Technical Report Documentation Page

1. REPORT No.
FHWA/CA/UCI-95-01

2. GOVERNMENT ACCESSION No.

3. RECIPIENT'S CATALOG No.

4. TITLE AND SUBTITLE
Assessment of Cross-Tie Performance in Bridge Pier Walls

5. REPORT DATE
December, 1994

6. PERFORMING ORGANIZATION
UC Irvine

7. AUTHOR(S)
Haroun, M.A., Pardoen, G.C., Shepherd, R., Haggag, H.A., Kazanjy, R.P.

8. PERFORMING ORGANIZATION REPORT No.

9. PERFORMING ORGANIZATION NAME AND ADDRESS
Civil and Environmental Engineering
4130 Engineering Gateway
UC Irvine
Irvine, CA 92717-1875

10. WORK UNIT No.

11. CONTRACT OR GRANT No.
RTA-59S986

12. SPONSORING AGENCY NAME AND ADDRESS
Caltrans- State Department of Transportation
1801 30th Street
Sacramento, CA 95816

13. TYPE OF REPORT & PERIOD COVERED
Final Report

14. SPONSORING AGENCY CODE
F925D24

15. SUPPLEMENTARY NOTES
This project was performed in cooperation with the U.S. Department of Transportation, Federal Highways Administration.

16. ABSTRACT

Seismic design standards are continually being upgraded to reflect latest seismological findings, most recent results of analysis and testing programs, and observations of the performance of structures during past earthquakes. Following the 1989 Loma Prieta earthquake, the California Department of Transportation intensified its efforts to verify and, if necessary, upgrade the seismic design of the structural components of highway bridges.

The very early design procedures of bridge pier walls assumed that these structural components behave as shear walls subjected to equivalent static loading. Lateral loads in the direction of the weak axis (flexural) of such walls were not considered in the design. As a result of this assumption, the pre-1971 pier wall design used relatively small reinforcement ratios in both the vertical and horizontal directions. An average ratio of 0.56% of the cross sectional area was used for the vertical reinforcement whereas an average ratio of 0.15% was used for the horizontal reinforcement. Horizontal bars were often placed on the inside of the vertical bars, unintentionally reducing a potential source of confinement. Furthermore, field lap splices were used between the vertical bars and the footing dowels. Class "A" splices, for which the splice length is 16 db, and class "C" splices, for which the splice length is 28 db, were commonly used where db is the diameter of the vertical bar.

17. KEYWORDS
pier wall; seismic design; ductility; cyclic load testing

18. No. OF PAGES:
118

19. DRI WEBSITE LINK
http://www.dot.ca.gov/hq/research/researchreports/1989-1996/95-01.pdf

20. FILE NAME
95-01.pdf

Technical Report Documentation Page

1. Report No.	2. Government Accession No.	3. Recipient's Catalog No.
FHWA/CA/UCI-95-01		

4. Title and Subtitle
Assessment of Cross-Tie Performance in Bridge Pier Walls

5. Report Date
December, 1994

6. Performing Organization Code
UC Irvine

7. Author(s) Haroun, M.A., Pardoen, G.C., Shepherd, R., Haggag, H.A., Kazanjy, R.P.

8. Performing Organization Report No.

9. Performing Organization Name and Address
Civil and Environmental Engineering
4130 Engineering Gateway
UC Irvine
Irvine, CA 92717-1875

10. Work Unit No. (TRAIS)

11. Contract or Grant No.
RTA-59S986

12. Sponsoring Agency Name and Address
Caltrans- State Department of Transportation
1801 30th Street
Sacramento, CA 95816

13. Type of Report and Period Covered
Final Report

14. Sponsoring Agency Code
F925D24

15. Supplementary Notes
This project was performed es
Department of Transportati

16. Abstract

95-01

Following the 1989 Loma Prieta on intensified its efforts to verify and, if necessary, upgrade the se idges.

The very early design procedure s behave as shear walls subjected to equivalent static loading. La such walls were not considered in the design. As a result of th ively small reinforcement ratios in both the vertical

The current design of bridge pi ismic performance of pier walls, specifically in the weak direc d the horizontal reinforcements, placing the horizontal re nding the vertical bars into the foundation, thereby eliminating ormly been distributed along the wall height to improve their fl

The present study intended, sp h the objective of establishing whether existing standards onfinement would be acceptable. In addition, two different rat ge and upper design limits in current Caltrans specifications were investigated. A computer program was developed to estimate both the pier wall ductility and strength. Furthermore, the current design method used by Caltrans designers was assessed. The calculated results were compared with the experimental findings, and recommendations for improved design procedures were devised.

17. Key Words	18. Distribution Statement
pier wall; seismic design; ductility; cyclic load testing	

19. Security Classif. (of this report)	20. Security Classif. (of this page)	21. No. of Pages	22. Price
Unclassified	Unclassified	104	

Form DOT F 1700.7 (8-72) Reproduction of completed page authorized

95-01

RTA-59696

[illegible] in cooperation with the United Stat[illegible]
[illegible] Federal Highway Administration.

[illegible] earthquake the California Department of Transportation [illegible] the structural components of highway [illegible] of piers [illegible] structural components [illegible] the weak axis (flexural [illegible] used [illegible] lateral section.

[illegible] has employed [illegible] to improve the se[illegible] such [illegible] the steel ratios of the vertical [illegible] the vertical bars, and exte[illegible] cross-ties have [illegible] strength and ductility in the weak direction.

[illegible] to examine a range of cross-tie provisions wit[illegible] conservative [illegible] If so, what level of [illegible] vertical steel [illegible] representing average [illegible]

FINAL REPORT TO

THE CALIFORNIA DEPARTMENT OF TRANSPORTATION

ASSESSMENT OF CROSS-TIE PERFORMANCE IN BRIDGE PIER WALLS

RTA No. 59S986

by

Medhat A. Haroun, *Professor and Chair*

Gerard C. Pardoen, *Professor*

Robin Shepherd, *Professor*

Hesham A. Haggag, *Graduate Research Assistant*

and Robert P. Kazanjy, *Senior Development Engineer*

DEPARTMENT OF CIVIL AND ENVIRONMENTAL ENGINEERING

UNIVERSITY OF CALIFORNIA, IRVINE

DECEMBER 1994

ACKNOWLEDGEMENTS

The financial support of the Division of Structures, the California Department of Transportation under Research Technical Agreement (RTA) no. 59S986 is appreciated. The technical advice from Caltrans bridge engineers Thomas Sardo, Craig Whitten and Ray Zelinski is acknowledged with gratitude. The numerous fruitful discussions with Mark Seyed of the Special Analysis Section of Caltrans is appreciated. The authors wish to express their appreciation to all who contributed to the success of the project, especially, Research Assistants Carrie Bischoff, Youhanna Labib, Kevin McCoy, Mathew Steiner and Brook Sutherland.

Contents

List of Figures

List of Tables

Chapter 1

Introduction

Seismic design standards are continually being upgraded to reflect latest seismological findings, most recent results of analysis and testing programs, and observations of the performance of structures during past earthquakes. Following the 1989 Loma Prieta earthquake, the California Department of Transportation intensified its efforts to verify and, if necessary, upgrade the seismic design of the structural components of highway bridges.

The very early design procedures of bridge pier walls assumed that these structural components behave as shear walls subjected to equivalent static loading. Lateral loads in the direction of the weak axis (flexural) of such walls were not considered in the design. As a result of this assumption, the pre-1971 pier wall design used relatively small reinforcement ratios in both the vertical and horizontal directions. An average ratio of 0.56% of the cross sectional area was used for the vertical reinforcement whereas an average ratio of 0.15% was used for the horizontal reinforcement. Horizontal bars were often placed on the inside of the vertical bars, unintentionally reducing a potential source of confinement. Furthermore, field lap splices were used between the vertical bars and the footing dowels. Class "A" splices, for which the splice length is 16 d_b, and class "C" splices, for which the splice length is 28 d_b, were

commonly used where d_b is the diameter of the vertical bar.

Because this design was based only on theoretical concepts without the benefit of experimental verifications, a comprehensive testing program [16] was conducted at the University of California, Irvine, to better understand the behavior of pier walls built to old design standards and to devise efficient retrofit schemes for deficient walls. The pier wall samples were subjected to cyclic loading in the directions of their strong and weak axes. The study concluded that the observed displacement ductility factor for the tested walls substantially exceeded the design ductility factor. Further observations at the later stages of loading indicated that the positioning of the horizontal bars to the inside of the vertical bars does not, as expected, provide any source of confinement and the slip between the vertical bars and the foundation dowels in the lap splice zone coupled with buckling of the vertical bars on the compression side of the wall could have significantly reduced the wall ductility.

The current design of bridge pier walls has employed clear measures to improve the seismic performance of pier walls, specifically in the weak direction, such as increasing the steel ratios of the vertical and the horizontal reinforcements, placing the horizontal reinforcement on the outside of the vertical bars, and extending the vertical bars into the foundation, thereby eliminating the need for lap splices. In addition, cross-ties have uniformly been distributed along the wall height to improve their flexural strength and ductility in the weak direction.

The present study examined a range of cross-tie provisions with the objective of establishing whether existing standards are unnecessarily conservative and, if so, what level of confinement would be acceptable. In addition, two different ratios of the vertical steel reinforcement representing average and upper design limits in current Caltrans specifications were investigated. A computer program was developed to estimate both the pier wall ductility and strength. Furthermore, the current design method used by Caltrans designers was assessed. The calculated results were

compared with the experimental findings, and recommendations for improved design procedures were devised.

Chapter 2

Historical Development

2.1 Introduction

Some of the problems observed in reinforced concrete bridges during earthquakes over the past twenty years have alerted designers that techniques to improve the seismic performance of bridges are necessary. In particular, investigations of the failure mechanism of bridges have led to enhancement of the design in many different ways. In general, damage to bridges may be categorized in three groups:

- Spans falling from their supporting piers under seismically induced large displacements as a result of inadequate seating provisions and lack of ties to pier caps or adjacent spans;
- Failure of piers or piles in flexure or shear, resulting from seismic inertia forces induced in the bridge superstructure; and
- Failure of foundation materials such as slumping of abutments and liquefaction of sandy foundations.

Research on bridges and their structural components has been carried out to estimate the strength and ductility demands. Both experimental and theoretical studies

have been performed to predict the strength and ductility capacities of bridge components. Pier walls, as bridge supporting systems, are the focus of study in this report. Previous investigations have experimentally modeled the pier as an individual element and simulated the superstructure actions on the bridge by a uniformly distributed axial load as well as quasi-static lateral loads at the top of the pier representing the inertia forces induced in the bridge superstructure by the earthquake.

An earlier study [16], which began at the University of California, Irvine, in 1990 investigated the seismic performance of bridge pier walls in their strong and weak directions. In the longitudinal direction (strong axis), it demonstrated a good performance of the walls. Shear failure was dominant and relatively large ductility was observed. In the weak direction, pier walls exhibited flexural failure more or less as rectangular columns. Due to the lack of general research on pier walls' performance under loading in the weak direction, and because of the expected similarity of their behavior to that of relatively wide rectangular columns, a summary of the literature on experiments conducted on bridge pier columns experiencing flexural failure is presented. Previous studies on pier columns had focused on two main issues:

- Investigation of the stress-strain characteristics of confined and unconfined concrete; and
- Investigation of the flexural strength and ductility of piers with different confining levels under simulated seismic loading.

2.2 Pier Failure in Past Earthquakes

Records of structural damage to bridges in past earthquakes have shown that damage was mainly confined to column piers and that there were no reports of damage to pier walls. This is attributed to the relatively low axial load ratio (applied

Figure 2.1: Shear failure at column top of the Foothill Boulevard undercrossing (1971 San Fernando earthquake)

load/capacity of the cross-section) carried by pier walls in comparison with columns, the larger ductility of the pier wall than that exhibited by columns, and lastly, because bridges supported on pier walls are generally less common than those supported by columns. It should be noted that pier walls excited along their longitudinal axis are efficient in transferring the shear forces exerted by the superstructure. In the weak direction, however, pier walls might experience the same type of damage exhibited by rectangular columns. Therefore, a brief summary of damage to pier columns in past earthquakes is introduced.

Flexural failure of pier columns is mostly attributed to the lack of confinement at plastic hinge zones. Spalling of the concrete cover followed by immediate increase of the x-sectional core stresses and buckling of the longitudinal reinforcement have contributed to the flexural failure of column piers. Figures 2.1 and 2.2 show shear

Figure 2.2: Flexural failure at column top at the San Fernando Road overhead (1971 San Fernando earthquake)

and flexural failures which occurred in the plastic hinge zone of bridge supporting columns during the 1971 San Fernando earthquake [31]. Another example of flexural failure is presented in Fig. 2.3 of the Corralitos Creek bridge (designed in 1936) during the 1989 Loma prieta earthquake where flexural cracks and spalling were observed at the top of the column pier [6]. Column failure below the confined zone at the Bull Creek Canyon Channel bridge during the 1994 Northridge earthquake is illustrated in Fig. 2.4.

2.3 Stress-Strain Relation of Confined Concrete

The traditional concrete cylinder compression test still is the common way to evaluate the compressive strength of the concrete, $f_c^{'}$. In most codes, the elastic design does not permit the maximum strain in the concrete section, ϵ_{cu}, to exceed 0.003. In the seismic evaluation of a reinforced concrete cross-section at relatively large defor-

Figure 2.3: Damage at top of column supporting the Corralitos Creek bridge (1989 Loma Prieta earthquake)

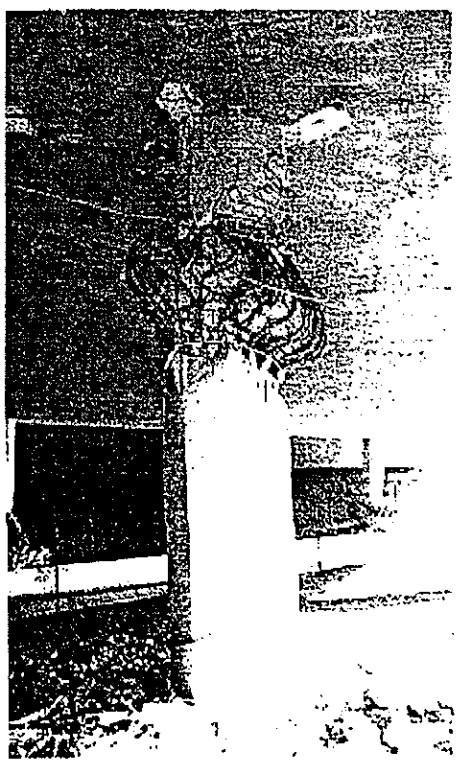

Figure 2.4: Column failure below the confined zone at the Bull Creek Canyon Channel bridge (1994 Northridge earthquake)

mation and compressive stress, the appropriate values for $f_c^{'}$ and ϵ_{cu} must consider the confinement stresses induced from the lateral reinforcement. Experiments to estimate the values of the confined concrete compressive strength, $f_{cc}^{'}$, and the maximum concrete strain, ϵ_{cu}, under multidirectional stresses have been classified according to the type of the confining stress, whether active or passive. Active confinement is conducted by applying direct lateral loads to the tested samples. Passive confinement is developed from the reaction of the lateral reinforcement to the lateral strain in the concrete section. The first type has been generally used to develop the general stress-strain relation of the concrete material, whereas the second type is more representative of the confinement in pier wall section.

In 1983, Mander [20] tested 16 half-scale pier samples of rectangular cross-section. The objective was to predict the concrete compression stress-strain relation under different configurations of the vertical and lateral reinforcement ratios. The specimens were monotonically loaded and tested under either quasi-static or high-strain rates representative of seismic conditions. The cross-section dimensions of the wall samples were 15 $\times$ 70 $\times$ 120 cm (5.9 $\times$ 27.5 $\times$ 47.2 inch). The samples were prototype of the walls in a hollow square column section.

This experiment was a step to suggest and experimentally evaluate an alternative design of the south Rangitikei Rail Bridge built of piers with hollow square cross-sections. The transverse hoop steel was designed to cover a typical range used for columns designed in accordance with the New Zealand concrete code, NZ3101 [25]. Three patterns for the confined reinforcement, allowed by that code, were examined. Figure 2.5 displays the different configurations of the lateral reinforcement: square hoops, overlapping square hoops, and rectangular hoops and cross-ties. Two equations governed the design of the area of the transverse reinforcement, A_{sh}, in each of the principal directions. A_{sh} is governed by the larger of

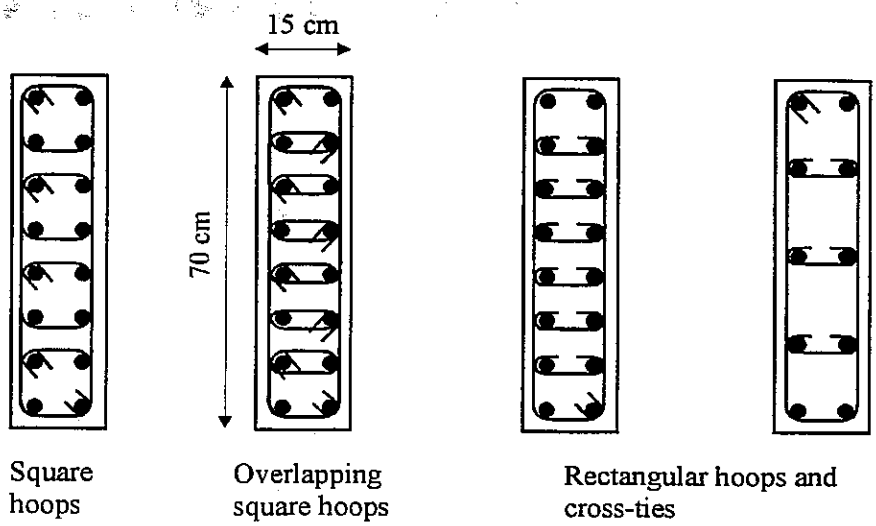

Figure 2.5: Cross-section of half-scale pier samples [20]

$$A_{sh} = 0.3 S_h \, h'' \left(\frac{A_g}{A_c} - 1 \right) \frac{f_c'}{f_{yh}} \left[0.5 + 1.25 \frac{P_e}{\phi f_c' A_g} \right] \tag{2.1}$$

or

$$A_{sh} = 0.12 S_h \, h'' \frac{f_c'}{f_{yh}} \left[0.5 + 1.25 \frac{P_e}{\phi f_c' A_g} \right] \tag{2.2}$$

where S_h is the vertical spacing of the lateral reinforcement, h'' is the concrete core dimension measured perpendicular to the horizontal hoop bars, A_g is the gross sectional area, A_c is the concrete core area, and P_e is the maximum subjected axial load. In these equations, the design reduction factor, ϕ, was set equal to 1.0. Two values of f_c' were employed. The hoop set spacing varied to achieve different ratios of the volumetric reinforcement ratio in the range of $\rho_s = 0.0\% \rightarrow 7.87\%$. This volumetric ratio of the transverse reinforcement, ρ_s, is calculated by adding up the transverse reinforcement ratios in each directions $(\rho_x + \rho_y)$. The vertical reinforcement ratios varied in the range of $\rho_v = 1.80\% \rightarrow 3.06\%$. The samples were set in the testing frame and axially loaded by monotonic loading. The test continued until the failure of the samples. Mander evaluated the maximum stress in the core section, f_{cc}', the corresponding strain, ϵ_{cc}, and the concrete strain at first hoop fracture, ϵ_{cu}, with and

without the confinement reinforcement and found that:

1. The increase of the volumetric ratio of the transverse reinforcement, ρ_s, between 0.0% $\rightarrow$ 7.87% showed an increase in the maximum concrete core stress, f'_{cc}, by a ratio of f'_{cc}/f'_c up to 2.00; an increase in the corresponding strain, ϵ_{cc}, from 0.0018 $\rightarrow$ 0.019; and an increase in the maximum concrete strain, ϵ_{cu}, in the range of 0.0045 $\rightarrow$ 0.045.

2. All samples with different configurations of the transverse reinforcement but having the same value of ρ_s behaved in a similar manner. It is worth noting that the interior square hoops are the most difficult to construct in field.

3. Induced larger axial stresses produce larger lateral forces which lead to early hoop fracture and buckling of the longitudinal bars. Therefore, in ductile design, it is preferable to keep the volume of the longitudinal steel low, and if necessary, use a larger concrete cross-section to relatively decrease the axial stresses.

4. An increase in the rate of loading resulted in an increase in the compressive strength of the concrete core, f'_{cc}; a decrease in the corresponding strain, ϵ_{cc}; an increase in the initial modulus of elasticity; and a decrease in the strain at first hoop fracture.

5. The analytical stress-strain model developed by Mander for the reinforced concrete rectangular section was suitable.

2.4 Strength and Ductility of Pier Samples

To evaluate the flexural strength and ductility of pier sections, tests were conducted on bridge pier samples subjected to variable lateral loads representing the earthquake action, accompanied by a constant axial load representing the vertical

Samples	X-section shape	Axial load(%)	ρ_v (%)	ρ_s (%)	ϵ_c at 1^{st} crushing	Max. concrete strain ϵ_{cu}		
						Ghee	Baker	Corley
1	Octagonal	20	2.43	0.756	.00837	.0405	.00498	.00975
2	Octagonal	56	2.43	1.527	.00832	.1271	.00597	.01161
3	Square	38	1.51	2.832	.00486	.0232	.00883	.01572
4	Square	25	1.51	2.218	.00839	.0359	.00827	.01136

Table 2.1: Experimental results of tested samples [10]

static loads. Due to the relatively large size of the tested samples and the large forces and displacements exerted in the samples, different testing setups were presented in the literature; some of these are displayed in Fig 2.6.

In 1981, Ghee [10] tested four pier samples including two octagonal and two square cross-sections. The testing involved slow static incremental loading followed by fast dynamic cyclic loading. The sample design and the testing parameters are summarized in Table 2.1, in addition to the observed ultimate strain. Ghee measured the maximum concrete strain at the edge of the core section and compared the obtained values with the following empirical equations presented by Baker and Amarakone [2] in 1964 and Corley [4] in 1966

$$\epsilon_{cu} = 0.0015\left(1 + 150\rho_s + (0.7 - 10\rho_s)\frac{d}{c}\right) \quad (by\ Baker\ and\ Amarakone) \tag{2.3}$$

$$\epsilon_{cu} = 0.003 + 0.02\frac{b}{L} + \left[\frac{\rho_s f_{yh}}{138}\right]^2 \quad (by\ Corley) \tag{2.4}$$

where c is the neutral axis depth at ultimate moment, d is the effective depth of member, f_{yh} is the transverse reinforcement yield stress in MPa, ρ_s is the volumetric ratio of the transverse steel to the volume of concrete core, b is the width of member, and L is the distance from the critical section to the point of contraflexure. The yield displacement, Δ_y, and curvature, ϕ_y, were evaluated from the load-displacement relation by extending a line passing through the origin and a load point corresponding to 75% of the calculated ultimate load. The plastic hinge length, L_p, was evaluated

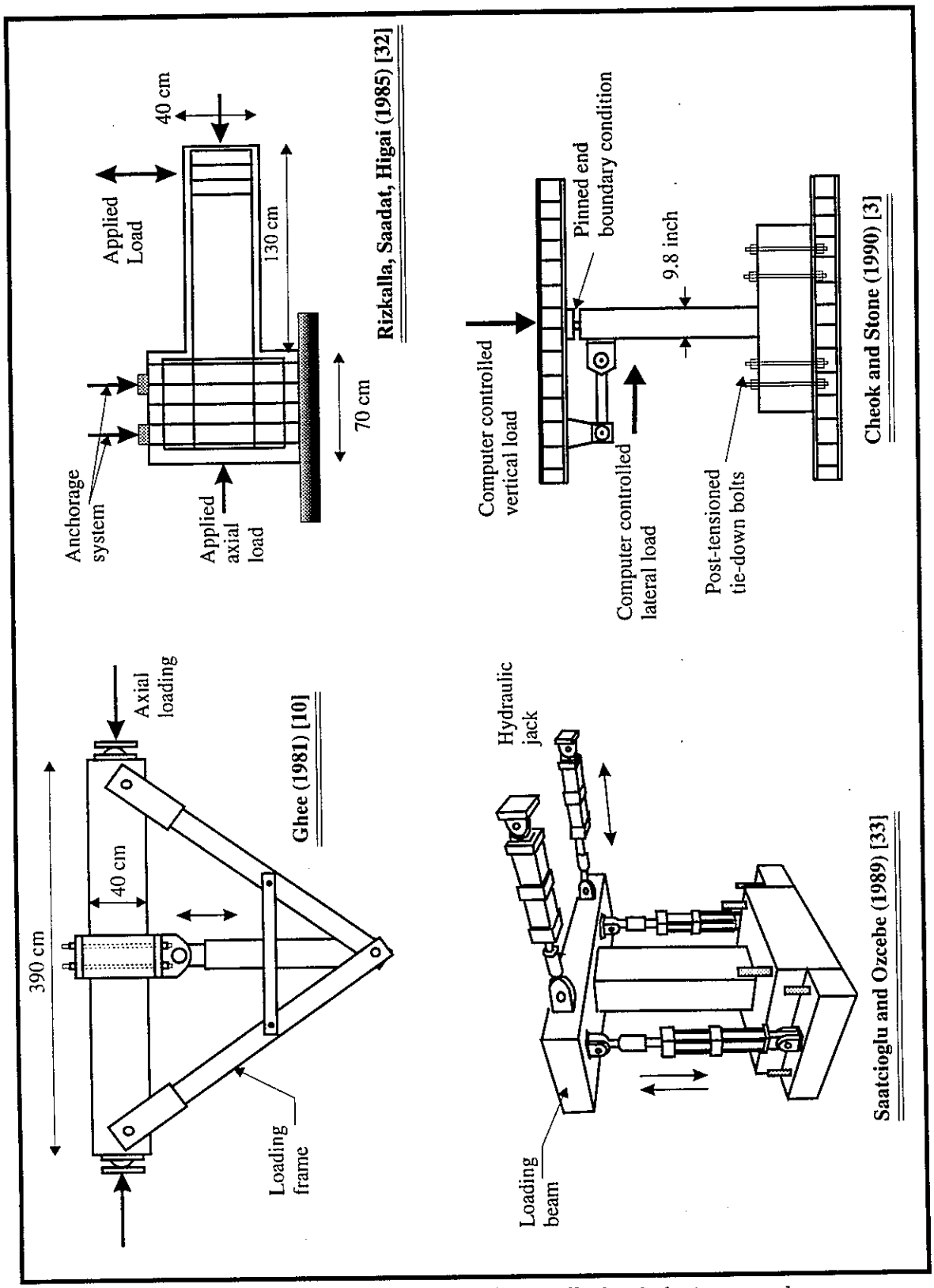

Figure 2.6: Different test setups of laterally loaded pier samples

from Eq. 2.5 using the experimental measured data

$$(\mu - 1)\Delta_y = (\phi_{max} - \phi_y)\, L_p \left(L - \frac{L_p}{2}\right) \tag{2.5}$$

where μ is the displacement ductility factor. Ghee compared the experimental values of L_p with the empirical equations developed by Baker [2] and Corley [4]

$$L_p = 0.8 K_1 K_3 \left(\frac{c}{d}\right) L \quad (by\ Baker\ and\ Amarakone) \tag{2.6}$$

$$L_p = 0.5d + \sqrt{d}\left(\frac{L}{d}\right) \quad (by\ Corley) \tag{2.7}$$

where K_1 and K_3 are factors dependent on the concrete and steel strengths, and c and d are defined in Eq. 2.3. The conclusion of Ghee's experiments can be summarized as follows:

1. The hysteresis behavior was not influenced by the cross-sectional aspect ratio when adequate confinement was provided.

2. The concrete strain at the first sign of crushing was 0.008 indicating that the value estimated by the ACI code for the concrete ultimate strain of 0.003 is low.

3. The curvature distribution over the sample height indicates that plasticity is concentrated in a small region around the critical section.

4. An increase of the flexural strength of the specimens in excess to the strength predicted by ACI charts due to the confining action was observed.

In 1985, Rizkalla, Saadat, and Higai [32] tested 16 large scale reinforced concrete specimens representing typical bridge piers in terms of material properties, section properties and construction details. The different parameters of the study were the shear span-to-depth ratio, L/d, longitudinal reinforcement ratio, ρ_v, frequency of the applied load, and level of axial compressive stress. No lateral reinforcement was considered. The samples were fixed at the base and horizontally cycled at the top. The

test parameters were varied for the ratio of (L/d) in the range of 3.29 $\rightarrow$ 6.05 and for ρ_v in the range of 0.46% $\rightarrow$ 1.95%. Ready-mixed concrete was used to construct all samples. According to parametric studies of the experimental results, Rizkalla *et al.* introduced a nondimensional factor, K, to describe the fundamental behavior of the pier members. The ductility factor, maximum shear stress, energy absorption/dissipation capacities and equivalent viscous damping coefficient were evaluated using this factor. The experimental yield displacement was evaluated when the experimental horizontal load equaled the calculated yield load. The suggested characteristic factor, K, is presented in Eq. 2.8

$$K = \frac{(L/d)f_t}{\rho_v f_y} \tag{2.8}$$

where f_t is the tensile strength of the concrete and f_y is the yield stress of the vertical reinforcement. The displacement ductility factor was evaluated as

$$\mu = \frac{1}{0.8 - 0.13K} \tag{2.9}$$

Using the K factor, they classified the failure mechanism to three modes. Mode I (K = 4.8 $\rightarrow$ 5.3) is observed by yielding of the longitudinal bars at the maximum moment section. Mode II (K = 4.0 $\rightarrow$ 4.8) is characterized by yielding of the longitudinal reinforcement within a distance, d, from the maximum moment section. Mode III (K = 2.3 $\rightarrow$ 4.0) is defined by the yielding within a distance, $2d$, from the maximum moment section. An increase of the K factor drives the failure towards a flexural failure mode. On the other hand, a decrease of the K factor drives the failure to a shear failure mode as shown in Fig. 2.7.

In 1987, Priestley and Park [30] evaluated the ductility and strength of different configurations of bridge pier columns. Figure 2.8 presents the cross-sections of the tested samples. The test variables included axial load level, cross-section dimension ratio, lateral reinforcement ratio, and lap splices. The lateral reinforcement was

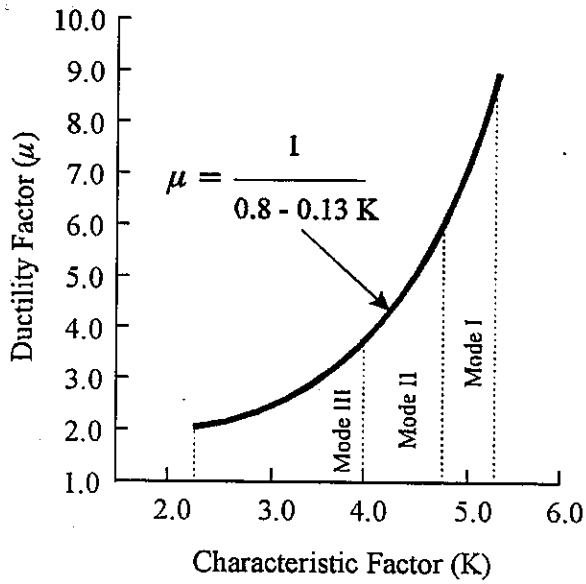

Figure 2.7: Relationship between ductility and the characteristic factor, K [32]

designed to satisfy the minimum and maximum ratios of Eqs. 2.1 and 2.2. The samples were hinged at their ends and loaded at the midspan. Investigating the load-displacement hysteresis loops, and from other test observations, Priestley and Park found that:

1. The load-displacement hysteresis loops were stable up to a ductility of $\mu = 6.0$.

2. The calculated design load, Q_i, based on the ACI code, was reached at $\mu = 2.0$ and the maximum horizontal load exceeded Q_i by almost 26%.

3. Very little load degradation was noticed during successive cycles of the same level of ductility.

4. Good energy dissipation potential was noted based on the width of the hysteresis loops.

5. The maximum measured strains ranged from 0.03 to 0.08 at the edge of the concrete core.

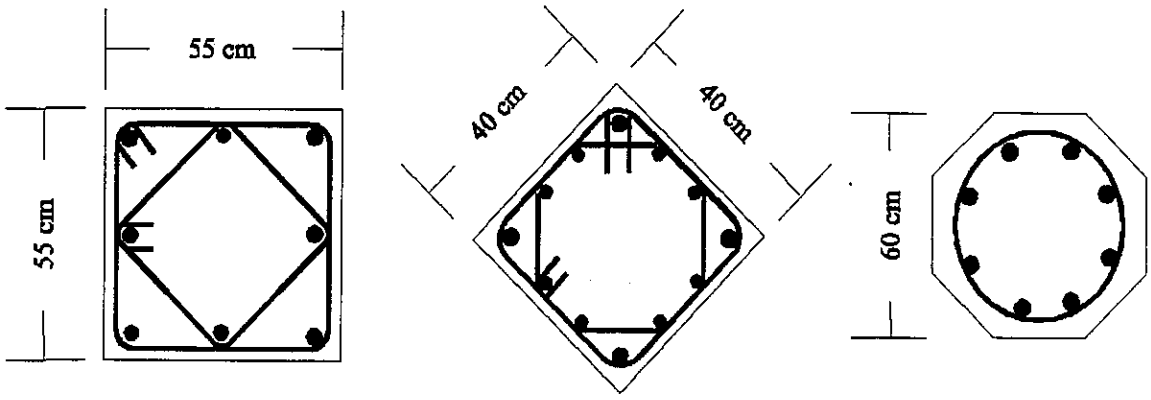

Face-loaded | Diagonal-loaded | Octagonal (circular reinforcement)

Figure 2.8: Cross-section of pier column samples [30]

6. The plastic hinge length, L_p, can be estimated using the proposed empirical equation (Eq. 2.10) which has no dependence on the axial load level nor on the vertical reinforcement ratio

$$L_p = 0.08\ L + 0.15\ d_b\ f_y \tag{2.10}$$

where d_b is the diameter of the vertical bars, L is the wall height and f_y is the yield stress of the vertical steel in ksi.

In 1989, Saatcioglu and Ozcebe [33] tested 14 full-scale square columns, modeling first-story columns between the foundation and the inflection point. The sample dimensions were 35 × 35 cm (14.3 × 14.3 inch) with a vertical reinforcement ratio of $\rho_v = 3.27\%$. The height of all samples was 100 cm (40.8 inch) which indicates that $L/d = 2.85$. The samples were tested under slowly applied lateral load reversals. Both uni-directional and bi-directional loadings were included. The axial loading and the confinement reinforcement were the varying parameters of the test. Closed hoops and cross-ties were used to induce confinement ratios between $\rho_s = 0.85\% \rightarrow 2.54\%$. Cross-ties with 135^o hooks at both ends and cross-ties with a 90^o hook at one end and a 135^o hook at the other end were used. The samples were fixed at the bottom and

loaded at the top. From observations of the tested samples and the testing results, Saatcioglu and Ozcebe concluded that

1. The axial tension caused a reduction in the flexural yield strength. In contrast, the axial compression increased the flexural yield strength followed by a rapid strength degradation.

2. Ductility of columns under combined axial compression and bending moment reversals was improved significantly with the use of proper confinement configurations. That was achieved by supporting every longitudinal bar by either a hoop or a cross-tie.

3. Cross-ties with a 135° hook at one end and a 90° hook at the other end behaved similarly to the cross-ties with 135° at both ends.

In 1990, Cheok and Stone [3] tested reduced scale samples of circular columns subjected to constant axial loads and horizontal cyclic forces. The objective was to evaluate the performance of bridge columns designed in accordance with the 1983 CALTRANS specifications. Three parameters were changed in that test: concrete mix, column aspect ratio, L/d, and axial load level. Six column samples were utilized to simulate a 1/6 scale model of a prototype bridge column. The samples were divided into two sets. In the first set, microconcrete was used whereas a ready-mixed concrete with pea gravel was used for the other set. The diameter of the column samples was 9.8 inches. Two columns of each set had a height of $4'\ 11''$ whereas the third column had a height of $2'\ 5.5''$. These specimens provided two aspect ratios, L/d, of 6.0 and 3.0. Flexural failure was expected for samples with $L/d = 6.0$ whereas shear failure was expected for $L/d = 3.0$. Deformed wire D6 was used for the longitudinal bars to reach a ratio of 2% for ρ_v. Confining reinforcement of volumetric ratios, ρ_s, of 0.68% and 1.41% were used for the flexure and shear samples, respectively. An axial load of

10% of $f_c' A_g$ was applied on the long samples while the ratios of 10% and 20% were applied on each of the shorter samples.

The column samples were fixed at their bottom and hinged at their top. A series of horizontal cyclic loads was applied at the top of the column while the axial load was kept constant. Evaluation of column performance was based on energy absorption capacity, displacement ductility, ultimate moment capacity, and qualitative observations concerning the ability of the confining reinforcement to prevent buckling of the longitudinal steel. The yield displacement was assumed to occur at 75% of the calculated ideal load, Q_i, based on the ACI-89 code. Cheok and Stone concluded that:

1. Ultimate displacement ductility factors of 10 and 5 were observed for specimens with $L/d = 3$ ($\rho_s = 1.41\%$) and $L/d = 6$ ($\rho_s = 0.68\%$).

2. A small increase of the displacement ductility factor and the energy absorption was observed using ready-mix concrete than the microconcrete.

3. Higher ductility and strength were observed for the $L/d = 3$ shear samples when the axial load ratio was increased from 10% to 20%.

4. The observed load capacity was higher than the calculated nominal load according to ACI-89 by 8% for the 10% axially-loaded samples and 27% for the 20% axially-loaded samples.

2.5 Pseudodynamic Versus Shaking Table Tests

The nature of earthquakes is to shake the structure from the ground up, and consequently, inertia forces are generated at the mass concentration. Most of the experimental work has modeled the bridge pier as a cantilever subjected to a constant axial load and excited by variable lateral displacements at the end of the can-

tilever. In 1988, Kawashima [18] investigated the difference of loading procedure on the seismic response of reinforced concrete bridge piers. Excitations using a shaking table and a dynamic actuator were compared. The cross-section dimensions of the samples were 40 × 80 cm (16.3 × 32.6 inch) with L/d ratio of 6.9. Longitudinal and cross-tie reinforcement ratios were 0.87% and 0.08%, respectively. Comparing the load-displacement hysteresis loops for both testing procedures, Kawashima concluded that in the shaking table tests the specimen showed biased response to one side at the principal motion, which was never developed by dynamic loading tests with symmetrical step-wise increasing load reversals under displacement control. He also concluded that less significant effects on the nonlinear hysteretic characteristics of reinforced concrete cantilever piers were found by comparing the two procedures.

2.6 Design of Bridge Piers

2.6.1 Requirements

Pier walls are classified as having a ratio of clear height to maximum width of the cross-section of less than 2.5. Minimum values of the concrete and steel strength, $f_c^{'} = 3,250$ psi and $f_y = 60,000$ psi, should be considered at a reinforced concrete section design. Deformed reinforcement shall be used except that plain bars or smooth wire may be used for spirals and ties. The modulus of elasticity and the effective inertia can be calculated according to the ACI code. The strength design method is used to control the design.

2.6.2 Loads

The design procedures specified by the Bridge Design Specifications Manual published by Caltrans [5] have been followed in this research for the design of the wall

samples. Parts of these specifications which govern the pier wall design are described here. Section 3 of this Caltrans manual, modified in June 1990, addressed the different types of loadings for which bridge components should be designed. In general, bridge structures shall be designed to carry the following loads and forces: dead load, live load, impact or dynamic effect of the live load, wind load, and any of the following forces if they exist: longitudinal forces, centrifugal forces, thermal forces, earth and drift pressures, buoyancy, shrinkage, rib shortening, erection stresses, ice and current pressure, earthquake stresses, prestressing and friction forces. All of these forces are described in Section 3 of the manual. In particular, the earthquake load should consider the relationship of the site to active faults, the seismic response of soils at the site, and the dynamic response characteristics of the total bridge. To determine the internal forces in the bridge components, two cases of loading shall be considered to account for the unknown direction of the earthquake which is the maximum of the following two equations

$$M = M_L + 0.30M_T \tag{2.11}$$

$$M = M_T + 0.30M_L \tag{2.12}$$

where M_L and M_T are the internal forces generated in the bridge components due to the effect of the earthquake forces in the longitudinal and the transverse directions, respectively. This straining action should be added to the internal forces induced from the vertical load of the bridge. In addition, Article 3.22 in the specifications, explains the different combinations of the loading factors.

Two methods are employed to determine the internal forces. The Equivalent Static Analysis method is used for bridges with well balanced spans and supporting bents of approximately equal stiffness. In this method, a factor ARS, dependent on the type of the soil at the site, the maximum expected acceleration and the period of the bridge, is multiplied by the dead load of the structure, W, to estimate the lateral force. Minimum value of 0.4 shall limit the factor ARS. For a bridge with irregular config-

uration, the Dynamic Analysis method shall be used. In the latter method, a modal analysis based on the application of a response spectrum of ground acceleration to a lumped mass space frame modeling the bridge structure is performed. Because of the large forces induced in the structure from earthquakes and the low probability of their occurrence, some allowance for inelastic action may be permitted. A ductility/risk reduction factor, Z, was introduced for the inelastic design. The seismic design force can be estimated by dividing the straining action calculated from Eqs. 2.11 and 2.12 by the Z factor. According to Article 3.21.1.2, Z=2 for piers, which may be increased for enhanced confined sections.

2.6.3 Reinforcement

The maximum ratio of the vertical reinforcement, ρ_v, shall not exceed 75% of the balanced reinforcement ratio, ρ_b. For pier walls with equal reinforcement area on the tension and compression side, the nominal moment and the balanced steel ratio can be calculated as

$$\phi M_n = \phi \left[A_s f_y d \left(1 - 0.6 \frac{\rho f_y}{f_c'} \right) \right] \tag{2.13}$$

or

$$\phi M_n = \phi \left[A_s f_y \left(d - \frac{a}{2} \right) \right] \tag{2.14}$$

where ρ is the tension reinforcement ratio and

$$a = \frac{A_s f_y}{0.85 f_c' b} \tag{2.15}$$

$$\rho_b = \left[\frac{0.85 \beta_1 f_c'}{f_y} \left(\frac{87,000}{87,000 + f_y} \right) \right] + \rho' \frac{f_s'}{f_y} . \tag{2.16}$$

where

$$f_s' = 87,000 \left[1 - \frac{d'}{d} \frac{87,000 + f_y}{87,000} \right] \leq f_y \tag{2.17}$$

To calculate the area of the lateral reinforcement, f_y shall equal 60 ksi. The lateral reinforcement shall be designed to consider the shear stress and to satisfy the confinement requirement. In addition to the above requirements, Article 8.18 added

- The minimum ratio of the vertical reinforcement, ρ_v, is 1% of A_g.
- The minimum ratio of the vertical shear reinforcement area to gross concrete area of a horizontal section in pier walls, ρ_n, is 0.25%, with a maximum spacing of 12 inches. ρ_n shall not be less than ρ_h which is the ratio of the horizontal shear reinforcement area to the gross concrete area of a vertical section in pier walls. The minimum value of ρ_h is 0.25% as stated in Article 8.18.2.3.
- All the bars shall be enclosed by lateral ties at least #3 in size for longitudinal bars #10 or smaller. Ties #4 shall be used for bars #11, #14, and #18.
- The total cross-sectional area, A_{sh}, of tie reinforcement for rectangular column shall not be less than

$$A_{sh} = 0.30 S_t h_c \frac{f_c^{'}}{f_y} \left(\frac{A_g}{A_c} - 1 \right) \tag{2.18}$$

  where S_t is the vertical spacing of the ties and h_c is the core dimension in the direction of the ties. In the plastic hinge zones, A_{sh} shall not be less than the minimum requirement above, or

$$A_{sh} = 0.12 S_t h_c \frac{f_c^{'}}{f_y} \left(0.5 + \frac{1.25 P_e}{f_c^{'} A_g} \right) \tag{2.19}$$

- Lap splices shall not be used in longitudinal reinforcing bars within zones of possible plastic hinging of the member.

Chapter 3

Experimental Program

The experimental program consisted of testing six samples representing a half-scale model of a bridge pier wall. Two ratios of the vertical reinforcement, approximately the average and the maximum design allowable by Caltrans specifications [5], were used. The samples were grouped to represent three distributions of cross-ties, for each ratio of the vertical reinforcement. A pseudo-dynamic horizontal load was applied on each sample along its weak direction while the wall was subjected to a constant axial vertical load. The horizontal loads at the top of the wall samples were cyclic and applied to generate prescribed displacement.

Measurement gages were used to evaluate the wall displacements and approximate values for the wall curvatures at different levels. In addition, strains in some of the vertical bars and the cross-ties were monitored. All data were digitally logged and the results were graphically represented for comparison.

3.1 Sample Description

The typical dimensions of the pier wall samples were 127 inches high, 96 inches wide, and 10 inches thick. These specimens were approximately a one-half scale model

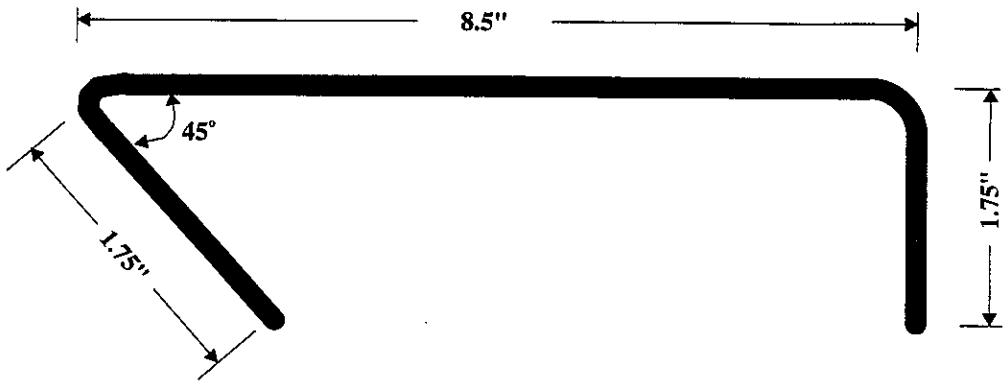

Figure 3.1: As-built dimensions of a cross-tie

of existing pier walls (the width has no influence on test results). Ready mix design of pea gravel concrete, of a nominal strength $f_c' = 4000$ psi, was used. This mix was agreed upon by Caltrans as an acceptable size mix for the half scale specimen. Cylinders representing the concrete mix in each wall were tested 7 and 28 days after concrete pouring and also at the time of testing. The specimens were divided to two groups: Group I has a vertical reinforcement ratio of 1.3% whereas Group II has a ratio of 2.3%. The vertical reinforcement ratio is equal to the total cross-sectional area of the vertical bars divided by the gross cross-sectional area of the concrete section. These ratios were chosen to represent approximately both the average and maximum reinforcement ratios of the Caltrans specifications [5] ($\rho_{min} = 1.0\%$ and $\rho_{max} = 0.75\rho_{balance}$). The spacing of the vertical reinforcement bars was the same for both groups, whereas bar sizes #6 and #8 were used for group I and II, respectively. The vertical bars were terminated in the footing with standard hooks. For each group, three distributions of cross-ties were used: none, uniform and partial. The partial distribution is represented by the concentration of the cross-ties at the lower part of the wall sample at the expected plastic hinge. Deformed wire D5 was used for the cross-ties with a standard shape of 90 and 135 degree legs. The cross-ties were placed in such a way that the vertical and the horizontal bars were enclosed by the

ties' hooks. Figure 3.1 presents as-built dimensions of a cross-tie. Each sample was denoted by two letters: the first is either "H" or "L" indicating high or low vertical reinforcement ratio, whereas the second letter "N", "P" or "U" indicates the cross-ties distribution. Figures 3.2 to 3.7 show the sample dimensions and their reinforcement details.

Horizontal reinforcement using #3 bars was placed on the outside of the vertical bars with a vertical spacing of 9 inches ($\rho_h = 0.25\%$) to satisfy the Caltrans recommended values ($\rho_{min} = 0.25\%$ and maximum spacing = 12 inches) in Sec. 8.18.1.5 [5]. In the "P" walls, the spacing of the horizontal reinforcement was reduced to 4.5 inch up to a height of 20.25 inches which represents approximately the expected plastic hinge length. This length was calculated based on the empirical formula by Priestley [30]

$$L_p = 0.08L + 0.15\ f_y\ d_b \tag{3.1}$$

where L is the wall height, f_y is the yield stress of the vertical reinforcement (in ksi) and d_b is the diameter of the vertical bars. U-shaped #3 bars were placed at each end of the wall at the horizontal reinforcement level where no cross-ties were present. According to Caltrans recommendations for seismic design [5], the first row of the horizontal reinforcement of the "P" and "U" samples was placed at heights of 2.25 and 4.5 inches, respectively, which represent half of the repeated vertical spacing.

Eight #7 bars were placed at the top of the wall with closed #3 stirrups to form an embedded concrete beam. The function of this beam was to uniformly distribute the actuator load and to increase the shear strength at the top of the wall.

3.2 Construction of the Samples

Footings, 18 inches thick, 116 inches long, and 56 inches wide, were designed to carry the wall samples. The footings and their corresponding walls were constructed in

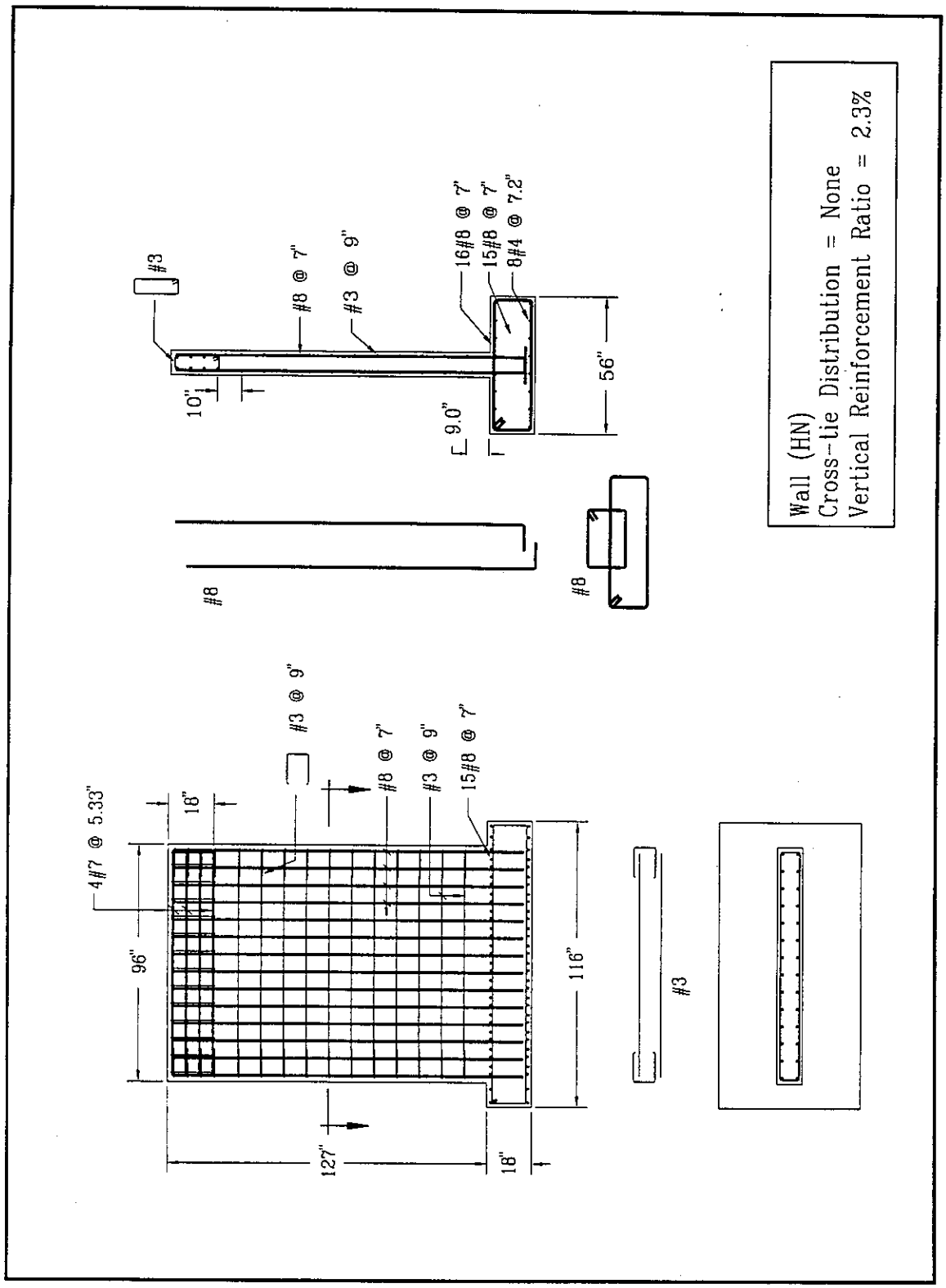

Figure 3.2: Reinforcement details of wall "HN"

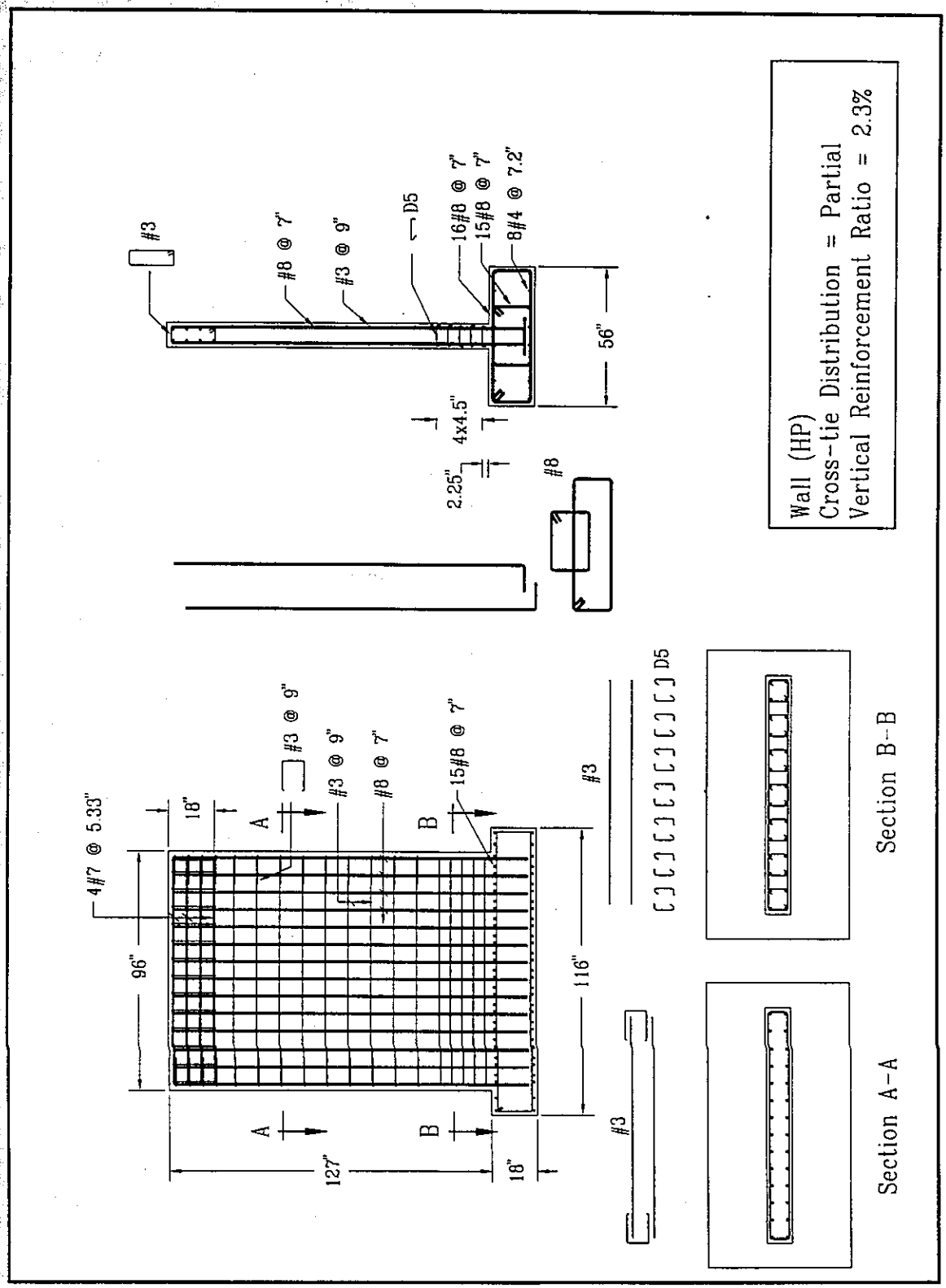

Figure 3.3: Reinforcement details of wall "HP"

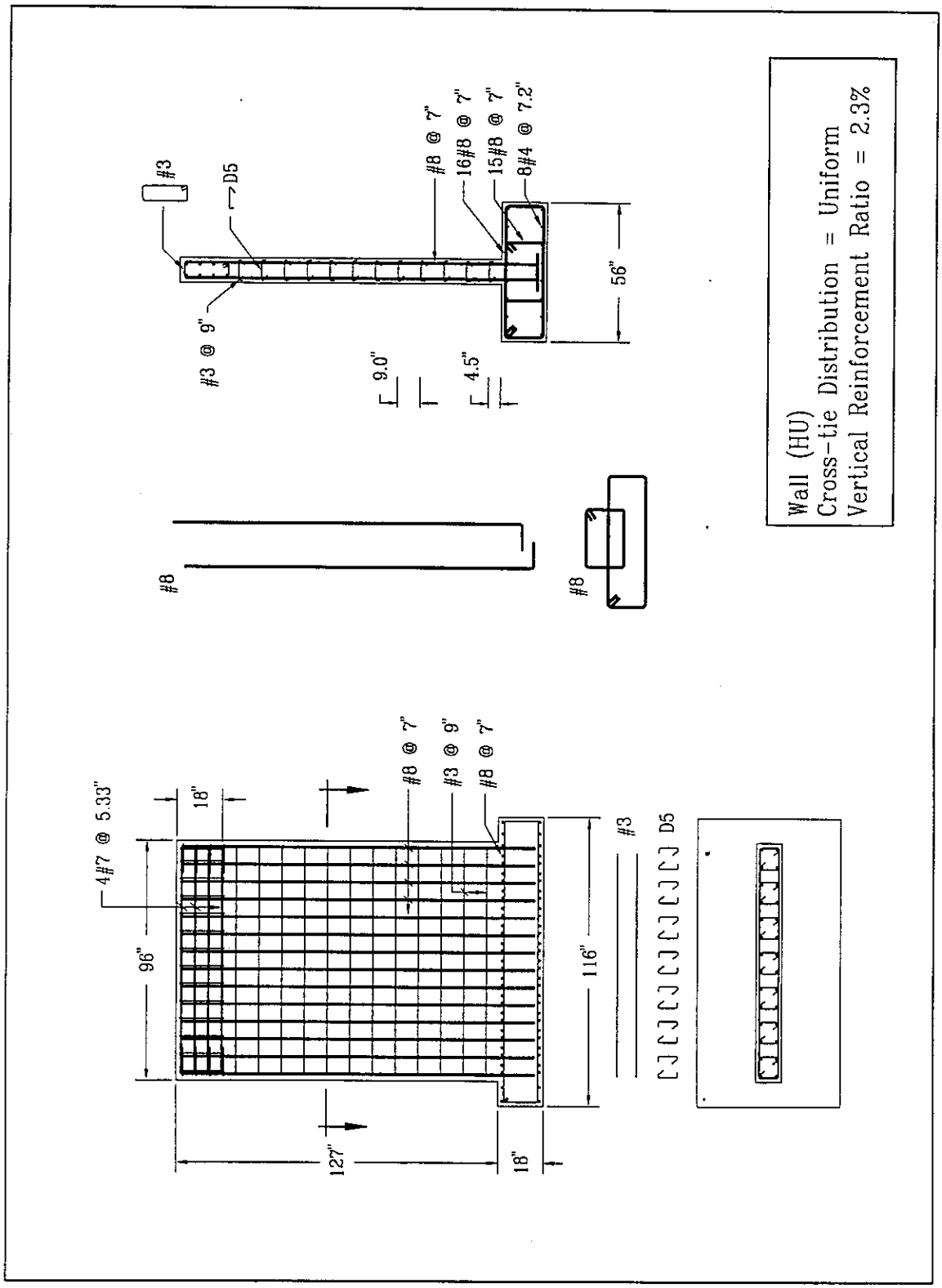

Figure 3.4: Reinforcement details of wall "HU"

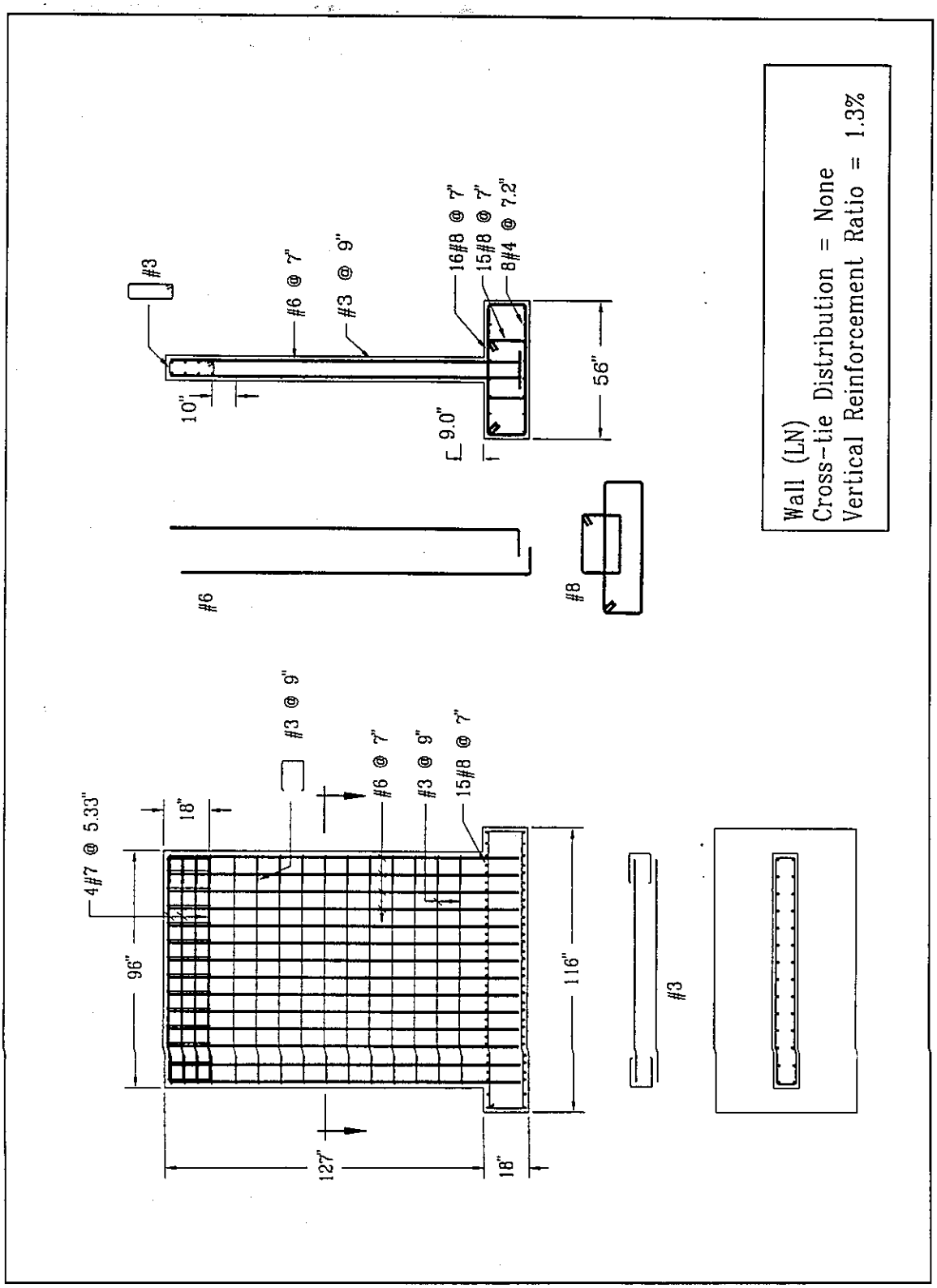

Figure 3.5: Reinforcement details of wall "LN"

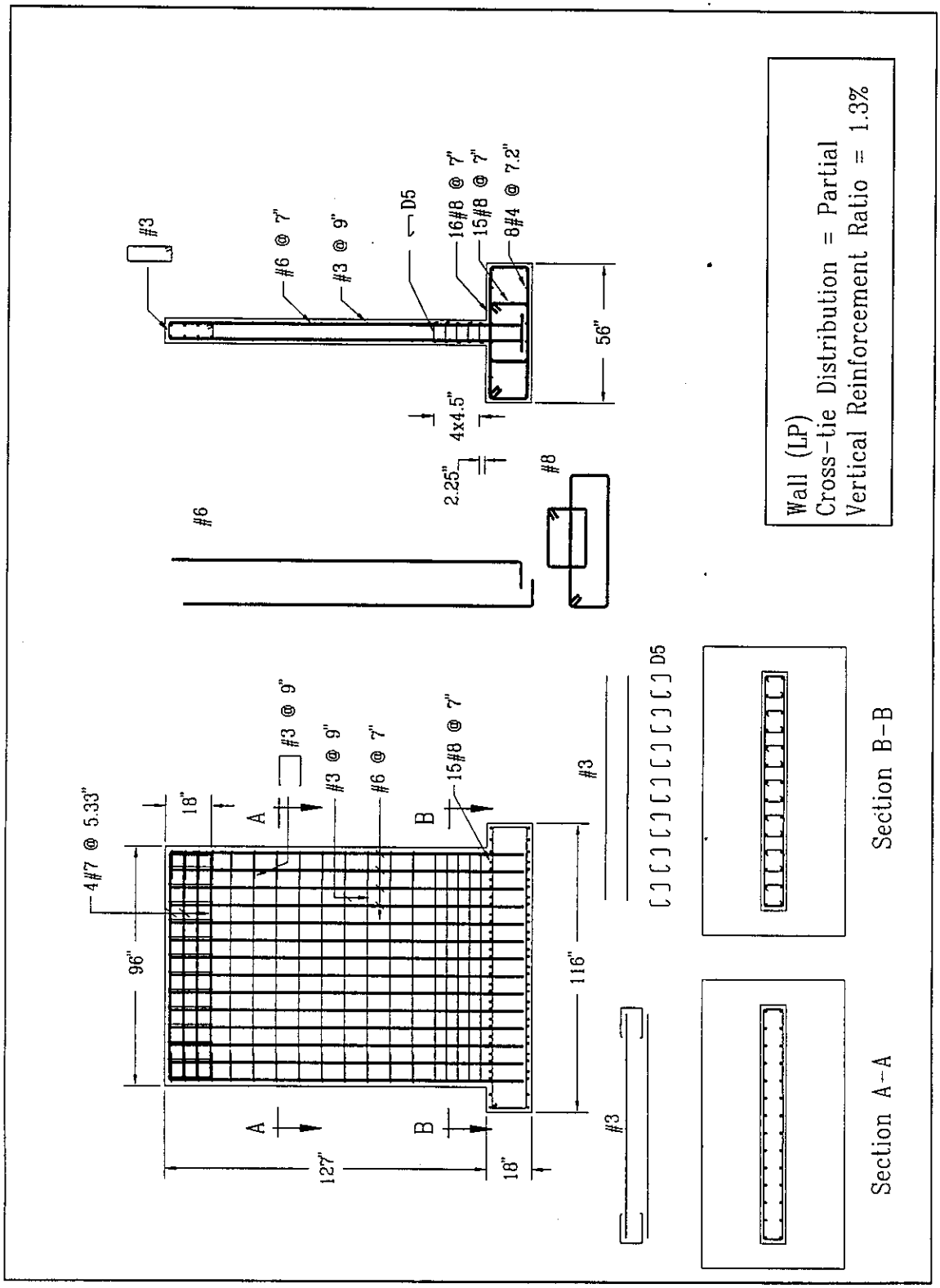

Figure 3.6: Reinforcement details of wall "LP"

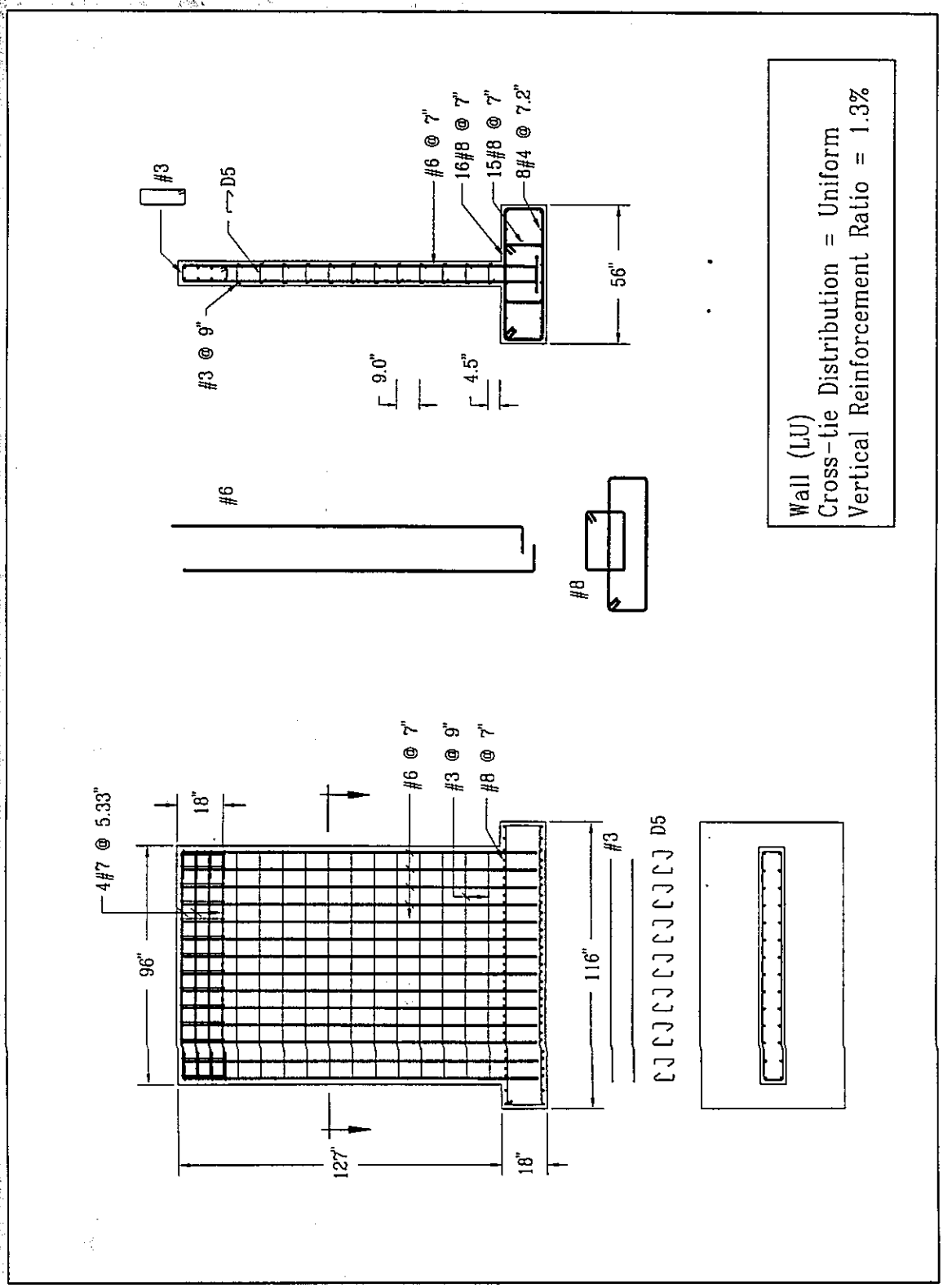

Figure 3.7: Reinforcement details of wall "LU"

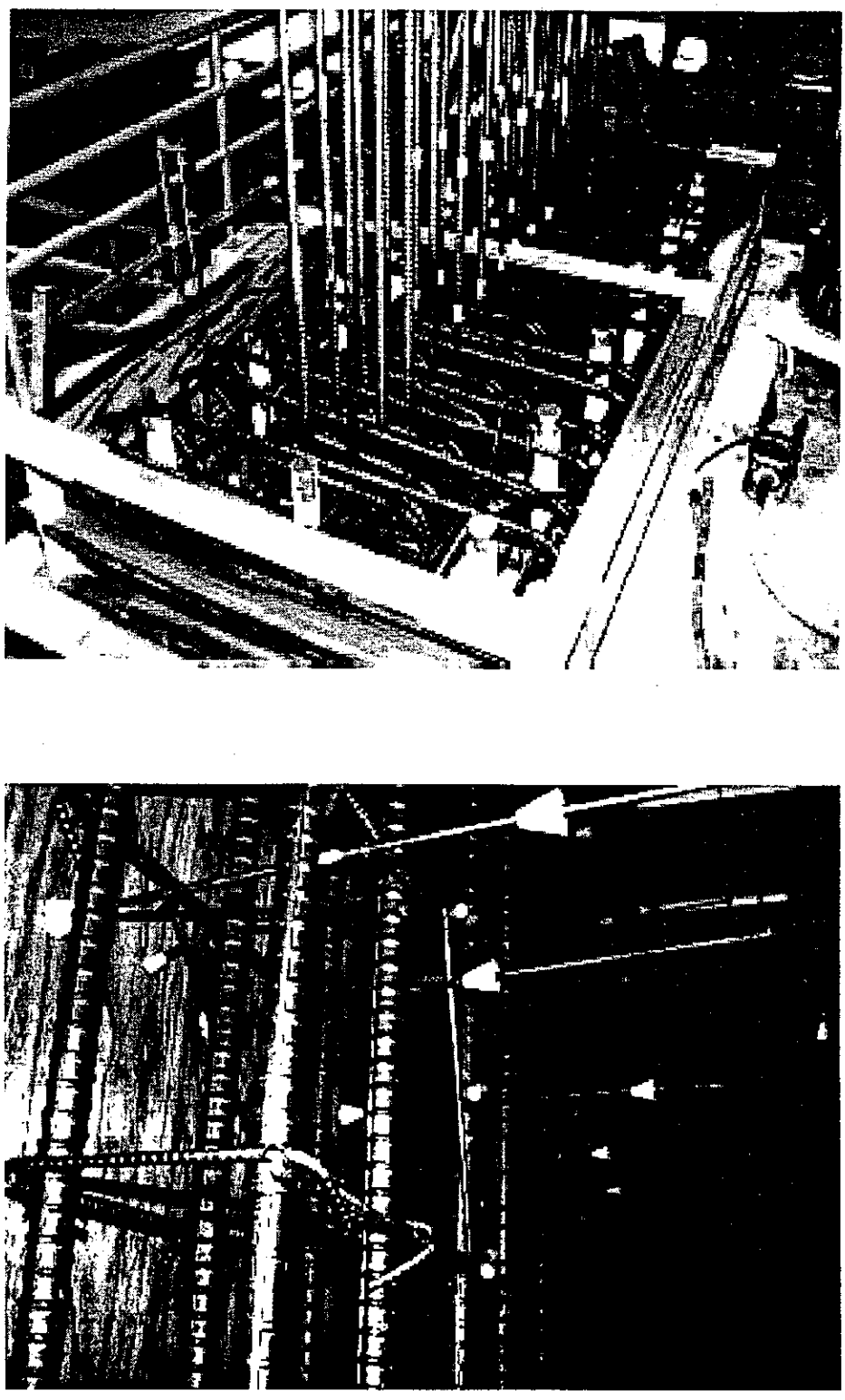

Figure 3.8: Reinforcement Placement

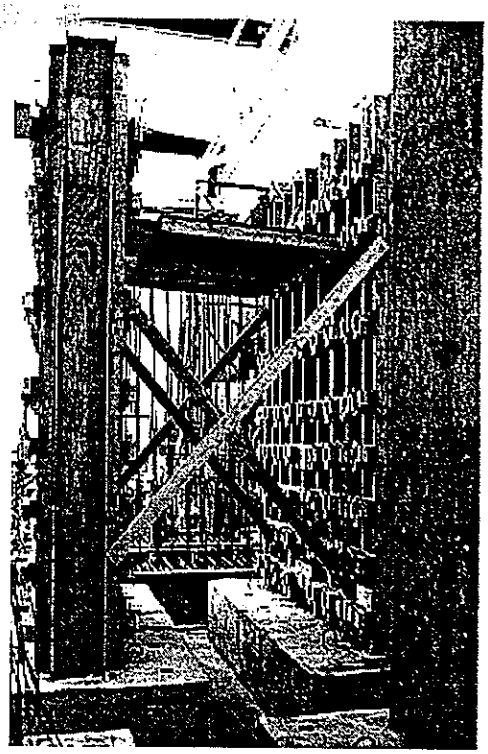

Figure 3.9: Bracing of wall forms during construction

two consecutive steps to simulate the actual construction stages. They were designed to carry a horizontal load at the top of the wall equal to 90 kips which is almost 1.5 times the expected strength of the "H" walls. Sixteen #8 closed bars were used to carry the flexure loading whereas 15 #8 closed bars were used to resist the shearing forces. Reinforcement bars #4 were used in the footing in the longitudinal direction to represent the minimum allowable design ratio. The footings were designed considering that they would be pretensioned to a rigid floor where no movements are allowed in any direction during testing. Concrete with the nominal strength of $f_c^{'} = 4000$ psi was used to construct the footings. Again, at least 3 cylinder samples of the concrete mix were examined after 7 and 28 days of pouring. The reinforcement details of the footings and of all constructed samples are shown in Fig. 3.2 to 3.7. Figure 3.8 displays photographs of the footing reinforcement and one of the wall samples.

Pouring of the concrete for the footings and the wall samples was done in two

Group No.	Pouring of		Tested at (days)	Strength (psi) of sample No.					Mean (psi)
	Footings	Walls		1	2	3	4	5	
I	HN, HU, HP		7	3136	3145	2756	-	-	3012
			28	4594	4841	4770	-	-	4735
II	LN	HN, HU	7	3180	2986	3357	3004	-	3132
			28	4594	4950	4734	4420	-	4675
III	LP, LU	HP, LN	7	3339	3251	2792	3180	3463	3205
			28	4240	4028	4099	-	-	4122
IV		LP,LU	7	2792	2686	2615	3180	2827	2820
			28	3534	3746	4064	3357	-	3675

Table 3.1: Compression strength of concrete cylinders after 7 and 28 days

consecutive steps to better reproduce the construction procedures in the field. Four pouring stages were scheduled to complete the construction of the six pier wall samples. Table 3.1 summarizes these steps and the typical compression test of the concrete cylinders in each group. After building the footing, the wall reinforcement was fabricated and the strain gages were attached to selected reinforcement rebars. Snap ties with fixed lengths were used to hold the two sides of wood form together and maintain constant thickness for the walls. Wall samples were constructed and cast in pairs. The wall forms were cross-braced to achieve self lateral stability during the concrete pouring, as shown in Fig. 3.9.

3.3 Test Setup

Each sample was fixed to the strong floor of the Structure Test Hall using twelve prestressed 1.25 inch diameter high strength bars, as shown in Fig. 3.10. Thick plate washers were used to prevent any local crushing of the footing due to stress concentration of the prestressing forces. A load cap fabricated from channels and plates was placed atop the wall to uniformly distribute the axial loads. Two 1.5 inch diameter steel bars were used to exert axial loads on the wall sample. These bars were attached to a hinge mechanism placed on the laboratory floor, and at the upper

end, they were connected to the load cap. The hinges at the wall base level were provided to reduce any bending effects on these bars due to large rotations of the wall. Figure 3.11 shows a picture of the hinge. The bars were tensioned using hydraulic cylinders placed on top of the load beam to provide an axial load approximately equal to 5% of the calculated wall axial capacity. A 155-kip Ortman hydraulic jack with a long stroke ($\pm$ 16 inch) was attached to the top of the wall sample at a height of 118 inches to apply horizontal cyclic loading. The actuator was free to rotate at its base and at the wall surface. The sample structure, under this setup, behaved as a cantilever excited by cyclic flexural load under a constant axial force.

3.3.1 Effect of the Test Geometry on the Measured Values

The axial and flexural forces are the two objective measurements of the straining actions on the critical section of the tested walls. The critical section of a cantilever is at its base. Correction factors may be required due to the large displacement of the wall top. Figure 3.12 shows the setup geometry and the load directions at large displacement. From that figure, the straining action at the critical section may be calculated as

$$Axial\ force = P\cos\theta = P\ \ C_p \tag{3.2}$$

where $\theta = \arctan(\Delta/118'')$ and C_p is the correction factor of the axial load. Similarly, the moment can be calculated as

$$Moment = (118H)\frac{\sqrt{118^2+\Delta^2}}{118} = (118H)\ \ C_m \tag{3.3}$$

where C_m is the correction factor of the moment. Evaluating the correction factors for $\Delta = 15$ inches yields $C_p = 0.992$ and $C_m = 1.008$. Since the maximum observed displacement of the test was less than 15 inches and the correction factors are close to unity, no modification of the measured values were considered.

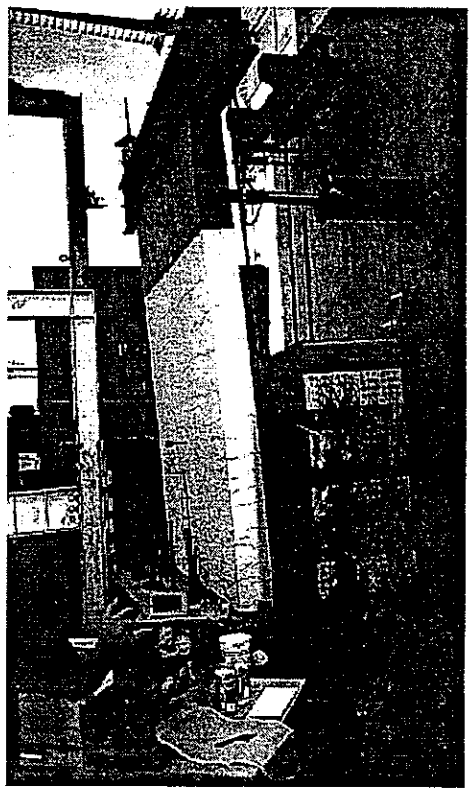

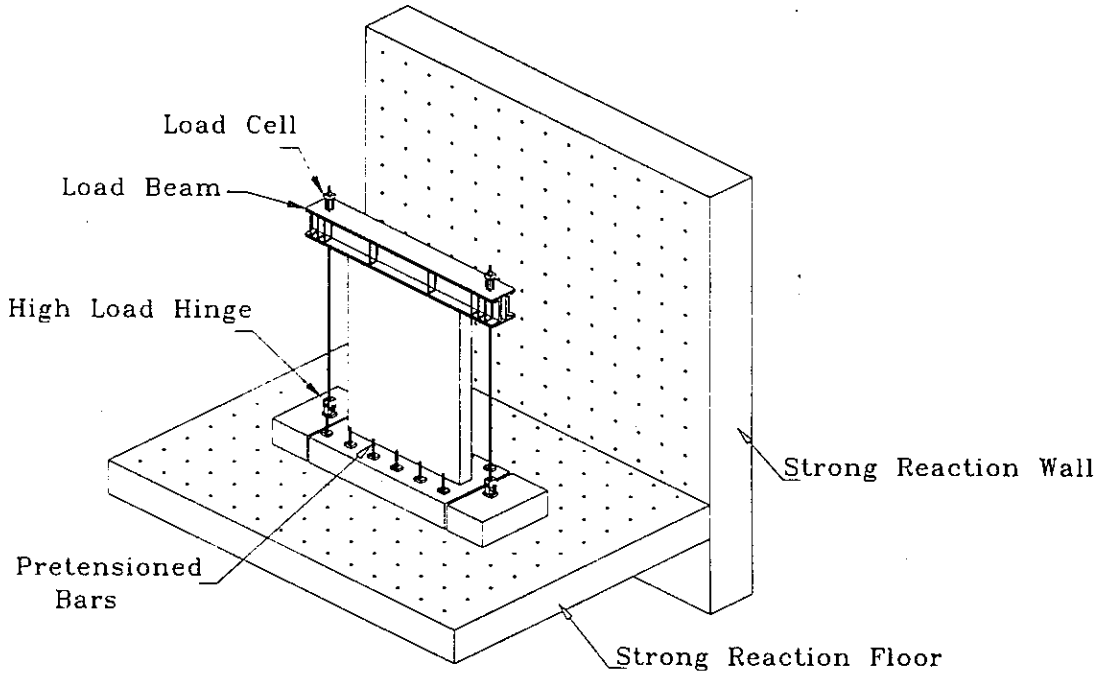

Figure 3.10: Test setup

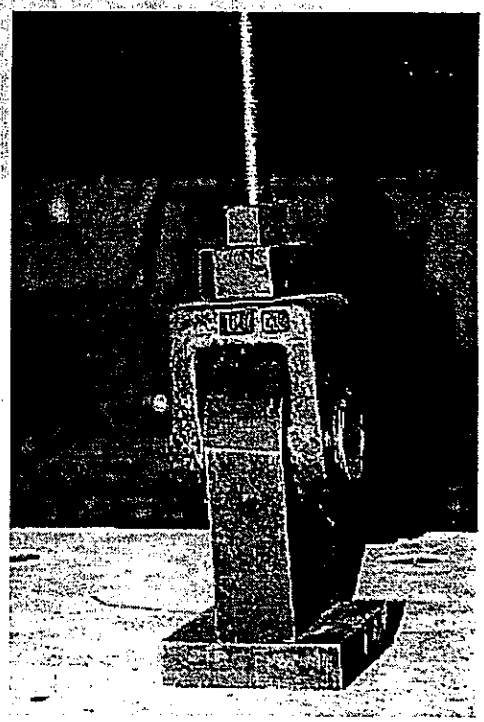

Figure 3.11: Hinge details

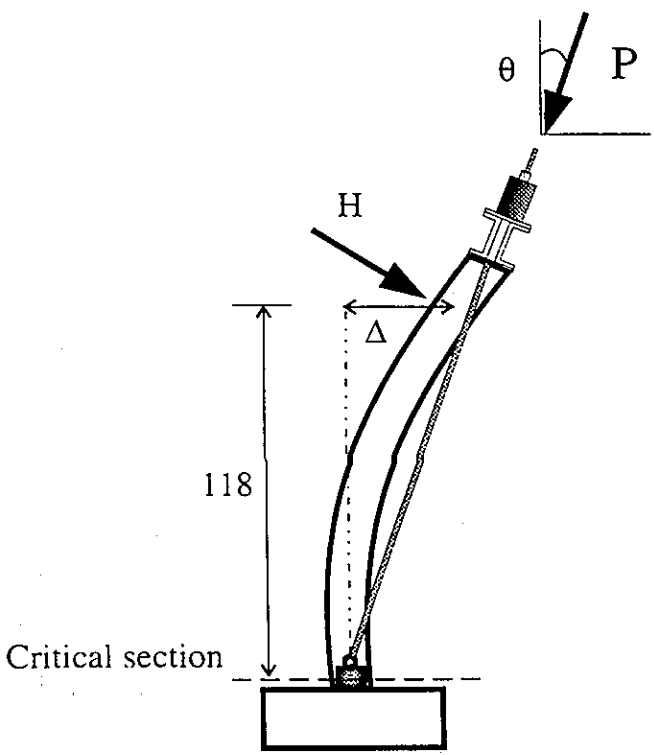

Figure 3.12: Test geometry at large displacement

3.4 Instrumentation

Displacements imposed by the hydraulic jacks were manually controlled. The values of these displacements and their corresponding loads were captured by a data logging system as described below. Twelve linear potentiometers were used to determine the curvature of the wall as it was subjected to cyclic loads. As shown in Fig. 3.13, the potentiometers were mounted to horizontal threaded rods which were embedded in the samples. These potentiometers were placed to measure the elongation and the contraction on the tension and compression sides of the wall. The lower part of each wall was divided to six strips and the curvature was calculated for each of these strips. Figure 3.13 shows the strips and their position. The curvature, which is measured by this method, is an average value for a strip of the wall and is not a value at a certain section. In addition, six string potentiometers were used to measure the horizontal displacements of the wall samples at different levels marked in Fig. 3.13. Strain gages (Micro Measurements) were attached to the vertical bars at two levels, approximately 2 and 20 inches, above the wall base to monitor strains (and consequently stresses) in the rebar. Strain gages were also attached to the cross-ties at different levels. The position of the strain gages on the vertical bars and the cross-ties is displayed in Fig. 3.14. Signals from the gages were amplified and conditioned (Measurements Group) and then passed to the data logging system.

The data logging system used in these experiments included four 8-channel terminal boards (Strawberry Tree T51). These boards were used to collect the analog input signals and transfer them to the Strawberry Tree analog-to-digital board through a Mac computer. Strawberry Tree's Workbench data acquisition software was used to collect and log data for the duration of the test. The Workbench program was set up to continuously log the applied loads and the corresponding displacements of the jacks as well as the potentiometers' and strain gages' signals.

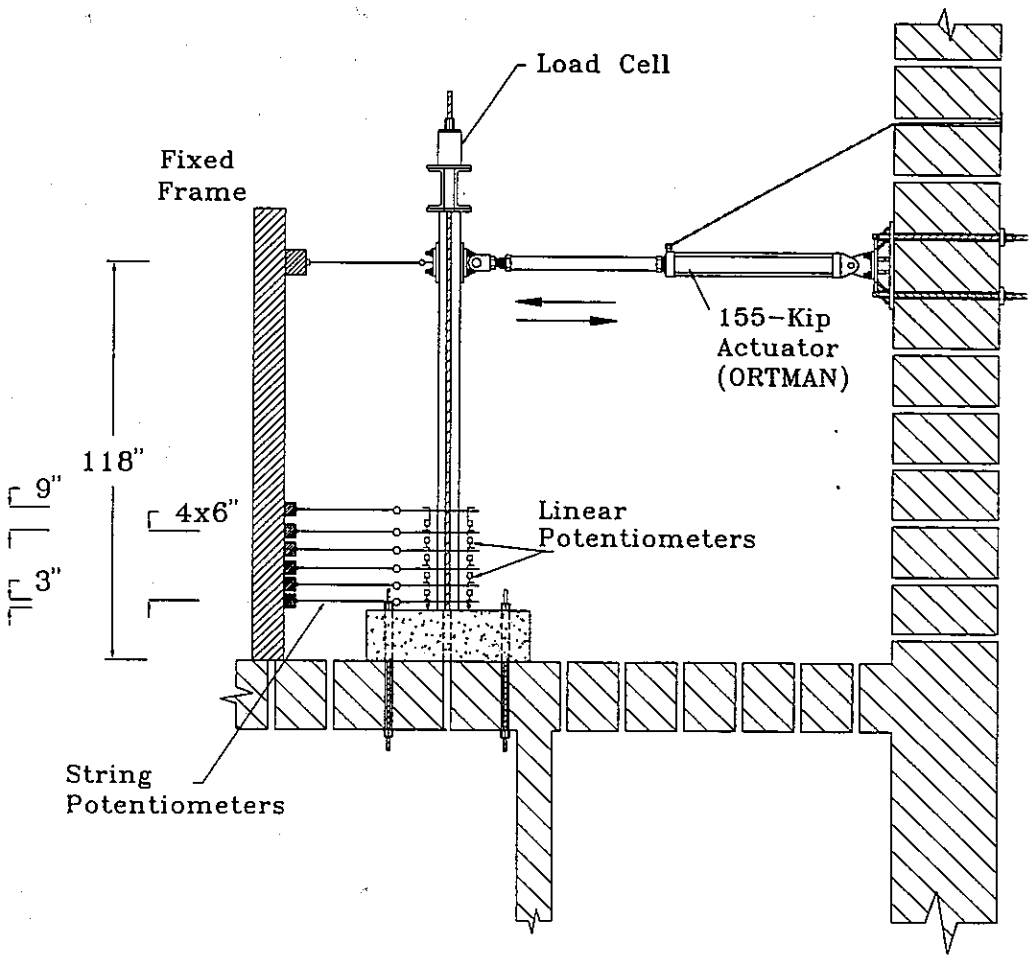

Measurements:

String potentiometers to measure horizontal displacements.
Linear potentiometers to measure vertical displacements.
Load cell to measure the axial load.
Ortman actuator to determine the horizontal load.

Figure 3.13: Instrumentation

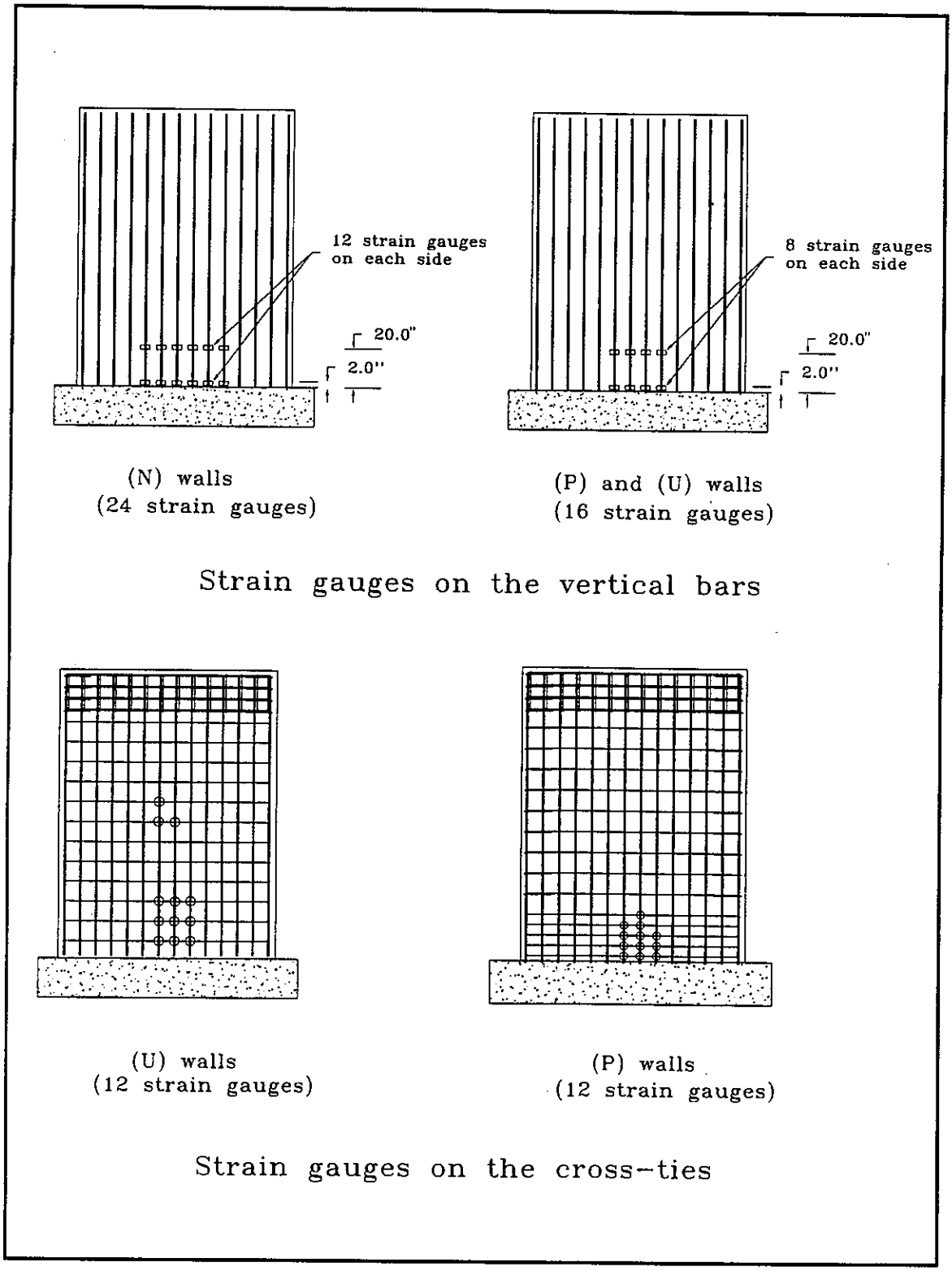

Figure 3.14: Position of strain gages

3.5 Test Procedure

All tests followed the same well-specified steps. At each step, the specimens were cycled horizontally three times at their top by the Ortman actuator. The maximum displacement of each cycle was limited by predesignated displacement level. The test was paused at the end of each step to record crack development. The test continued up to the failure of the wall. The test procedure is described briefly as follows:

1. The vertical rods were tensioned to apply axial loads equivalent to almost 5% of the wall axial strength. These values were 225 kips and 198 kips for the "H" and "L" walls, respectively, and are calculated as

$$P = 0.05\left(0.85f_c^{'}(A_g - A_{st}) + f_y A_{st}\right) \tag{3.4}$$

2. The Ortman jack was driven to a displacement less than the calculated yield displacement of the wall (about ± 0.3 inch).

3. The wall was cycled three times for that displacement level.

4. The jack load was increased until a nonlinear behavior of the load vs displacement was observed on the analog-plotter. This value is considered an approximation of the yield displacement.

5. The wall was cycled three times by this yield displacement.

6. The test was paused to record any crack development.

7. Steps 5 and 6 were repeated by increasing the displacement limits by factors of the yield displacement and the number of cycles. Table 3.2 shows the assigned cyclic displacement limits and the number of cycles at each loading step.

8. The test was stopped when the wall lost most of its strength (more than 30% reduction of the horizontal load capacity.)

Cycle No.	HN wall			HP wall			HU wall		
	Δ	μ	Cycles	Δ	μ	Cycles	Δ	μ	Cycles
1	0.30	0.12	3	0.30	0.11	3	0.30	0.12	3
2	1.00	0.40	3	1.00	0.37	3	1.00	0.39	3
3	1.50	0.60	3	1.50	0.56	3	1.22	0.47	3
4	2.25	0.91	3	2.23	0.84	3	1.83	0.71	3
5	3.00	1.21	3	2.98	1.12	3	2.44	0.95	3
6	3.75	1.51	3	3.72	1.39	3	3.05	1.19	3
7	4.5	1.81	3	4.47	1.67	3	3.66	1.42	3
8	5.25	2.12	3	5.21	1.95	3	4.27	1.66	3
9	6.00	2.42	3	5.96	2.23	3	4.88	1.90	3
10	6.75	2.72	3	6.70	2.51	3	5.49	2.14	3
11	7.5	3.02	3	7.45	2.79	3	6.10	2.37	3
12	8.25	3.33	3	8.19	3.07	3	6.71	2.61	3
13	9.00	3.63	3	8.93	3.34	3	7.32	2.85	3
14	10.00	4.03	3	9.68	3.63	3	7.93	3.09	3
15	18.00		1	10.42	3.90	3	8.54	3.32	8
16				11.17	4.18	3	9.15	3.56	6
17				11.91	4.46	4	9.76	3.80	6
18							10.37	4.04	6

Cycle No.	LN wall			LP wall			LU wall		
	Δ	μ	Cycles	Δ	μ	Cycles	Δ	μ	Cycles
1	0.30	0.16	3	0.30	0.17	3	0.30	0.17	3
2	0.86	0.46	3	0.91	0.51	3	0.87	0.49	3
3	1.29	0.69	3	1.37	0.76	3	1.30	0.73	3
4	1.72	0.92	3	1.82	1.02	3	1.70	0.95	3
5	2.58	1.39	3	3.64	2.03	3	2.10	1.17	3
6	3.44	1.85	3	4.55	2.54	3	2.53	1.41	3
7	4.30	2.31	3	5.46	3.05	3	3.37	1.88	3
8	4.73	2.54	3	6.37	3.56	8	4.22	2.36	3
9	5.16	2.77	3	7.28	4.07	8	5.06	2.83	3
10	5.59	3.01	3	7.74	4.32	3	5.90	3.30	8
11	6.02	3.24	8	8.19	4.58	8	6.75	3.77	8
12	6.45	3.47	8	8.65	4.83	6	7.59	4.24	8
13	6.88	3.70	8	9.10	5.08	5	8.43	4.71	8
14	7.31	3.93	6	10.01	5.59	5	9.28	5.18	8
15	7.74	4.16	8	10.92	6.10	7	10.12	5.65	4
16	8.17	4.39	4						

Table 3.2: Displacement limits of each cycle

At ductility levels beyond about 3.5, the number of cycles at each step was increased. The reason for this modification was to examine the effect of cycles on the deterioration of the wall at levels that may be reached only under very severe earthquake motions.

Prior to testing, it was expected that the maximum displacement of the wall samples would be rather low, and accordingly, the setup for the first test allowed for a maximum displacement of 10 inch. As the first sample (specimen "HN") was cycled, it became apparent that the wall would undergo displacements beyond those anticipated in the setup. Therefore, sample "HN" was cycled to a ductility factor of 4.0 and then pushed in one direction without any further cycling until failure.

After testing, the yield displacement was recalculated from the logged data of the load-displacement curve. The yield displacement was taken corresponding to a load equal to 75% of the ideal load which is calculated from the moment capacity of the wall section using the ACI-89 code approach in which ϵ_{cu}, the maximum concrete strain, is assumed 0.003. To simulate the load-displacement relation as an elasto-plastic relation the yield displacement, Δ_y, was projected to the ideal load value to estimate an idealized value of the yield displacement, Δ_y' as shown in Figure 3.15. The displacement ductility factor is considered as a multiple factor of the idealized yield displacement.

3.6 Test Observations

Concrete cylinder samples were examined at the time of testing and the results are presented in Table 3.3. All samples were examined after failure and the major relevant observations are summarized in Table 3.4.

It is noted that cracks started at the corner of the wall and spread to the middle. All observed cracks were almost horizontal. The cracks also started at the bottom of

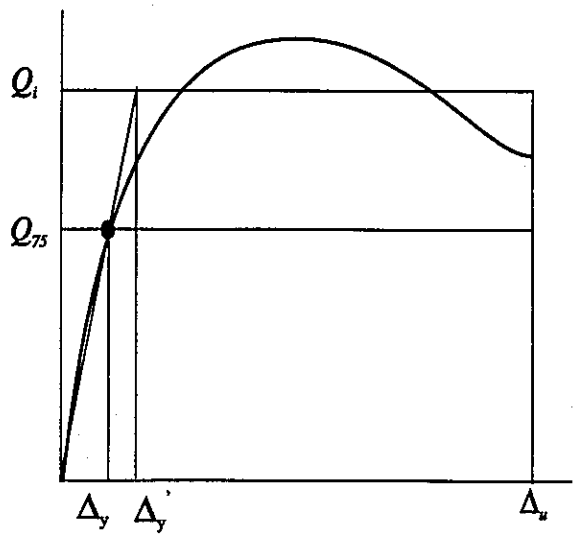

Figure 3.15: Idealized yield displacement

Wall	Sample No.					Mean
	1	2	3	4	5	
HN	5406	5650	5650	5370	5830	5581
HU	5795	5707	5371	5795	5830	5700
HP	6180	5480	5480	5300	5830	5654
LN	4947	5124	5636	5707	-	5354
LP	4947	4806	4912	4876	5300	4968
LU	4523	4876	5194	5053	-	4912

Table 3.3: Compressive strength of concrete cylinders at time of testing

Wall	H_{max} (kips)	Height of concrete spalling (inch)	Buckling length of vertical bars (inch)	Max. ductility factor
HN	58.95	30-35	25-30	4.03
HP	58.25	20-26	18-19	4.28
HU	58.50	28-29	17-18	4.00
LN	39.00	18-21	13-14	4.36
LP	40.84	15-17	9-12	6.11
LU	39.11	17-18	10-12	5.65

Table 3.4: Observations of tested walls

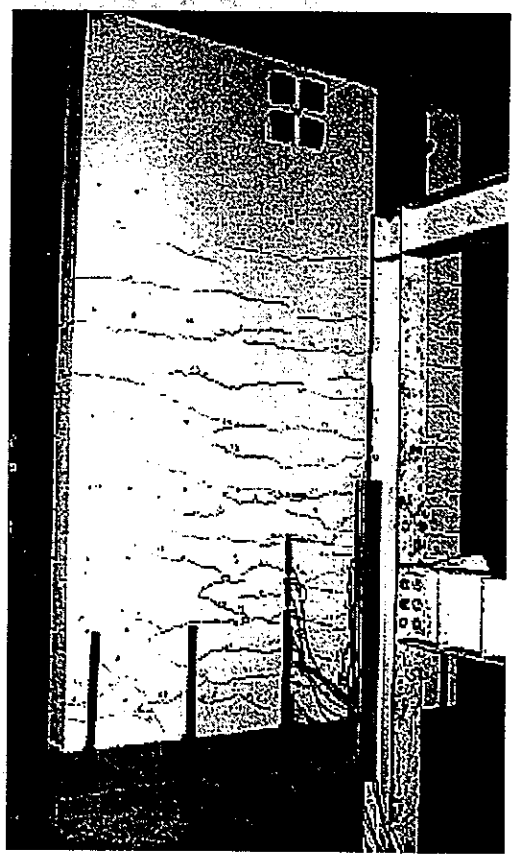

Figure 3.16: Crack distribution over wall "HN" just before failure

the wall and spread upward up to two-thirds of the wall height. Figure 3.16 shows the crack patterns of wall "HN" just before failure.

At a ductility level of nearly 3, the crack distribution became stable. At higher ductility factors, the lower cracks started to open widely. No damage was observed in the upper part of any of the tested walls. Plastic hinges of maximum length of 31 inches were observed (nearly 26% of the wall height). Figures 3.17 to 3.22 show the wall samples after failure. Low stress levels in the cross-ties at elevations higher than 25 inches were noted. End failure of the cross-ties was also noted all over the buckling length of the vertical bars as shown in Fig. 3.23. The end failure occurred through the opening of most of the 90 degree legs and some of the 135 degree legs. All walls exhibited similar failure mechanisms, however, damage in the "N" walls was relatively more severe than the "U" and "P" walls. It is noted also that the "P" walls

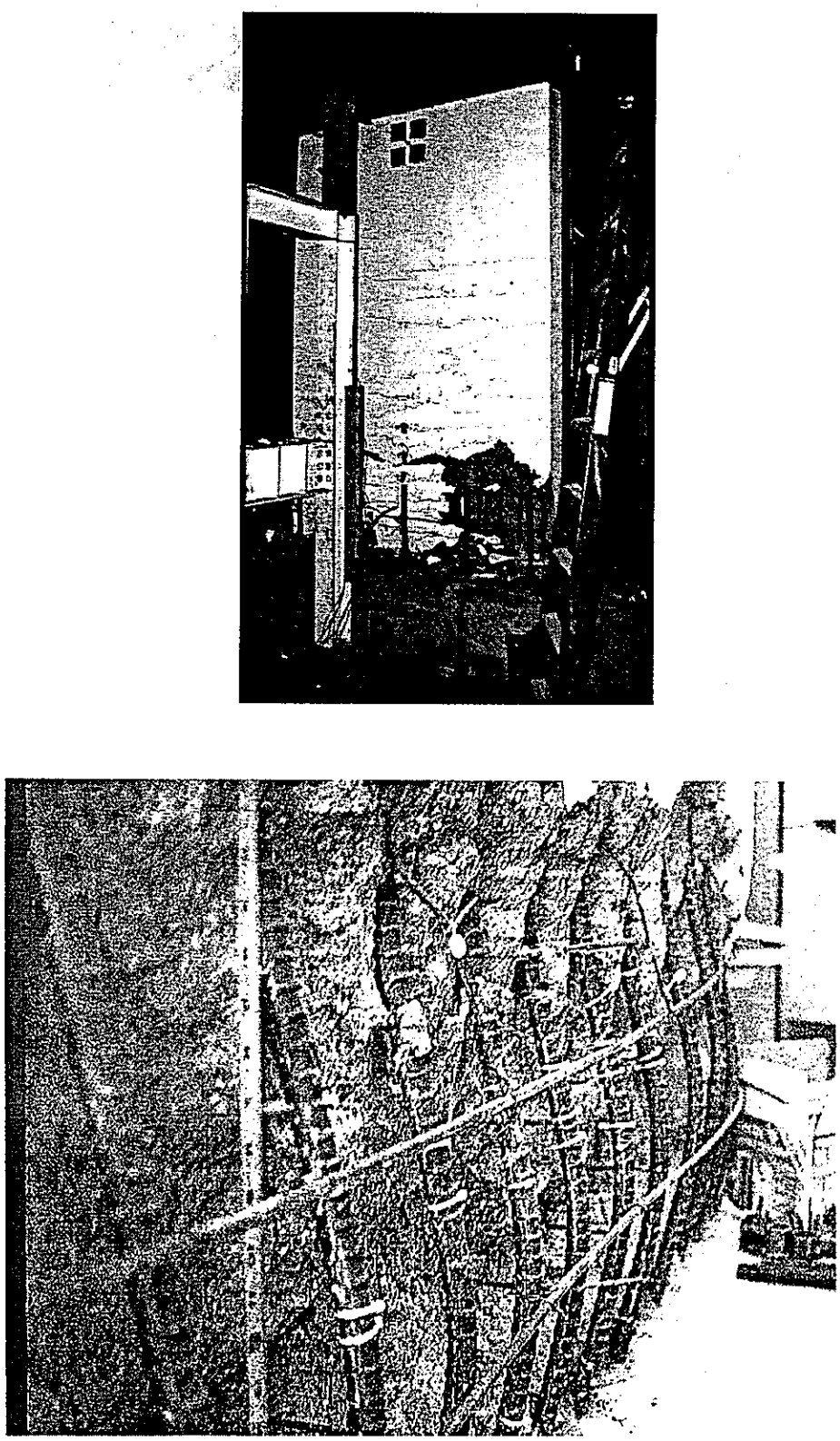

Figure 3.17: Wall "HN" after failure

Figure 3.18: Wall "HP" after failure

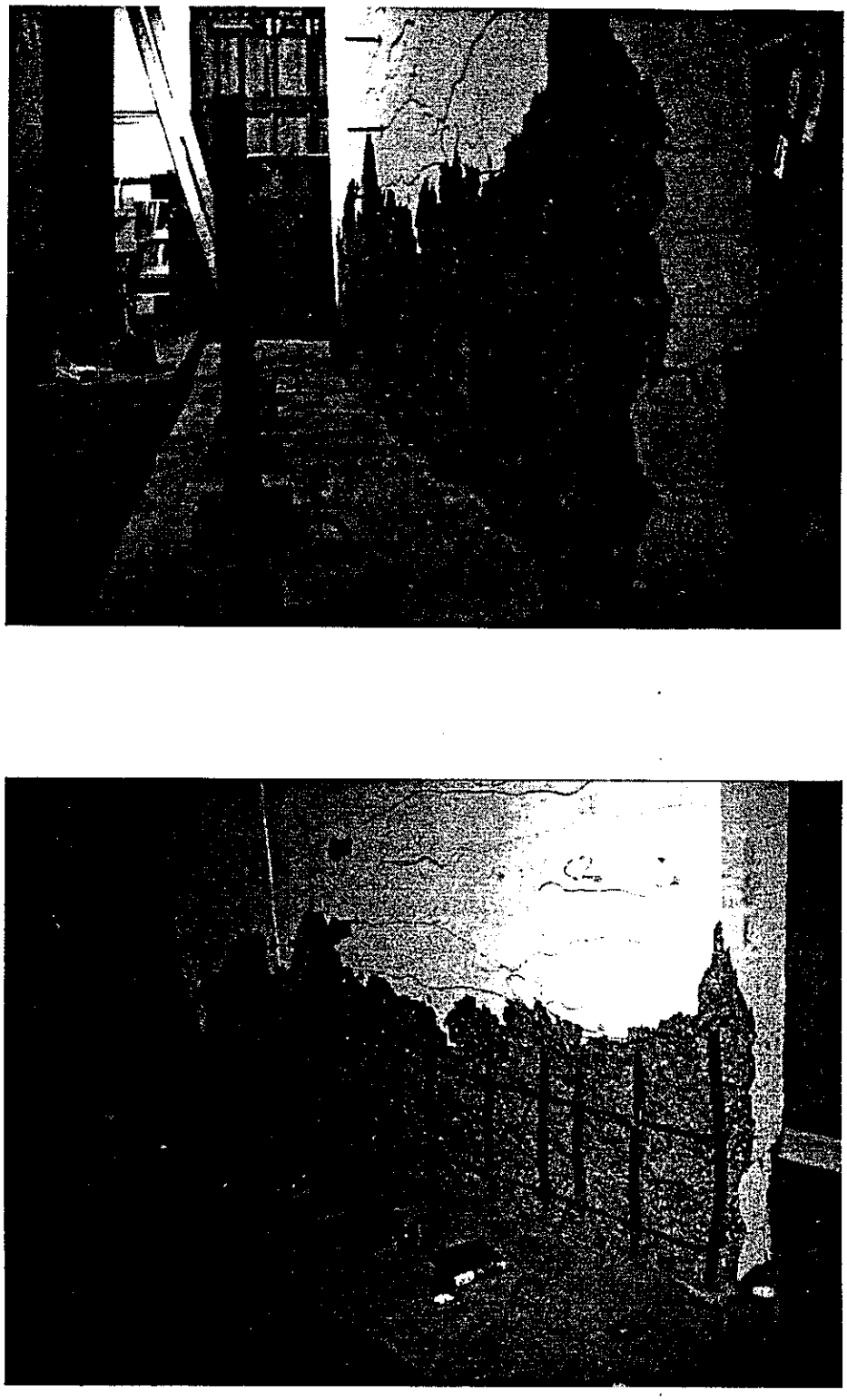

Figure 3.19: Wall "HU" after failure

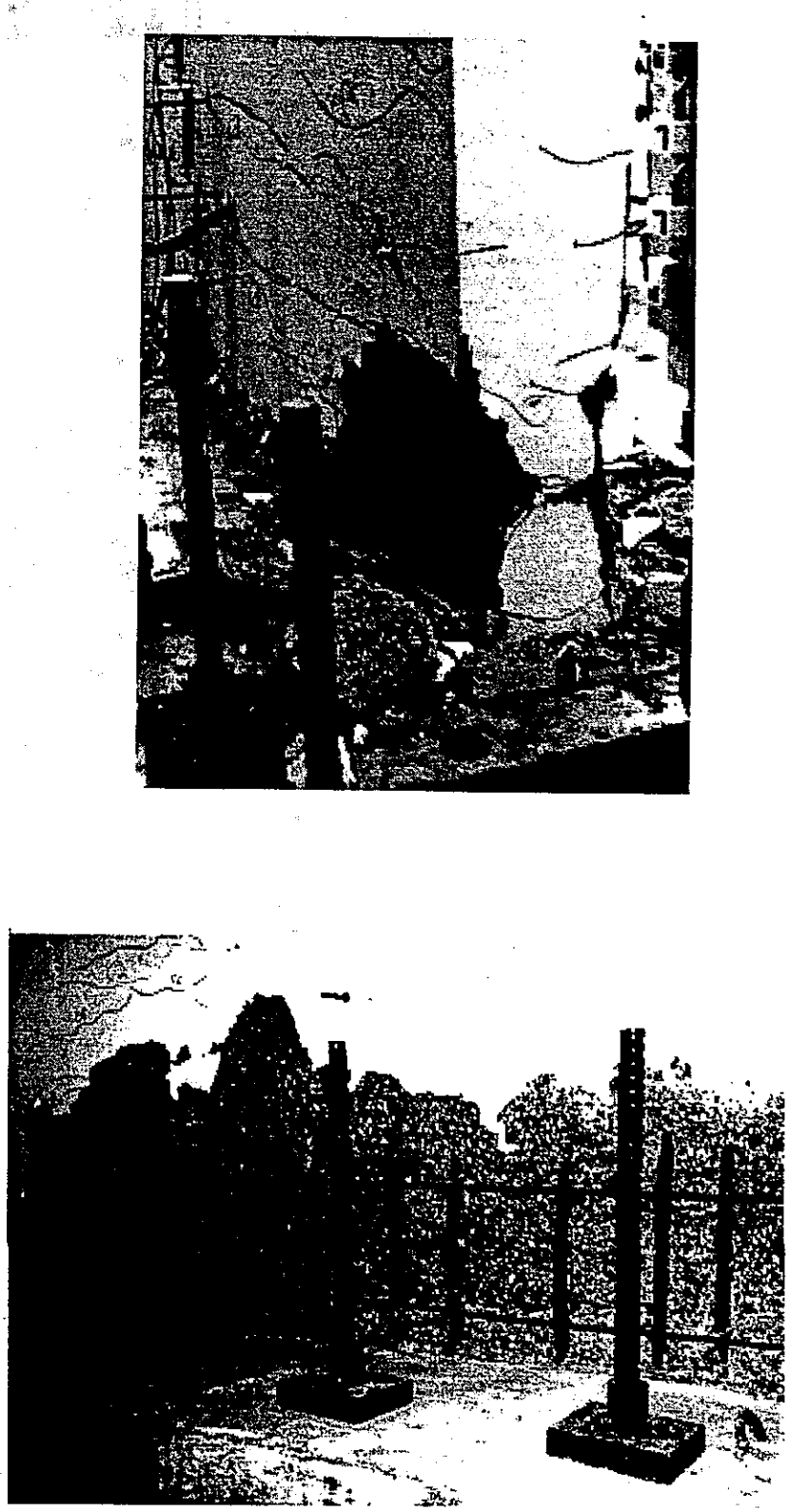

Figure 3.20: Wall "LN" after failure

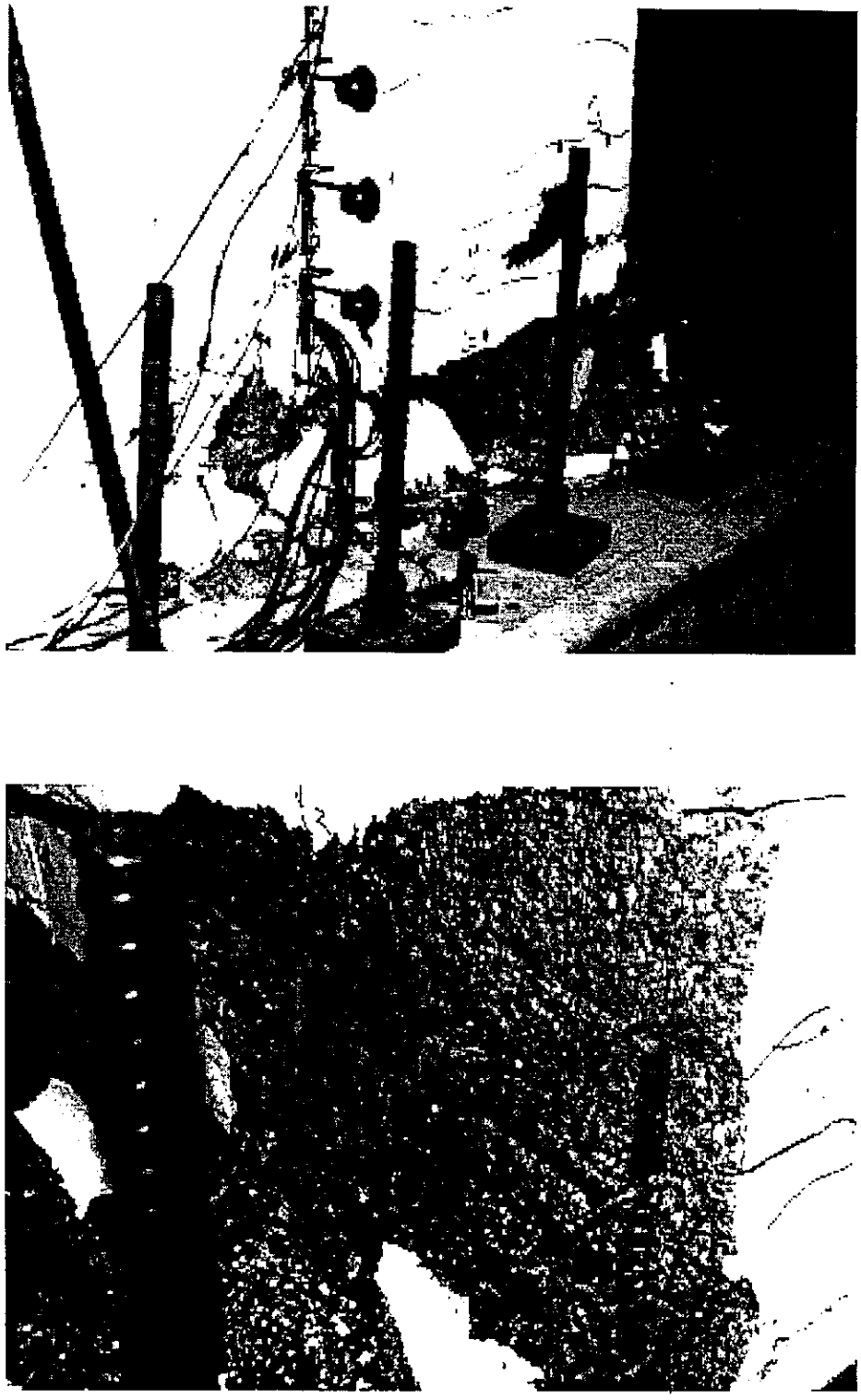

Figure 3.21: Wall "LP" after failure

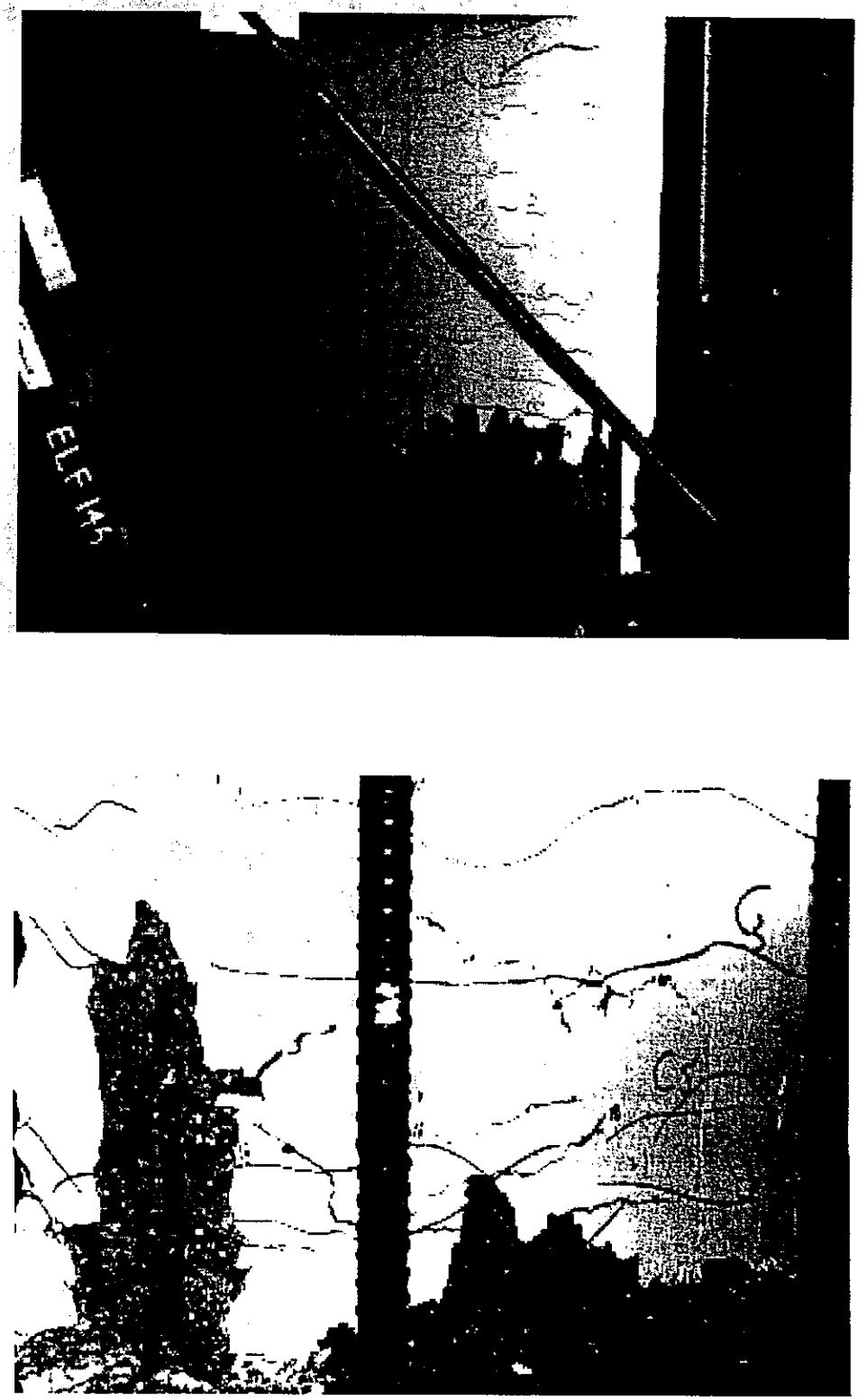

Figure 3.22: Wall "LU" after failure

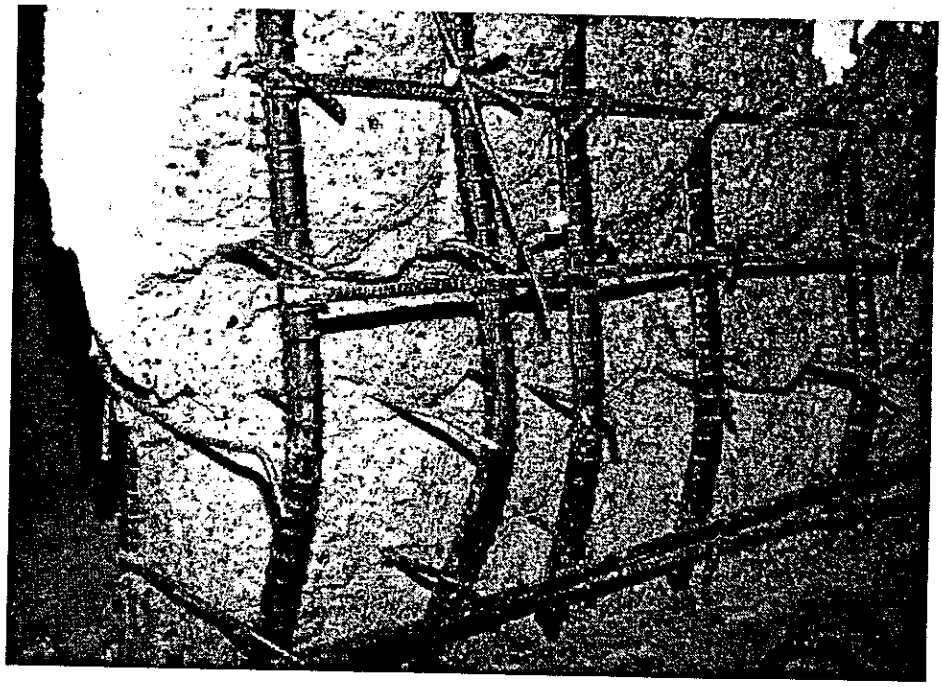

Figure 3.23: Failure of cross-ties by opening of their ends

sustained, relative to the other test specimens, the least damage and the shortest buckling lengths.

3.7 Definition of Ductility

The ductility of a structural element is generally defined as the member's ability to undergo deformations without a substantial reduction in its load resisting capacity. The ductility can be defined either by the curvature ductility factor which is the ratio of the section curvature at ultimate strength to the curvature when the tension reinforcement first reaches the yield state, or by the displacement ductility factor which is the ratio between the maximum horizontal displacement of the wall at ultimate and at first yield. Since it is difficult to pinpoint the yield state experimentally, an elasto-plastic model was proposed [20] to approximate the moment-curvature or the

load-displacement relations. The theoretical value for the yield displacement, Δ_y', is calculated from the following relation

$$\Delta_y' = \Delta_y \frac{Q_i}{Q_y} \tag{3.5}$$

where Δ_y and Q_y are the displacement and the applied load at the first yield of the vertical reinforcement and Q_i is the ideal load calculated from the moment capacity of the wall section using the ACI-89 code approach as stated before. Therefore, the displacement ductility factor is defined by

$$\mu = \frac{\Delta_u}{\Delta_y'} \tag{3.6}$$

where Δ_u is the displacement just before failure. The ultimate displacement is that displacement at which a reduction of the horizontal load by approximately 20% of the maximum horizontal load occurs.

3.8 Analysis of Test Results

The logged data of the loads, displacements and strains were filtered to eliminate any electrical noise. Different relations were constructed to evaluate and compare the ductility and strength behavior of each sample design.

3.8.1 Load-Displacement Relations

The relation between the applied horizontal load and the top horizontal displacement was plotted to form hysteresis loops for each wall. The maximum values of the applied loads in the push and pull sides were expected to be the same, however, small differences in the raw data were observed in the range of ± 4 kips. Subsequently, the load data were shifted to eliminate these differences. Figures 3.24 to 3.29 present these relations where the upper x-axis shows the displacement ductility factor. The

yield displacements, Δ_y', were calculated as described before using the envelopes of the load-displacement relations. The area enclosed within each loop represents the ability of the wall sample to absorb the seismic energy. Studying these figures shows that

- All samples exhibited good performance to absorb energy at large displacement levels.
- Except at the failure stage, reductions in the load capacity were observed to occur mainly after the first cycle at each displacement limit.
- In contrast, rapid reductions in the load capacity were observed to occur at all cycles near failure.

To compare the behavior of the wall specimens, the envelope of the hysteresis loops for each wall was plotted in Fig. 3.30. It is clear from this figure, along with other test observations, that

- The cross-ties distribution has not changed either the wall stiffness or the maximum load.
- Walls with the higher reinforcement ratio exhibited higher stiffness but lesser ductility than the walls with the lower reinforcement ratio.
- All walls with the higher reinforcement ratio failed at nearly the same ductility level regardless of the cross-ties distribution. On the other hand, cross-ties improved the ductility in the "LP" and "LU" walls by nearly 40% and 30%, respectively.
- A minimum ductility factor of 4.0 was achieved for all walls.

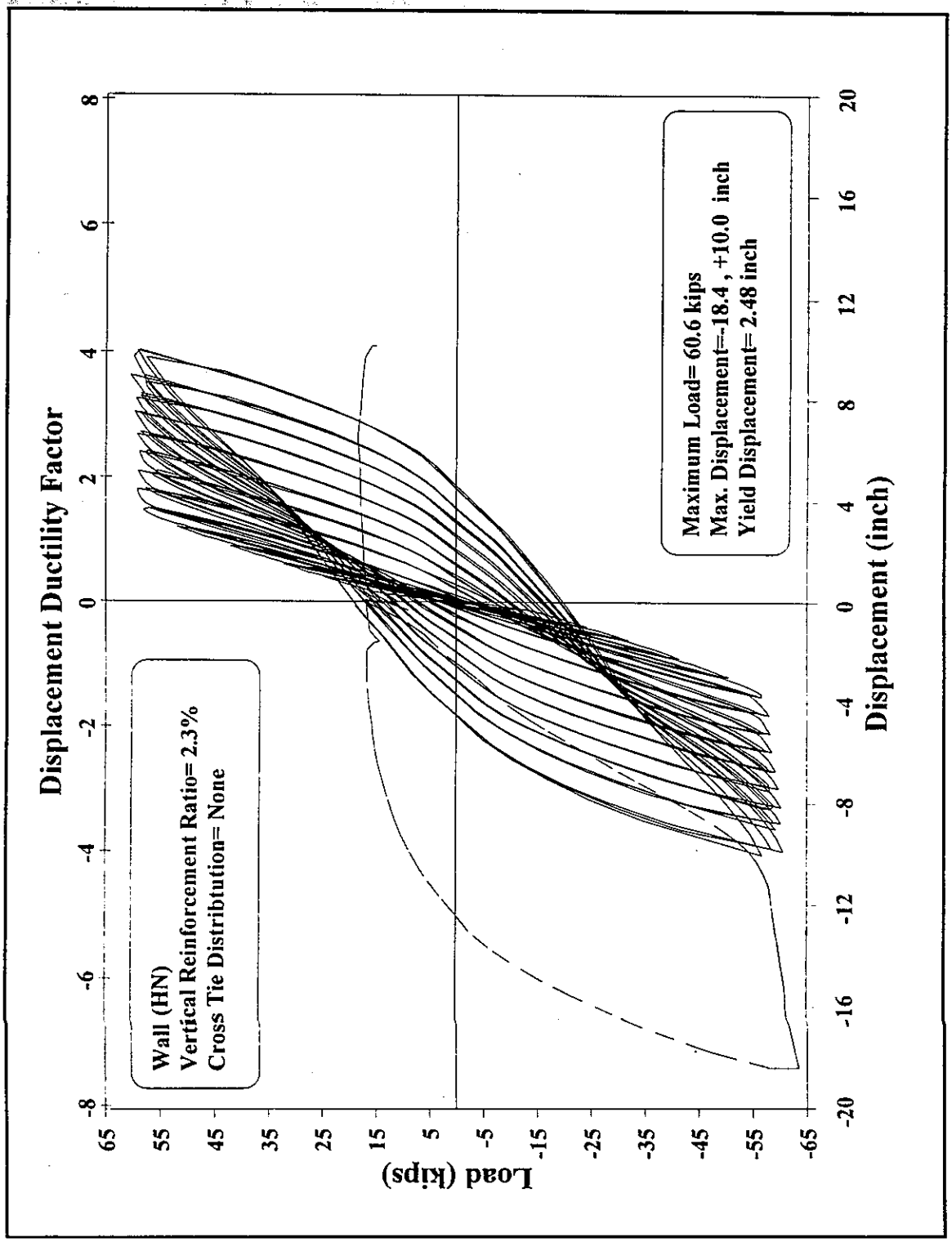

Figure 3.24: Hysteresis loops for load-displacement of wall "HN"

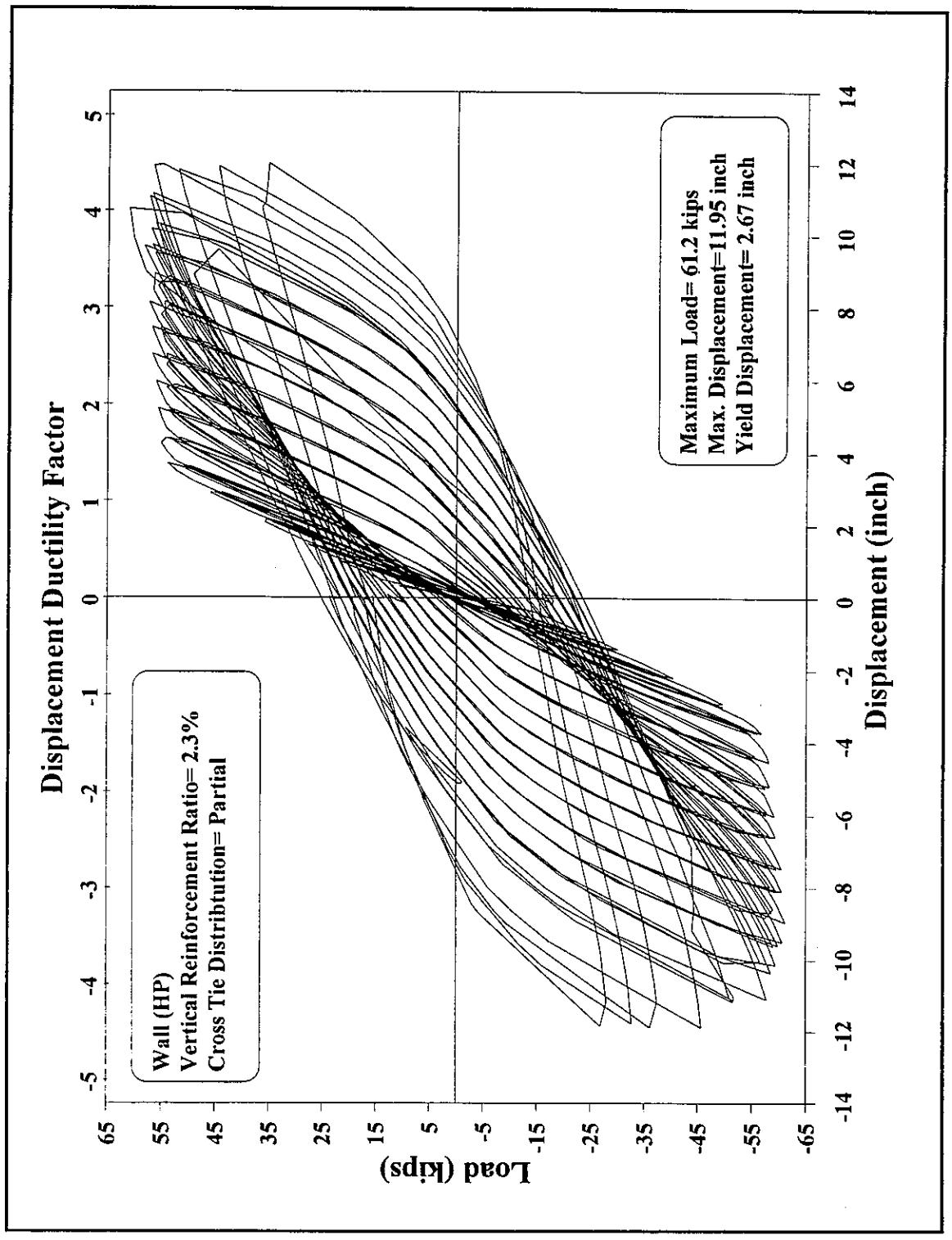

Figure 3.25: Hysteresis loops for load-displacement of wall "HP"

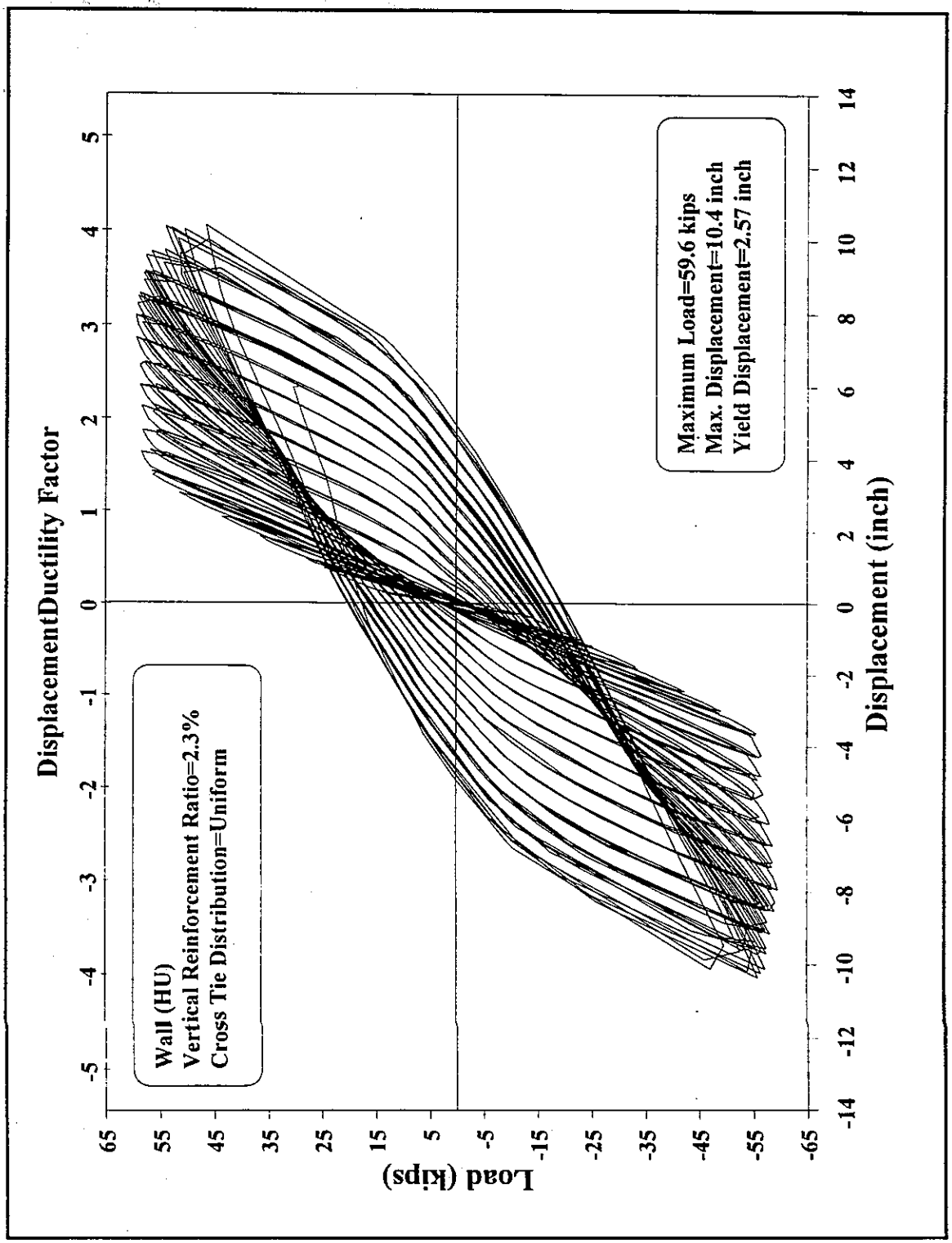

Figure 3.26: Hysteresis loops for load-displacement of wall "HU"

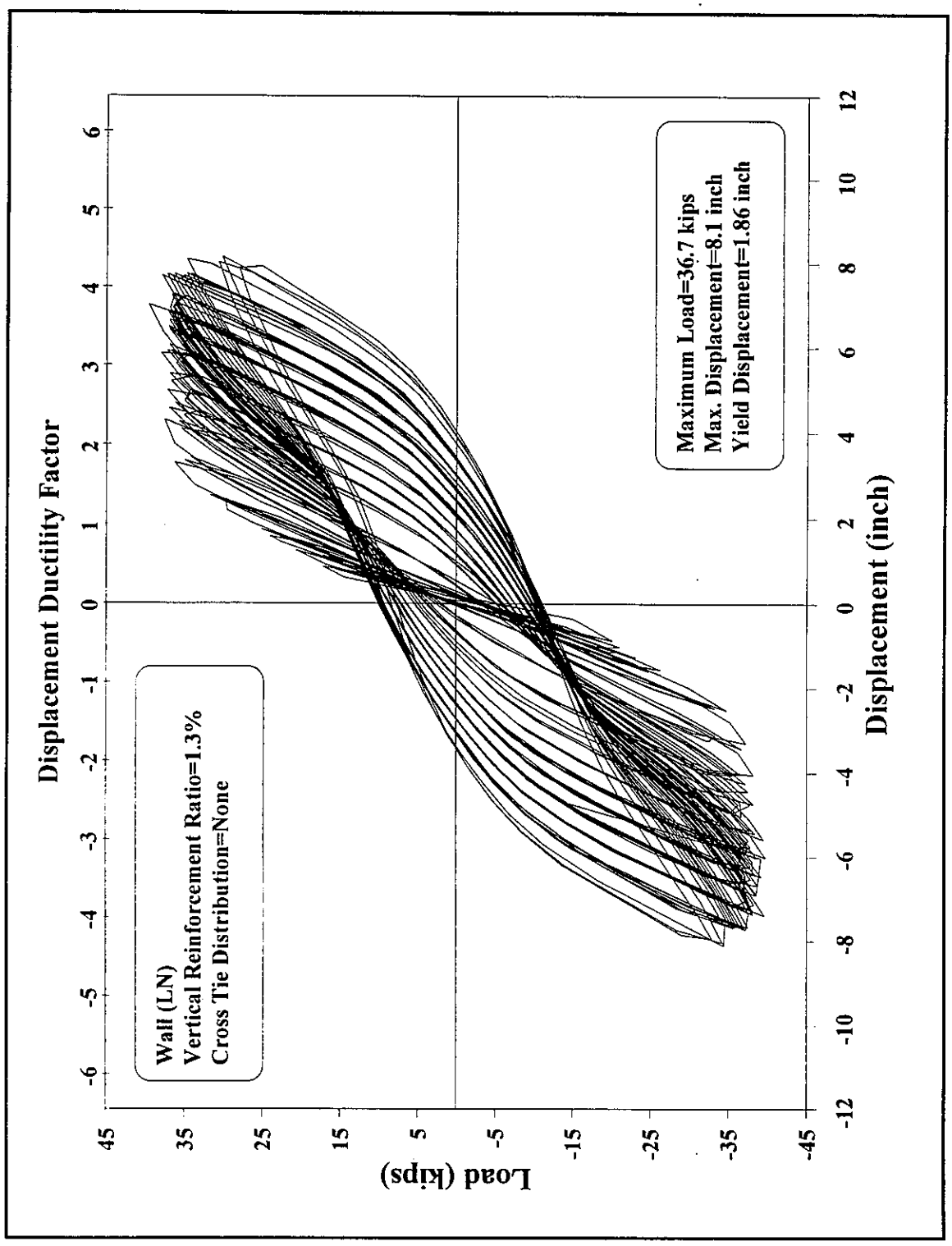

Figure 3.27: Hysteresis loops for load-displacement of wall "LN"

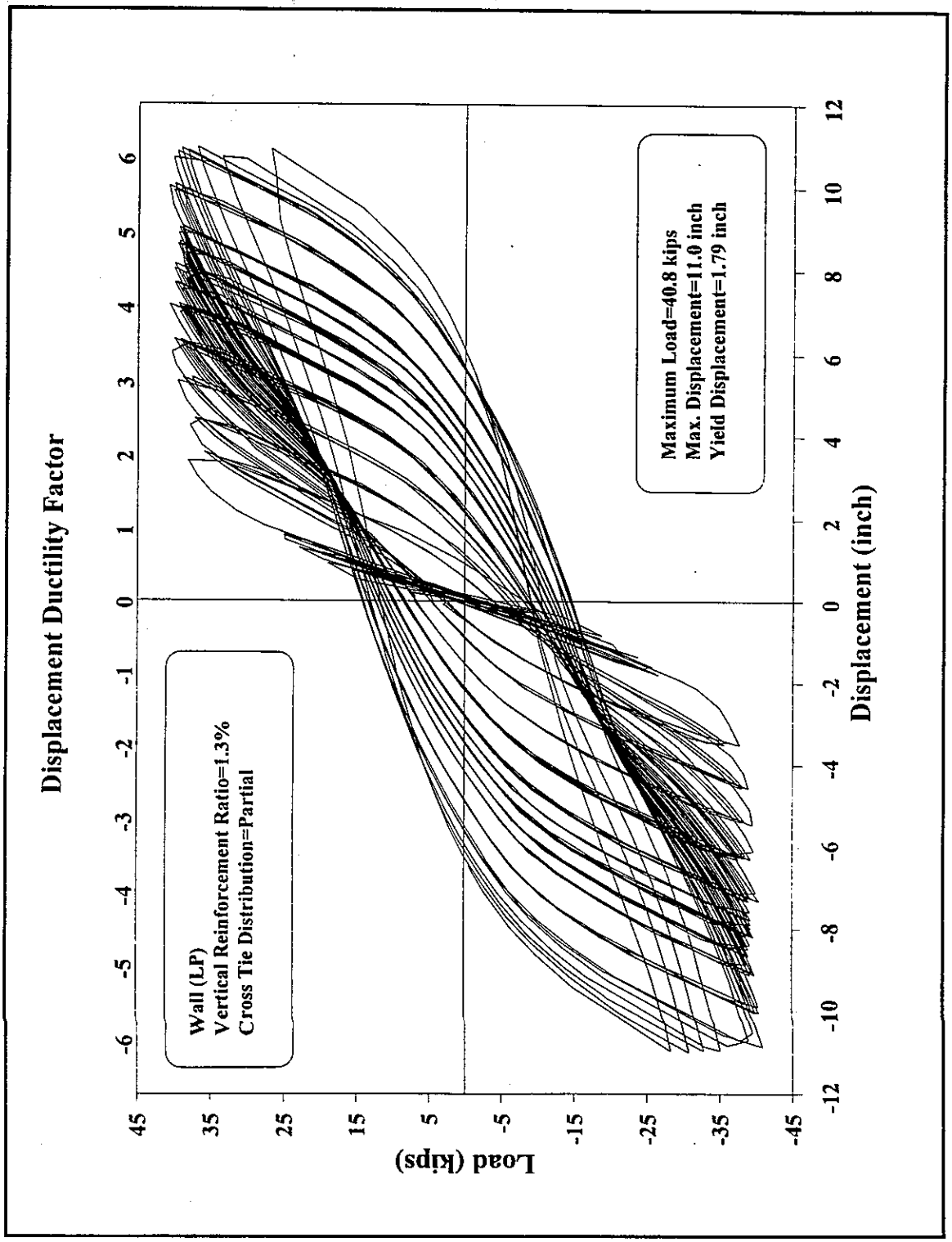

Figure 3.28: Hysteresis loops for load-displacement of wall "LP"

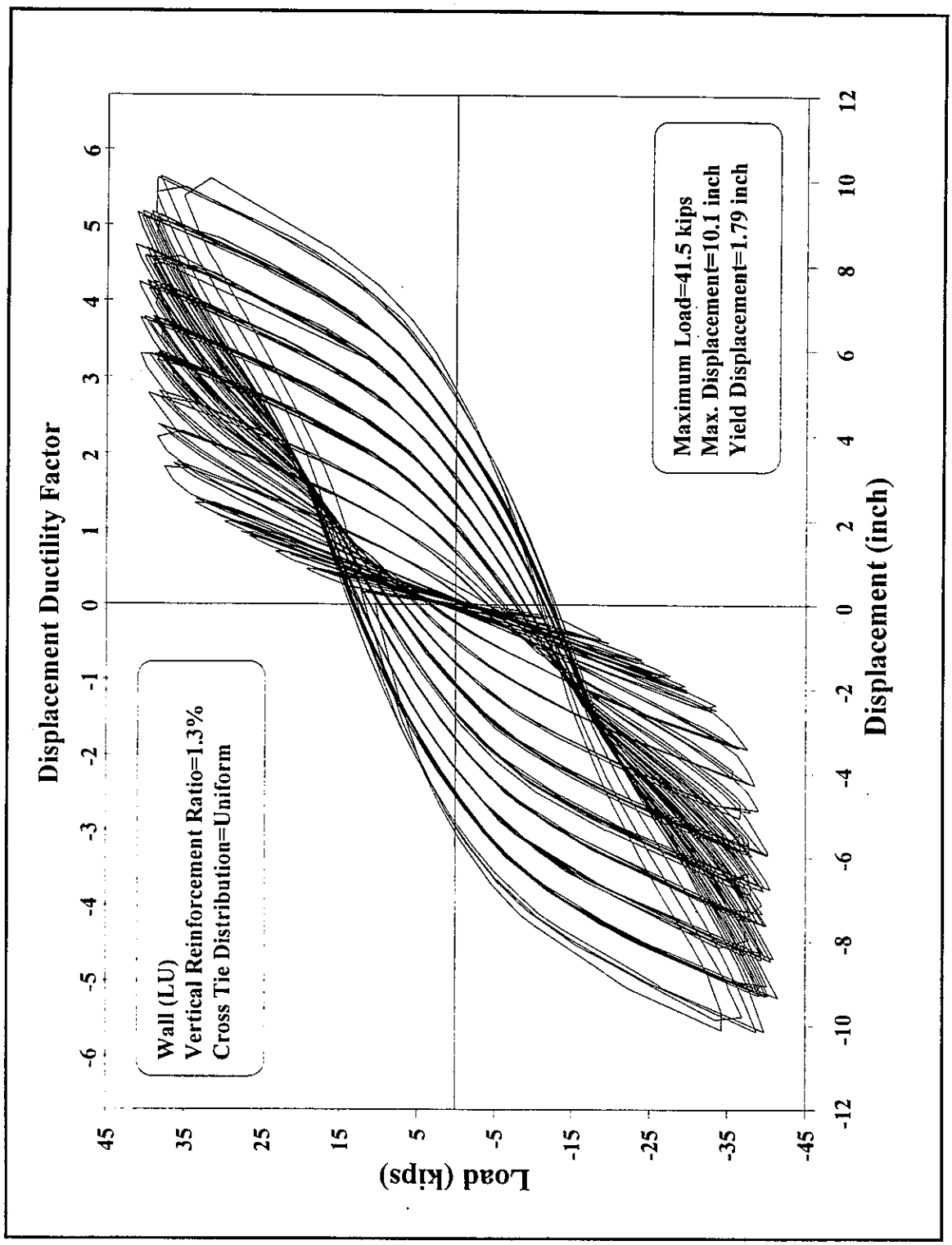

Figure 3.29: Hysteresis loops for load-displacement of wall "LU"

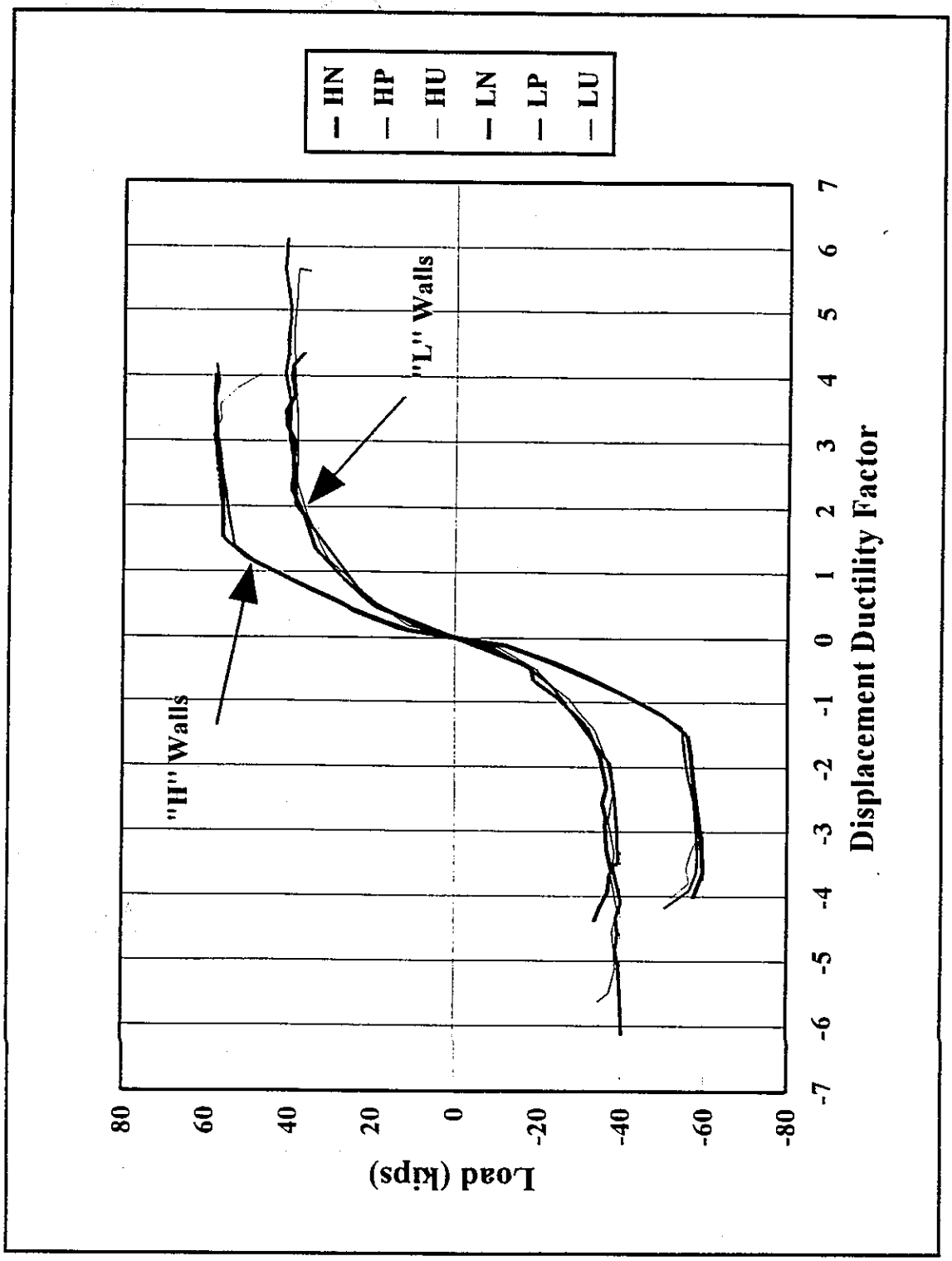

Figure 3.30: Envelope of hysteresis loops

3.8.2 Deformed Shape

Data from string potentiometers were used to determine the wall displacement at different elevations. Linear interpolation was used to estimate the deflected shape of the wall samples. Figures 3.31 to 3.36 display the deflected shapes of the wall samples at different displacement ductility factors. It is observed from these figures that no movement at the wall base had occurred and that the samples deflected as flexural members.

3.8.3 Curvature Distribution

Six levels in the bottom one-third of the wall were instrumented by a total of twelve linear potentiometers to measure the average curvature of the walls at these elevations. Figure 3.37 shows a strip of the wall sample with two potentiometers attached to its left and right sides. From that figure the average curvature, ϕ, of a strip is calculated as

$$\phi = \frac{\Delta_R - \Delta_L}{l_v \, l_h} \tag{3.7}$$

where Δ_R and Δ_L are the displacements of the right and left potentiometers, respectively.

The curvature distribution over the wall height was estimated by connecting the curvature at these levels. Zero curvature was assumed at the loading point. Figures 3.38 through 3.43 display the curvature distribution for all samples at different values of the displacement ductility factors. It is apparent from these figures that the curvature values remained low in the horizontal strips at the highest positions and that these values increased nonlinearly at the lower strips.

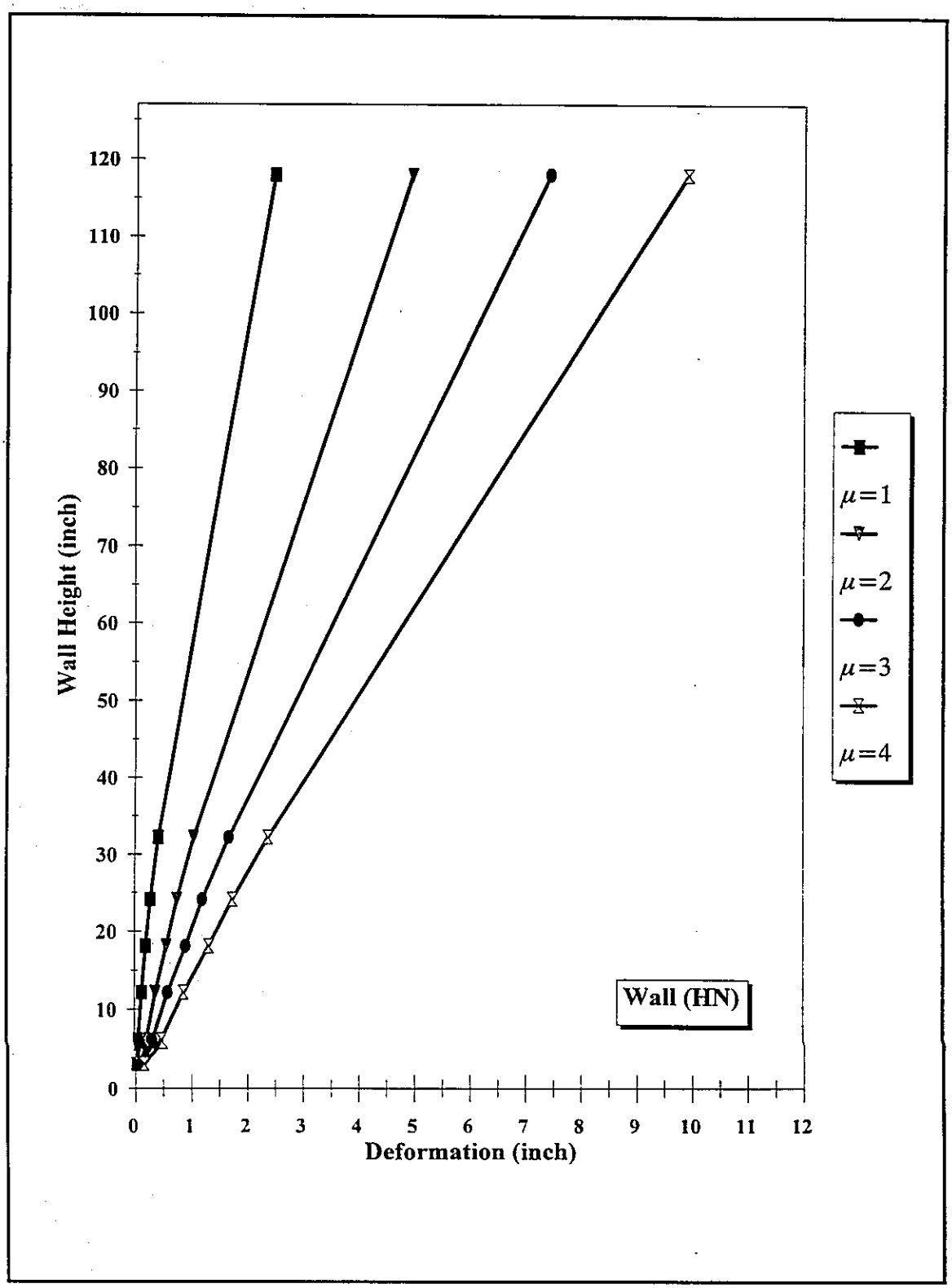

Figure 3.31: Deformed shape of wall "HN"

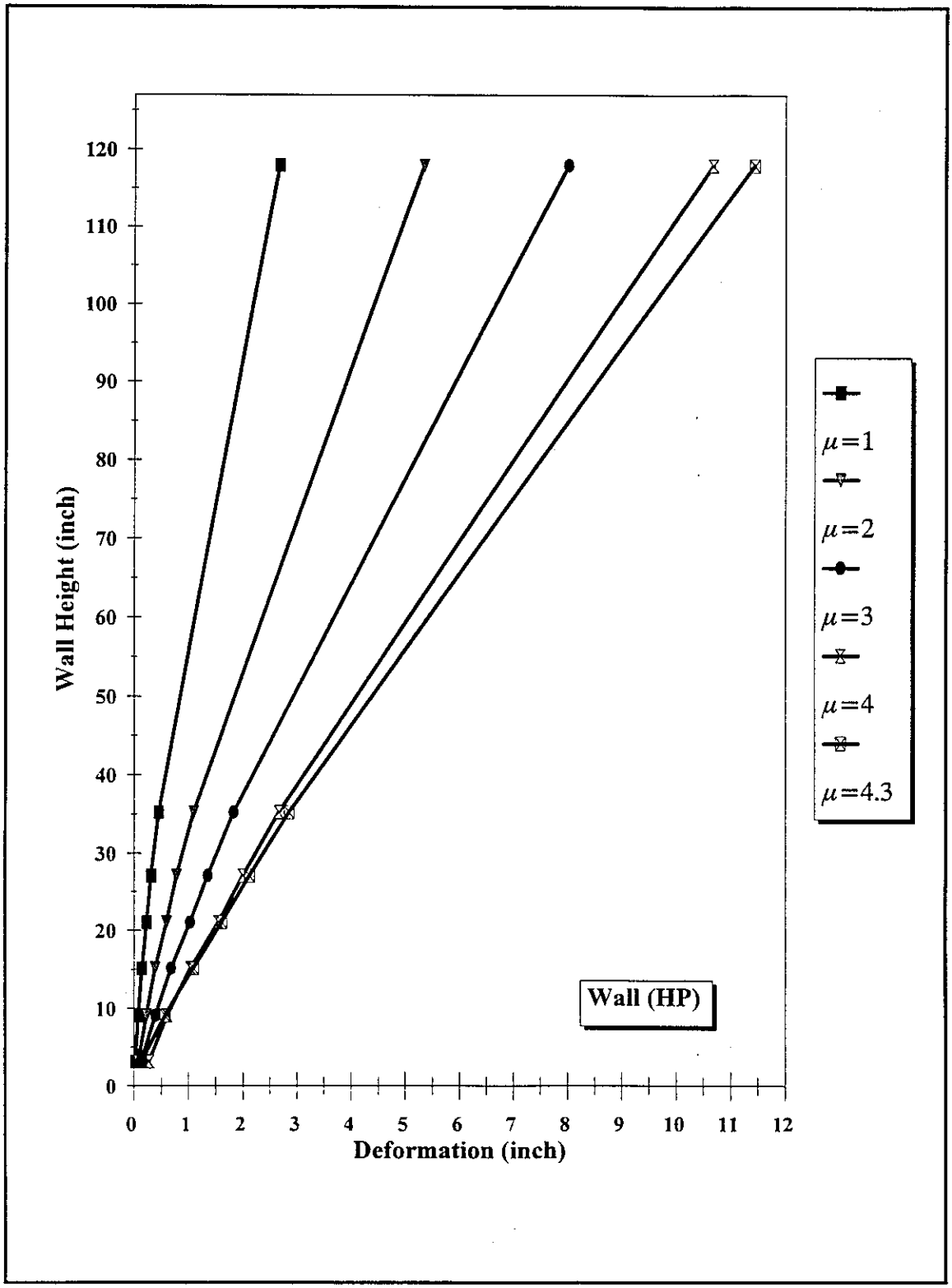

Figure 3.32: Deformed shape of wall "HP"

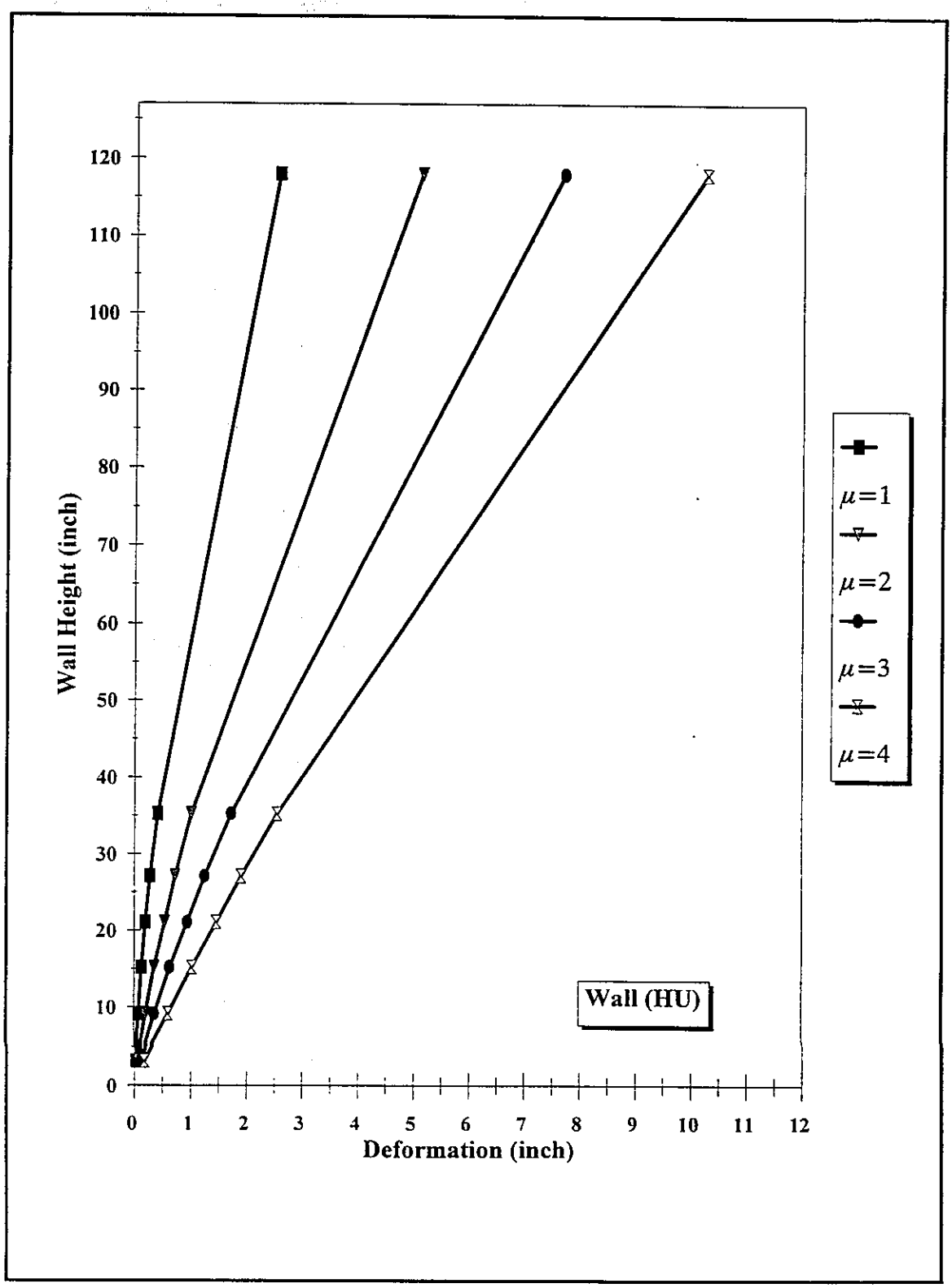

Figure 3.33: Deformed shape of wall "HU"

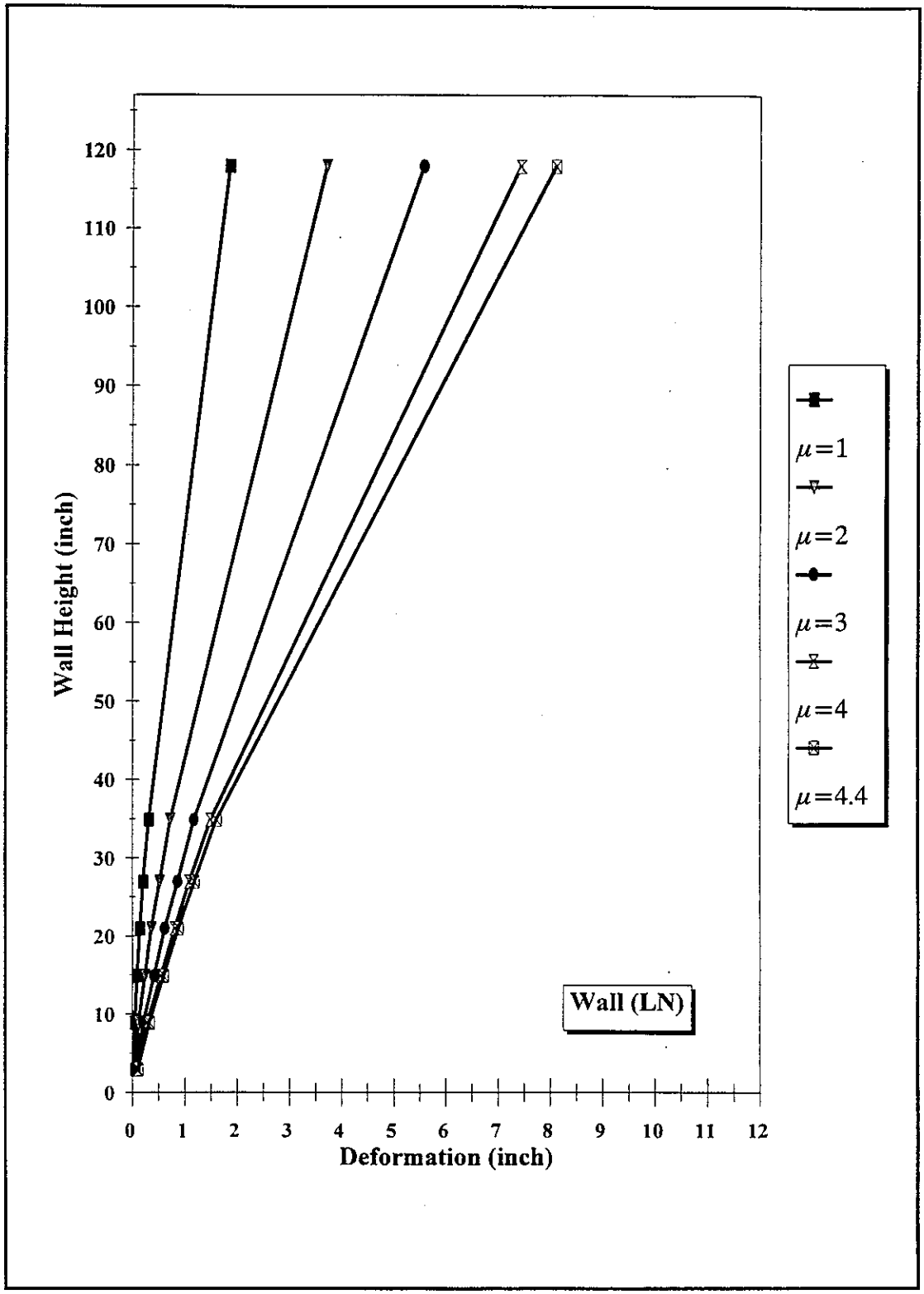

Figure 3.34: Deformed shape of wall "LN"

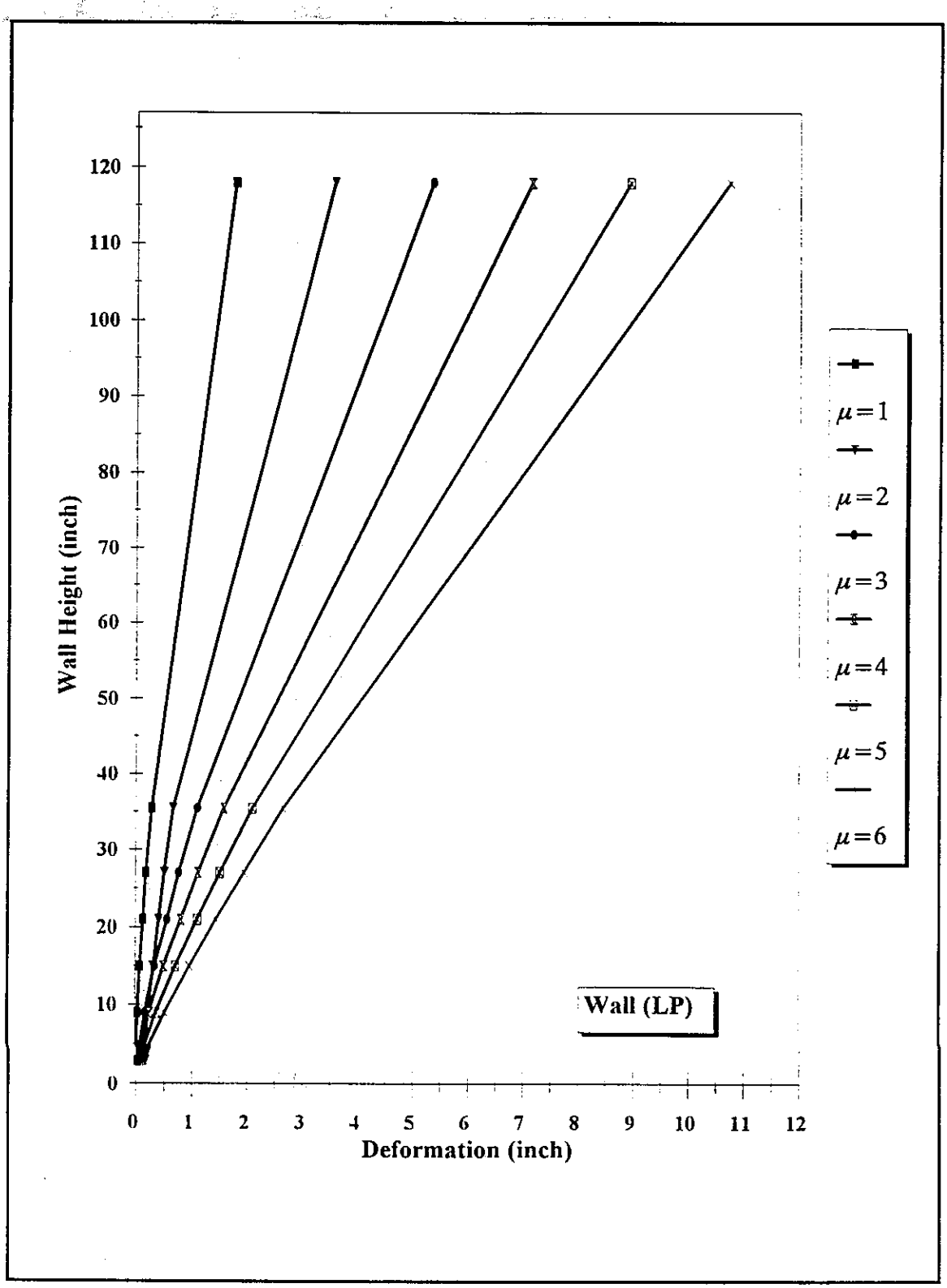

Figure 3.35: Deformed shape of wall "LP"

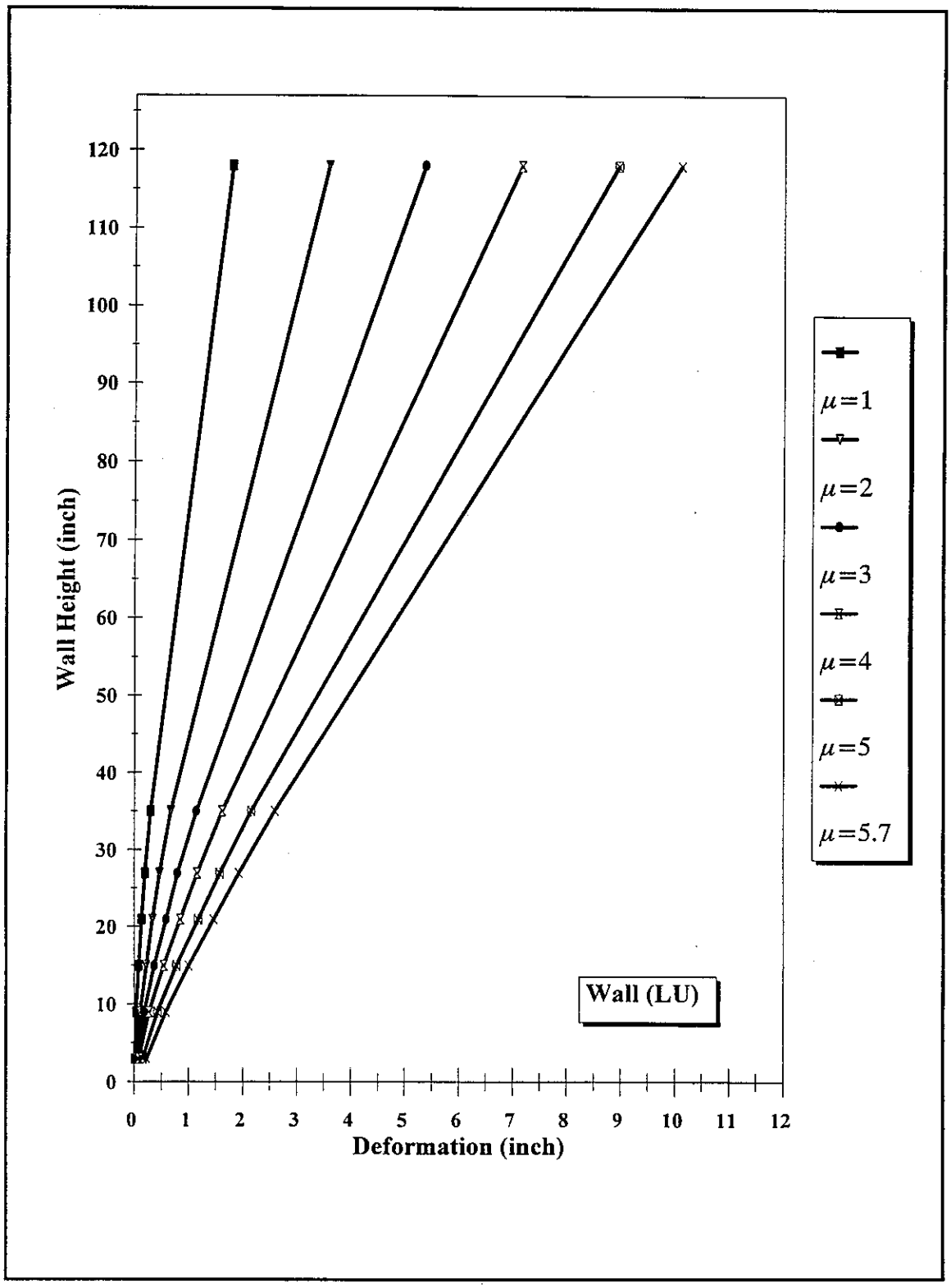

Figure 3.36: Deformed shape of wall "LU"

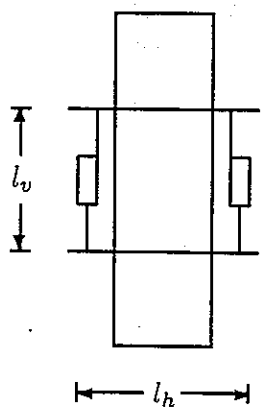

Figure 3.37: Parameters used to calculate the curvature

3.8.4 Strains in Cross-Ties

The strains in the cross-ties are averaged for each elevation and presented in Figs. 3.44 to 3.51. These figures are set to study the effect of the vertical reinforcement ratio on the amount of the strains in the cross-ties at different ductility levels. Examining these figures, one notes that the first row of the cross-ties in the "P" walls had low strain values and that the cross-ties in the wall with the higher reinforcement ratio "HP" had significantly larger strains than the "LP" wall. Figures 3.48 to 3.51 showed that the cross-ties at the higher elevations of the "U" walls experienced very low stress even at late stage of testing. One thus concludes that the use of cross-ties at the upper part of the wall is of little value. The failure mechanism of the cross-ties through the opening of their ends emphasizes the need to change current fabrication details.

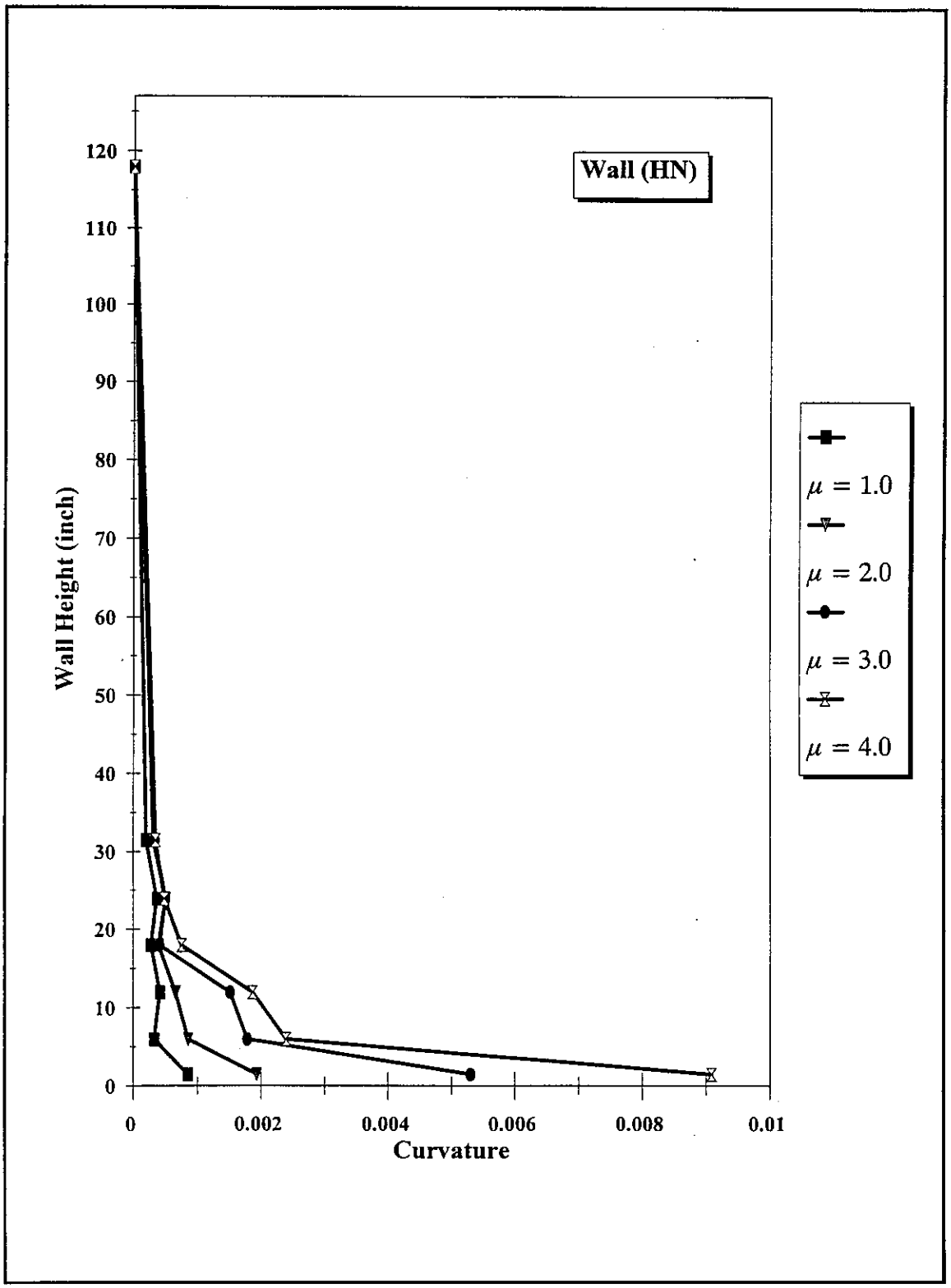

Figure 3.38: Curvature distribution of wall "HN"

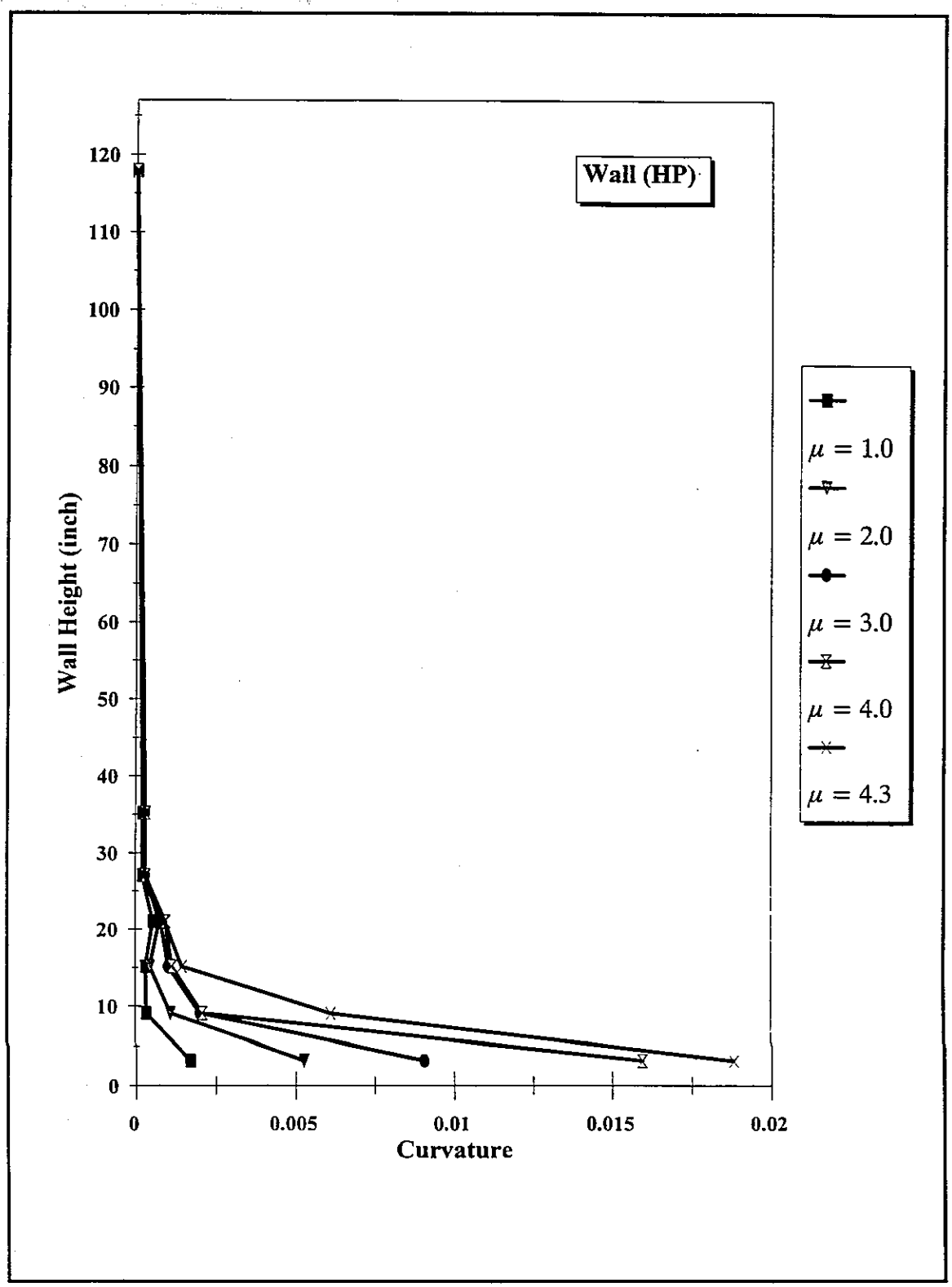

Figure 3.39: Curvature distribution of wall "HP"

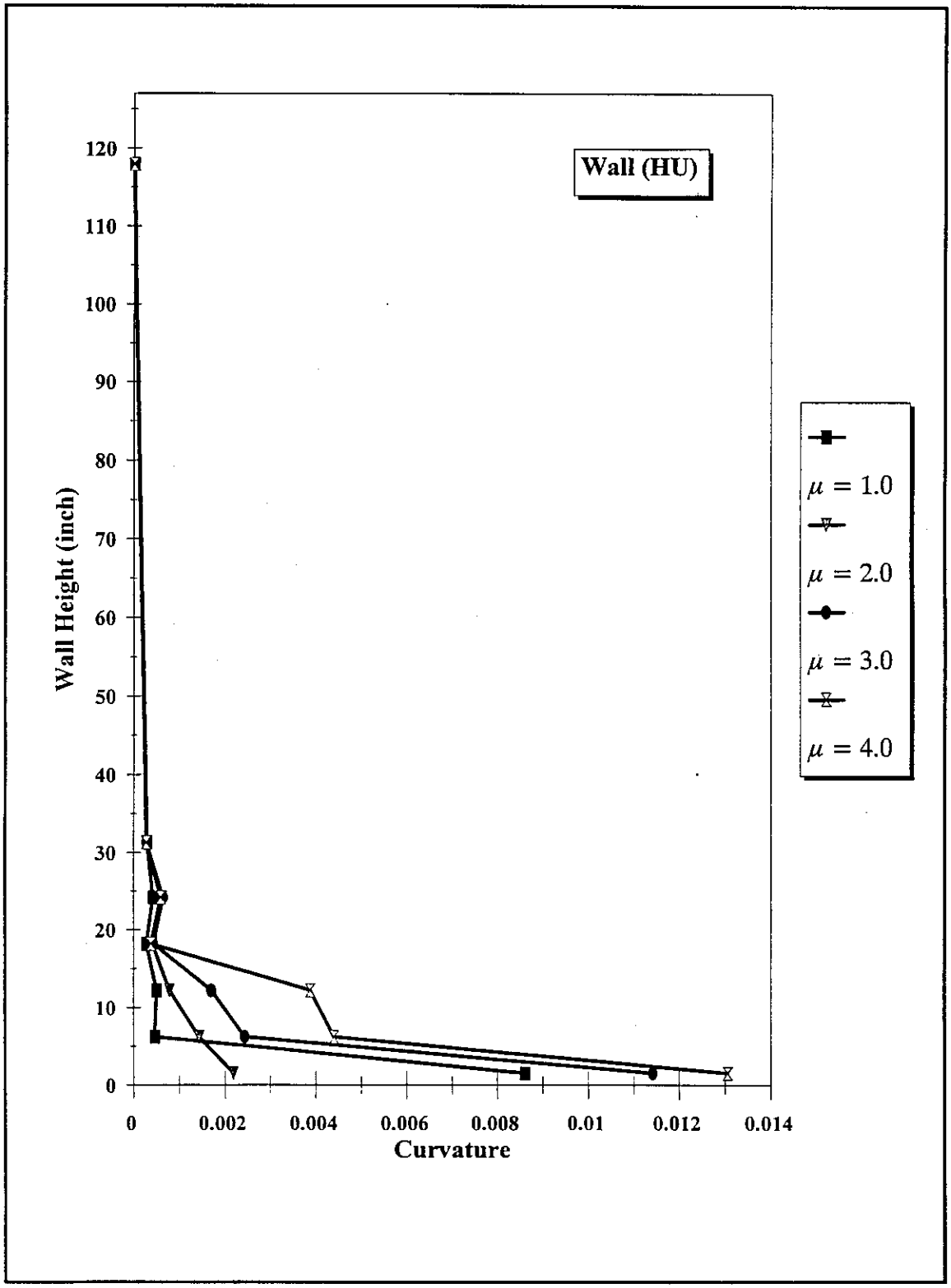

Figure 3.40: Curvature distribution of wall "HU"

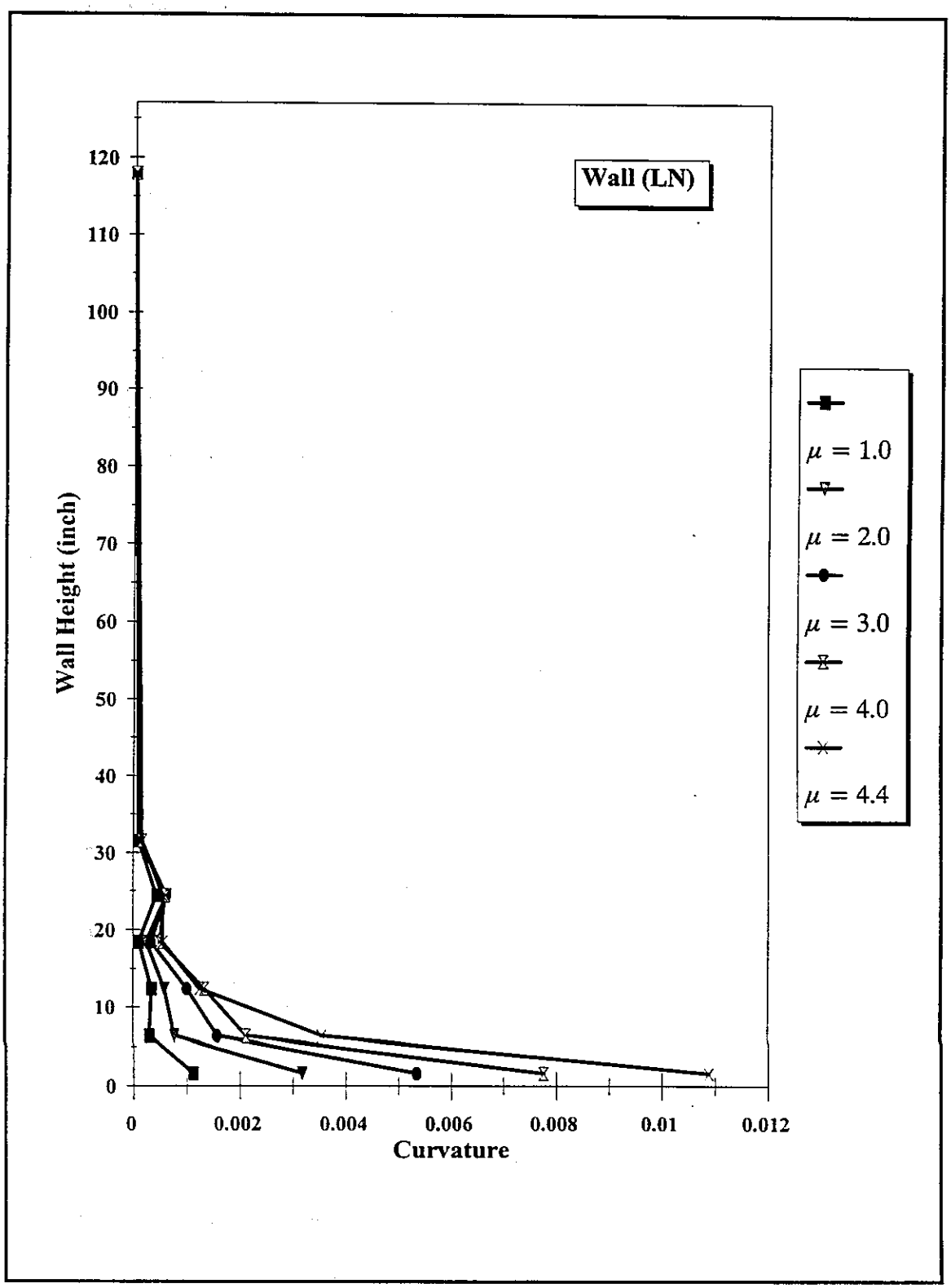

Figure 3.41: Curvature distribution of wall "LN"

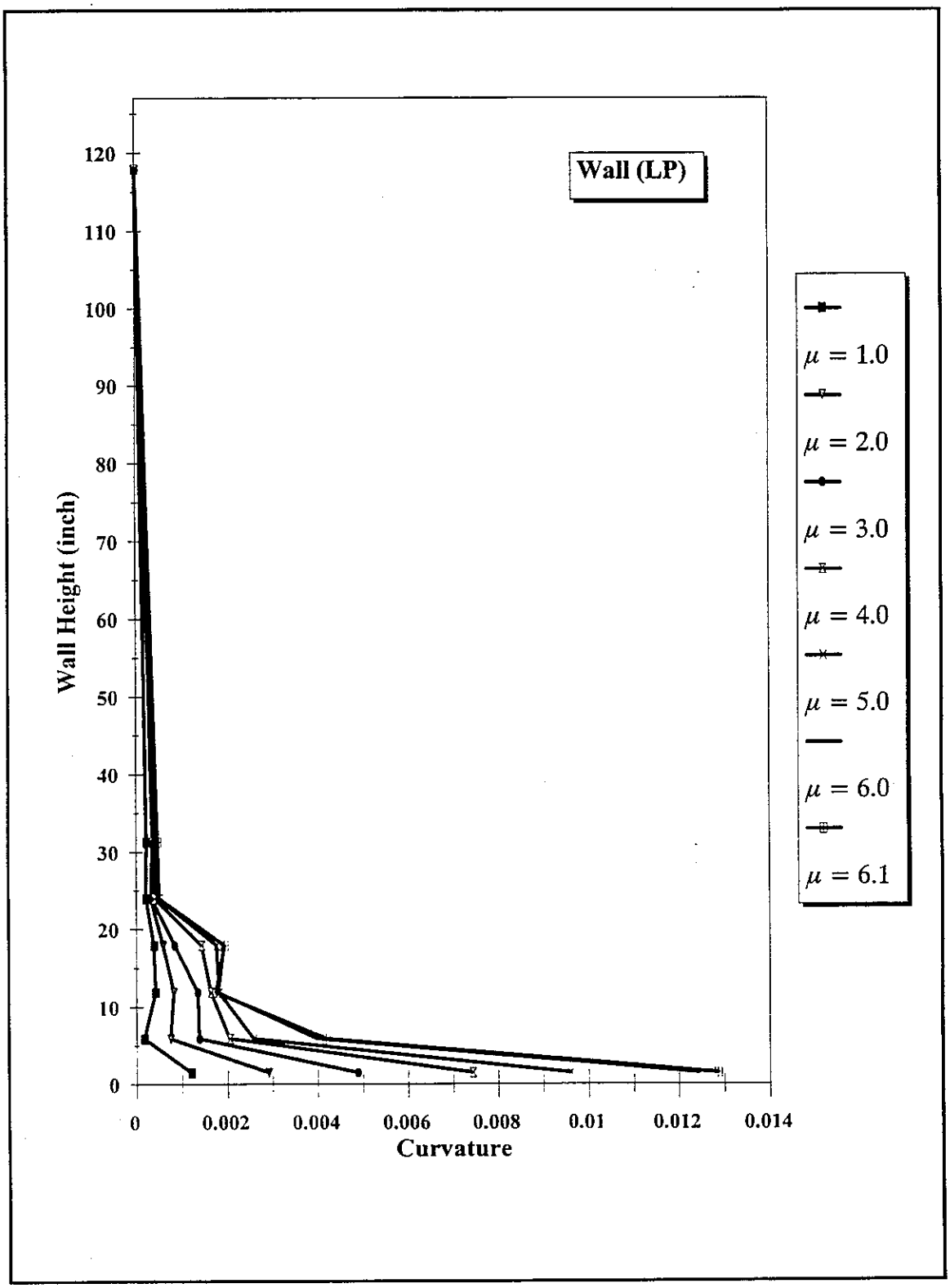

Figure 3.42: Curvature distribution of wall "LP"

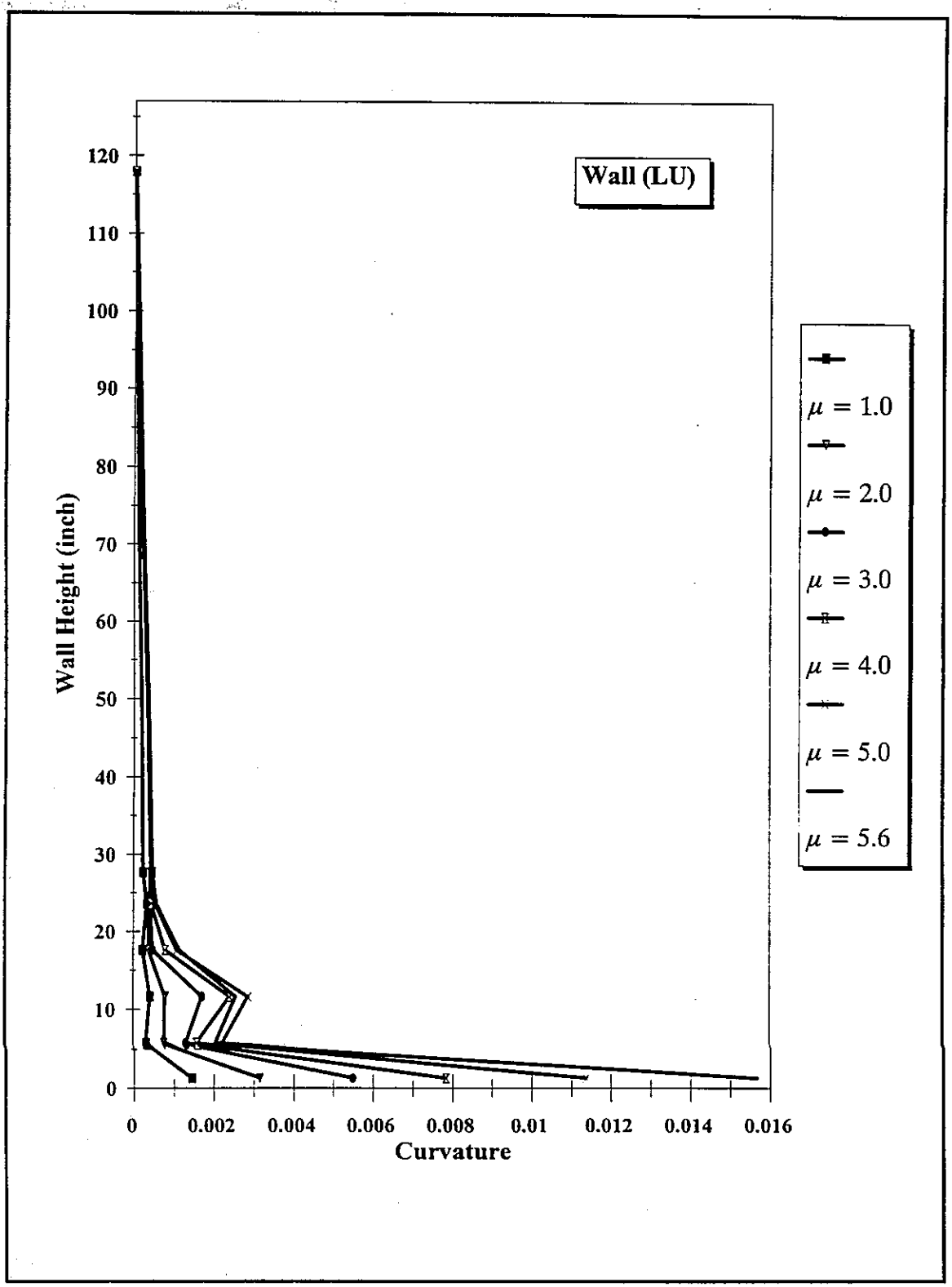

Figure 3.43: Curvature distribution of wall "LU"

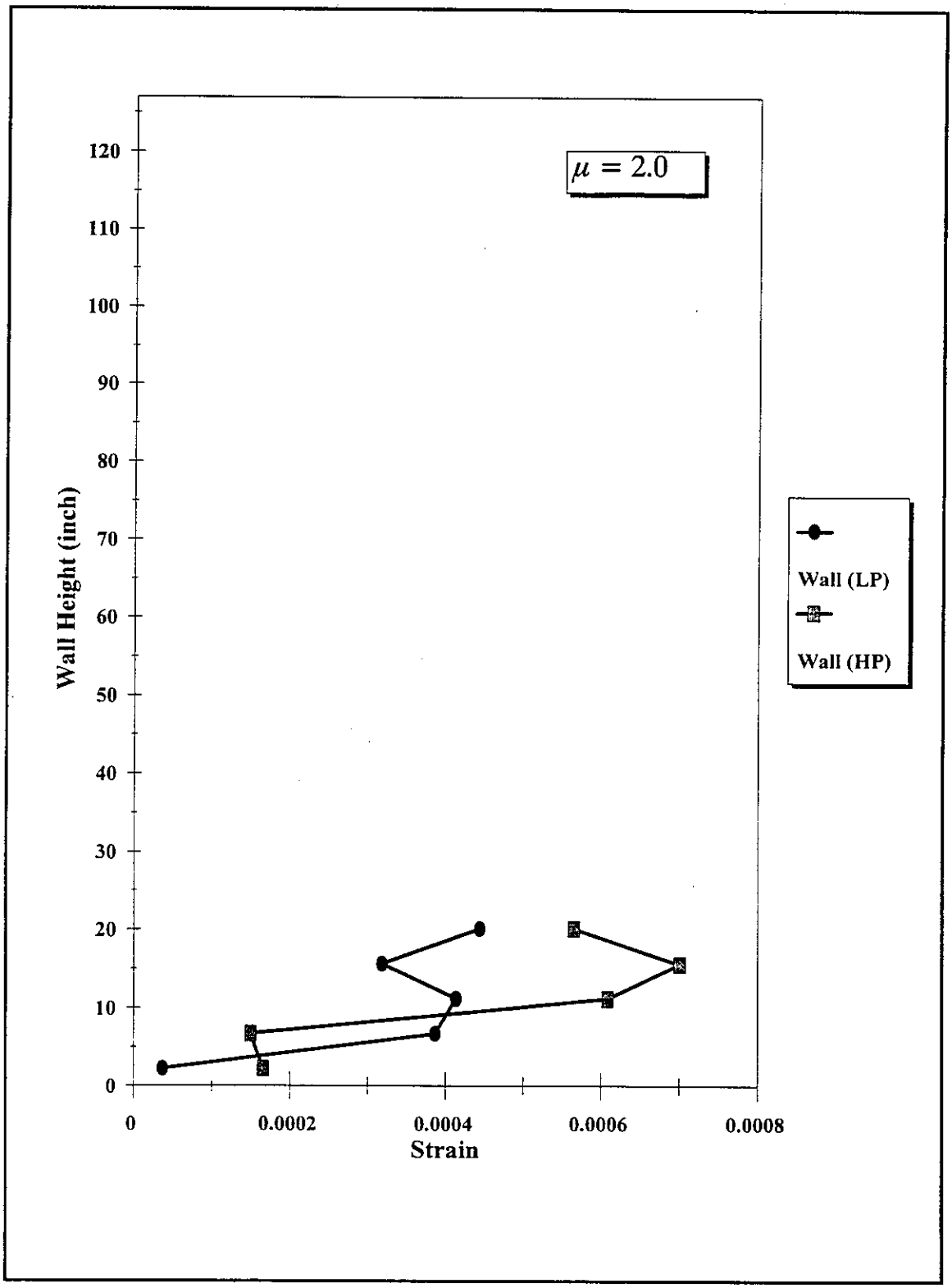

Figure 3.44: Distribution of strain in cross-ties over the height of the "P" walls at $\mu = 2.0$

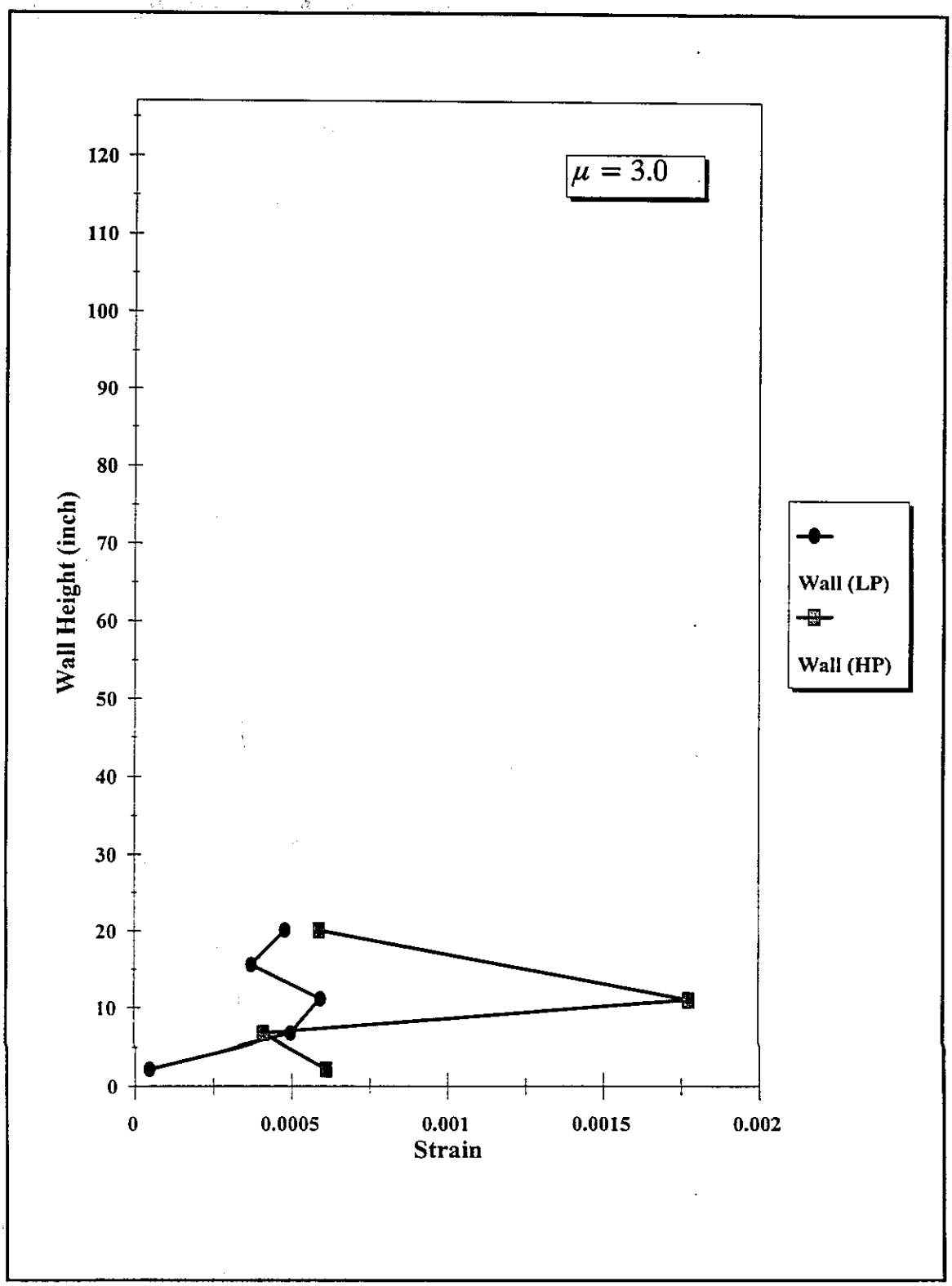

Figure 3.45: Distribution of strain in cross-ties over the height of the "P" walls at $\mu = 3.0$

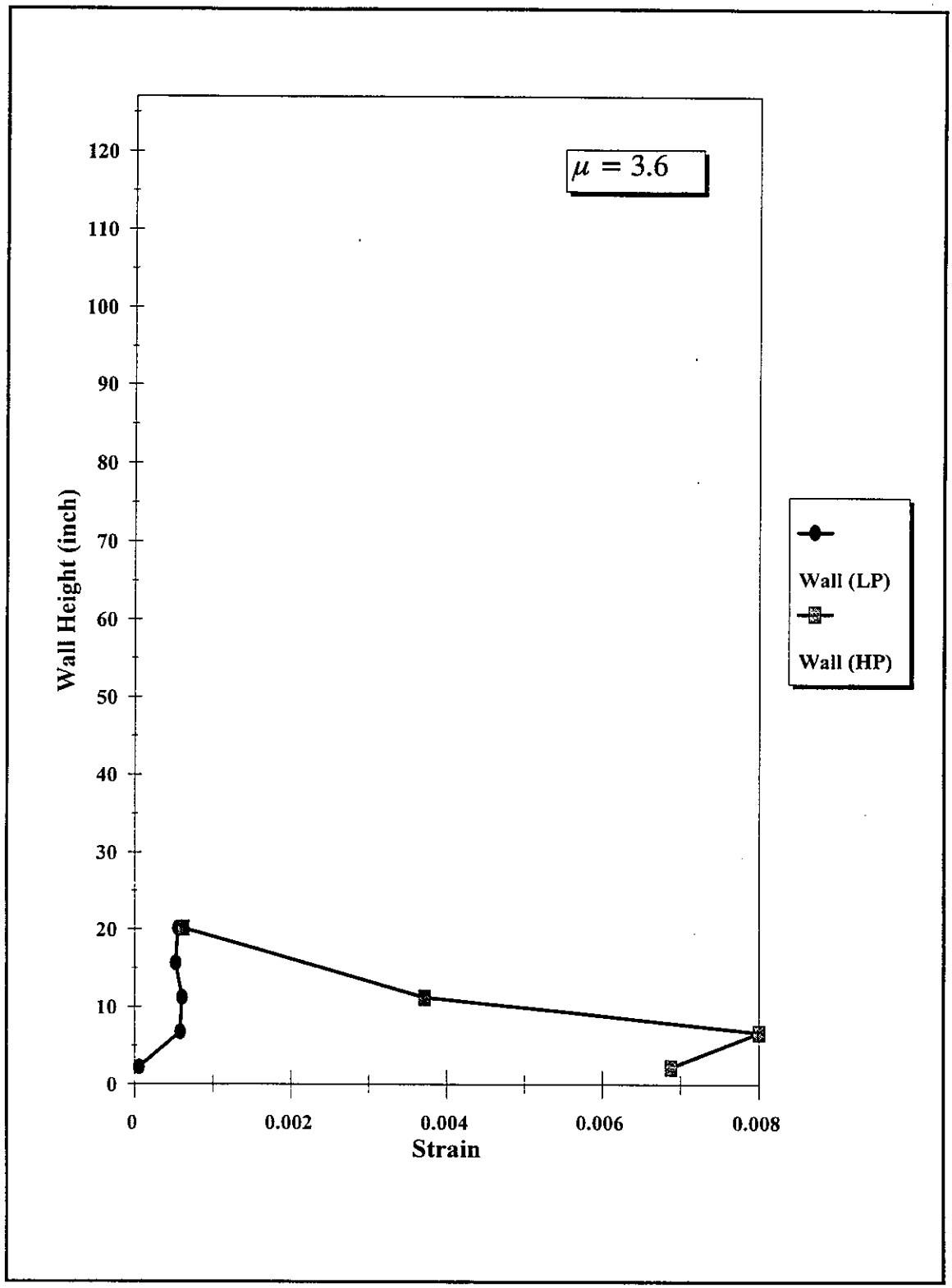

Figure 3.46: Distribution of strain in cross-ties over the height of the "P" walls at $\mu = 3.6$

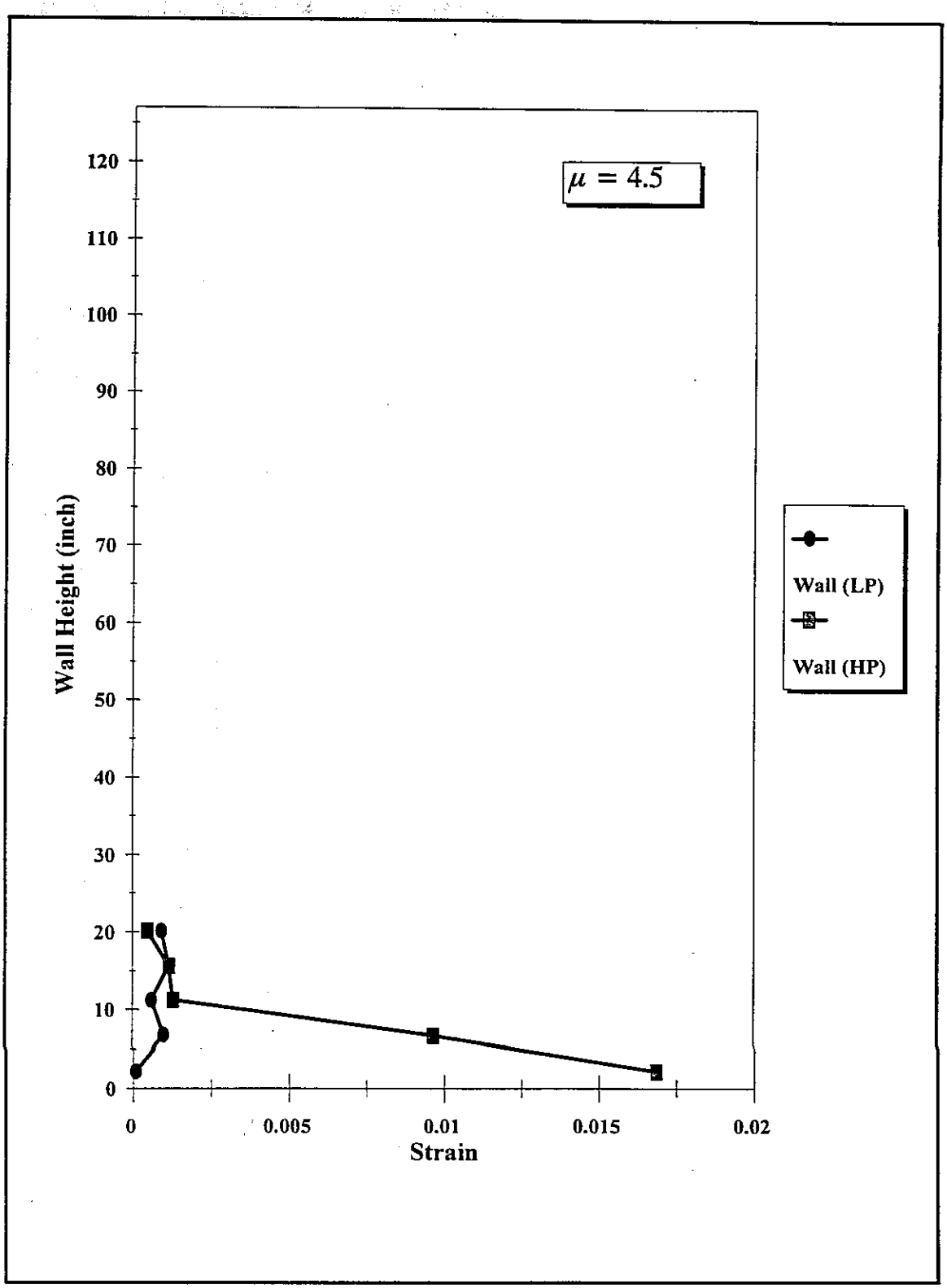

Figure 3.47: Distribution of strain in cross-ties over the height of the "P" walls at $\mu = 4.5$

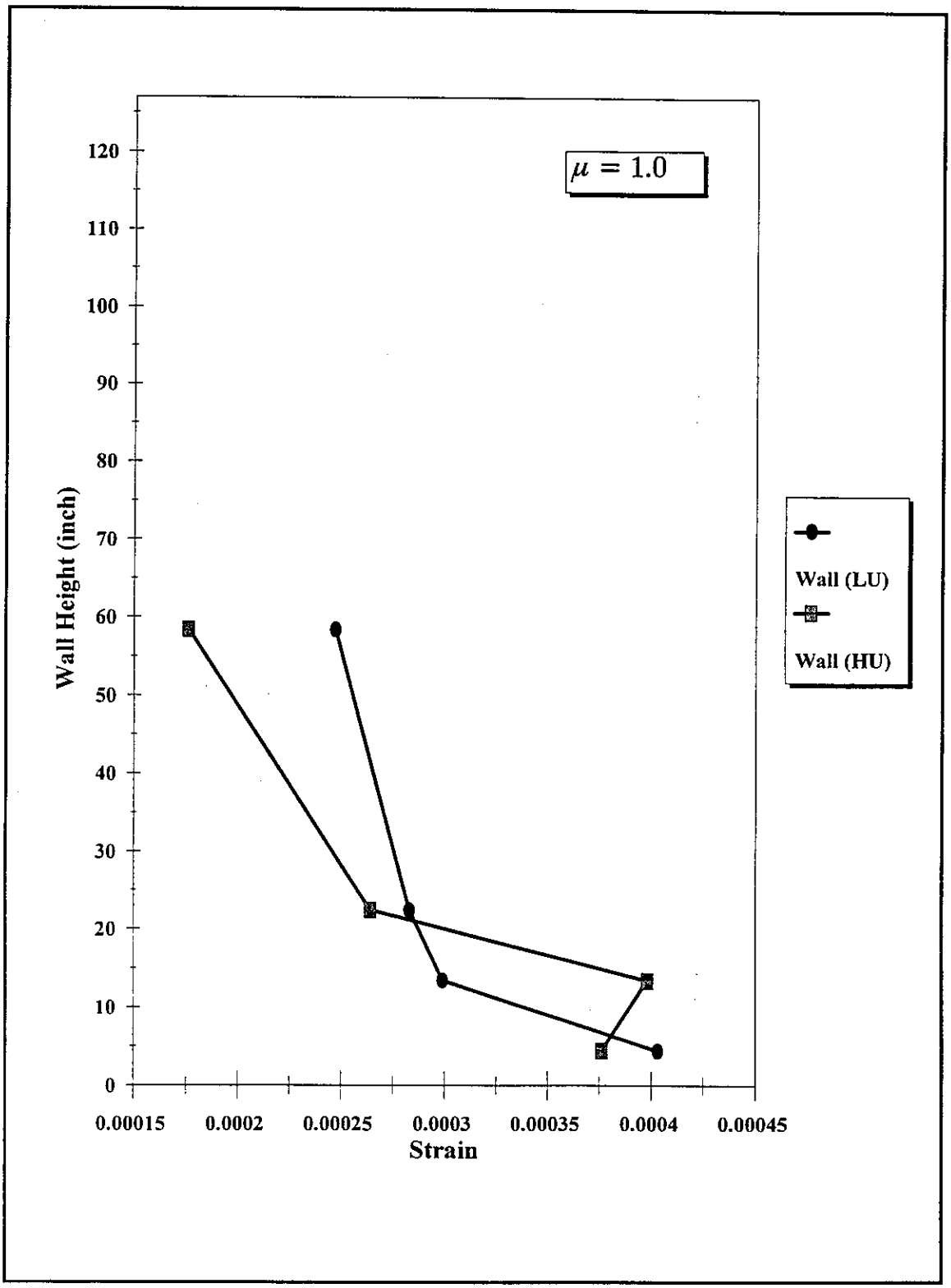

Figure 3.48: Distribution of strain in cross-ties over the height of the "U" walls at $\mu = 1.0$

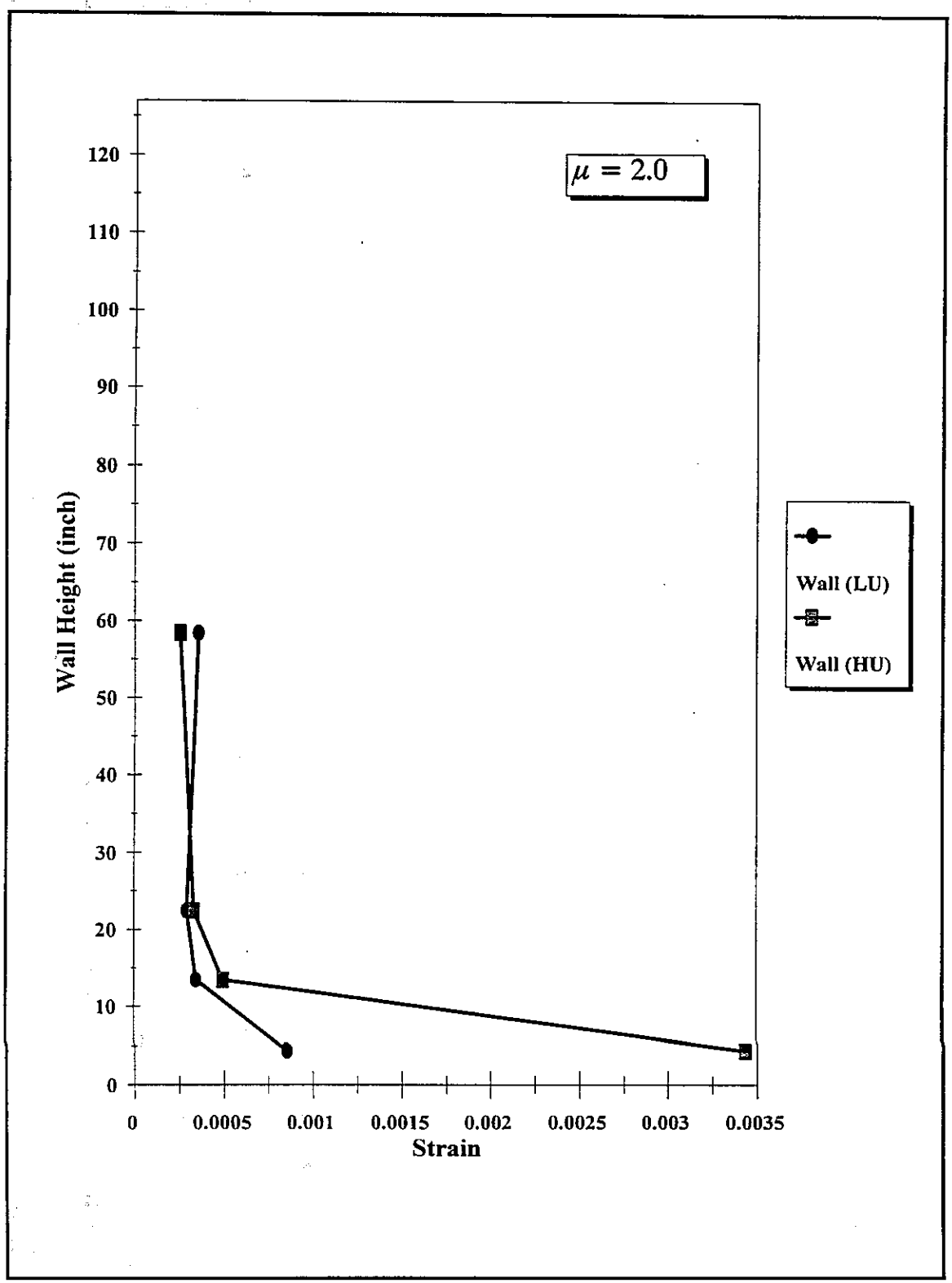

Figure 3.49: Distribution of strain in cross-ties over the height of the "U" walls at $\mu = 2.0$

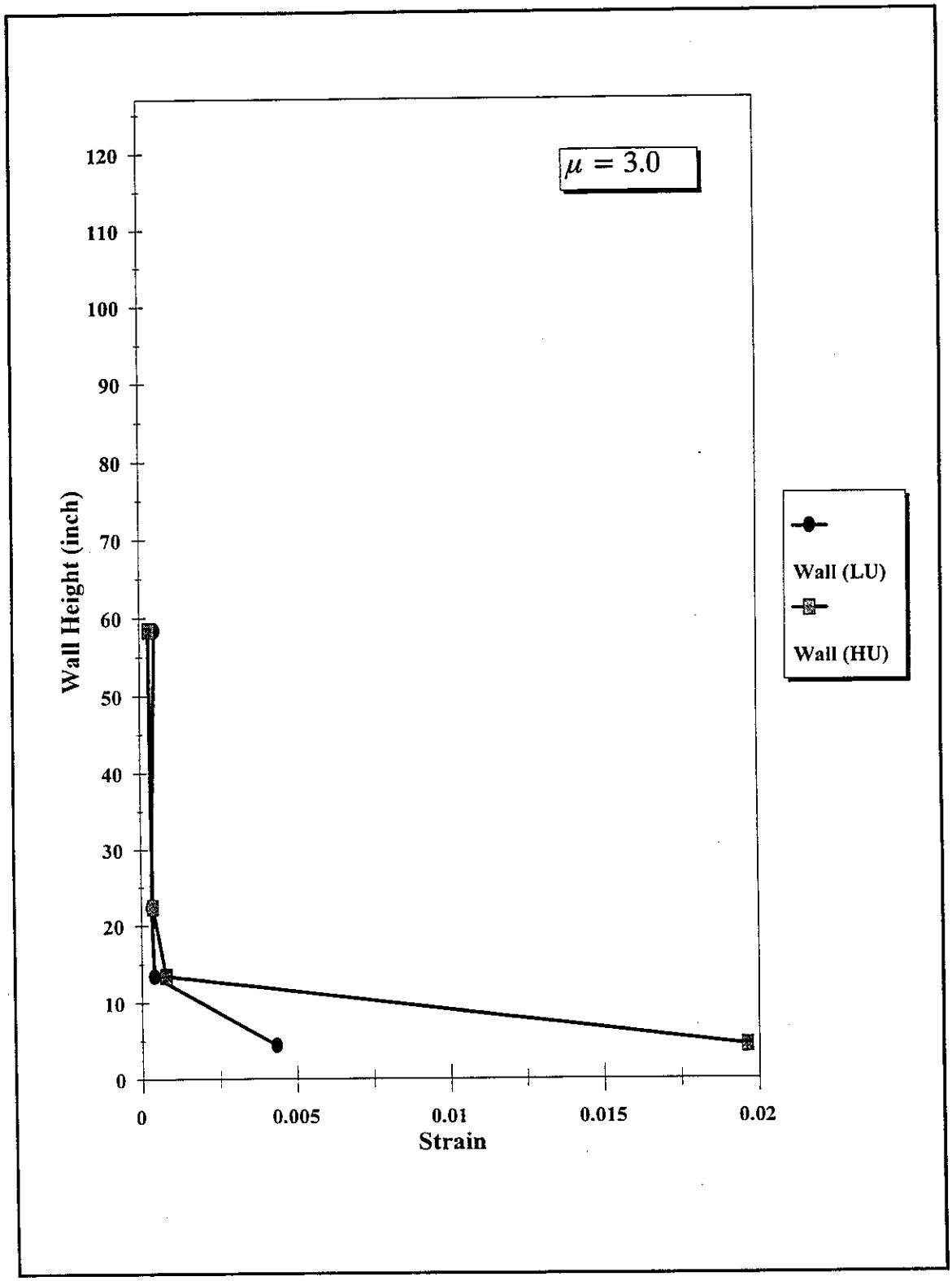

Figure 3.50: Distribution of strain in cross-ties over the height of the "U" walls at $\mu = 3.0$

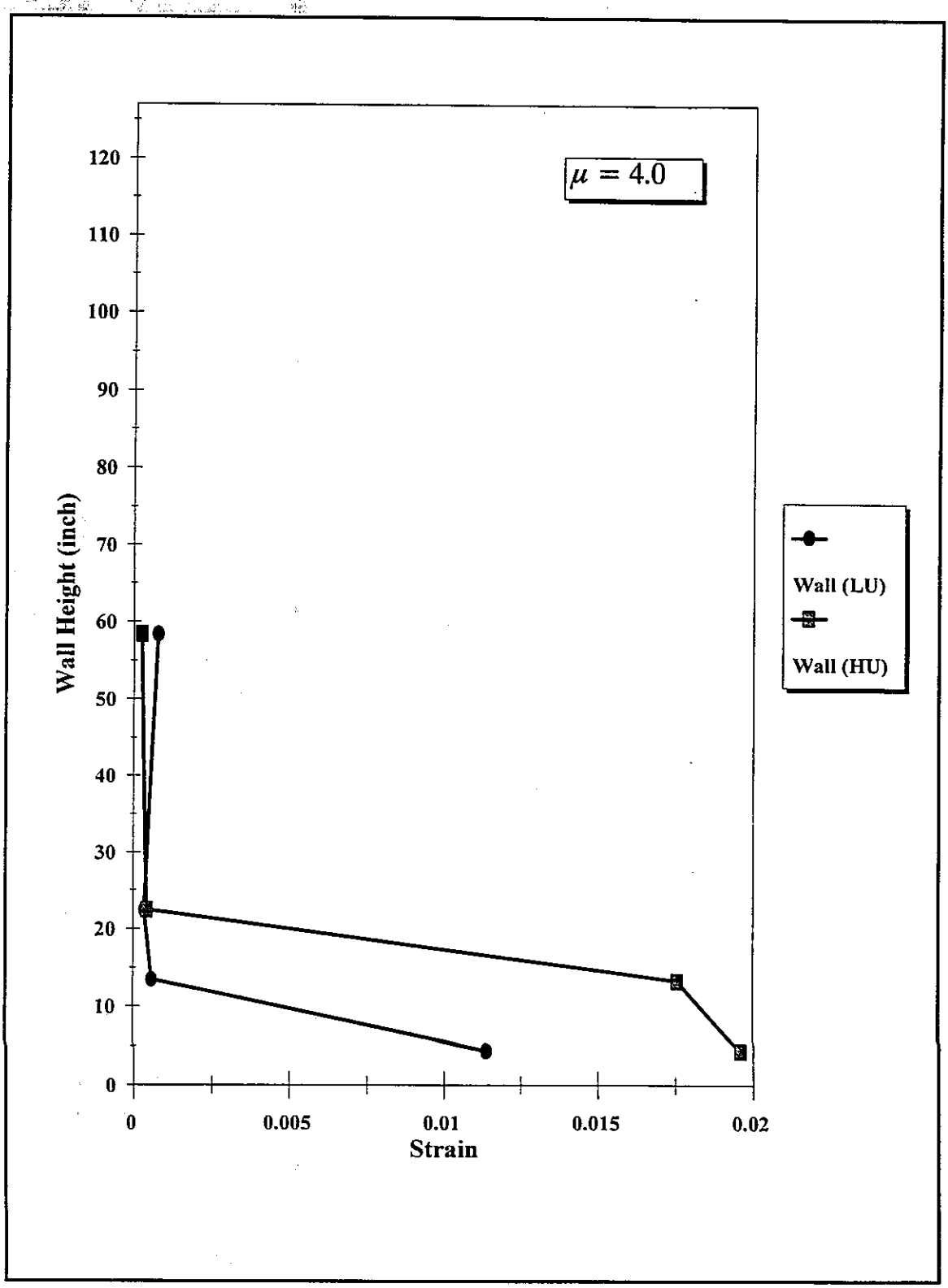

Figure 3.51: Distribution of strain in cross-ties over the height of the "U" walls at $\mu = 4.0$

Chapter 4

Analytical Program

The experimental study was performed to evaluate the strength, ductility and failure mechanism of six bridge pier wall samples. A theoretical program was also developed to predict the observed experimental parameters. In addition, the Caltrans method for evaluating the ductility was assessed. The behavior of pier walls in the weak direction is similar to the behavior of rectangular columns except for the degree of confinement and the vertical reinforcement ratio. Because the pier wall models investigated in this study were of the cantilever type, a one degree of freedom system was assumed in both the analysis and the experiments. Since the axial load exerted on a pier wall is mainly comprised of the weight of the bridge deck, the analysis assumed it as a constant load, invariable with the dynamic conditions.

The ductility of the pier wall samples was evaluated using the displacement ductility factor which was employed in the experimental measurement and described below. Also, the concrete and steel material were modeled analytically using verified empirical models.

4.1 Definition of Ductility

The ductility of a structural element, as described in the previous chapter, is defined by the displacement ductility factor as the ratio between the maximum horizontal displacement of the wall at ultimate and at first yield of the vertical reinforcement. Again, since it is difficult to pinpoint the yield state experimentally, an elasto-plastic model was proposed by Mander [20] to approximate the moment-curvature or the load-displacement relations in the theoretical analysis as well. The idealized value for the yield displacement $\Delta_y^{'}$ is calculated from the following relation (refer to Sec. 3.7)

$$\Delta_y^{'} = \Delta_y \frac{Q_i}{Q_y} \tag{4.1}$$

where Δ_y and Q_y are the displacement and the applied load at the first yield of the vertical reinforcement and Q_i is the ideal load calculated from the moment capacity of the wall section using the ACI-89 code approach. Therefore, the displacement ductility factor is defined by

$$\mu = \frac{\Delta_u}{\Delta_y^{'}} \tag{4.2}$$

where Δ_u is the displacement corresponding to the ultimate strain of the concrete.

4.2 Material Modeling

In seismic zones, the concrete section is expected to experience large strain. The concrete normal stress resulting from the common compression cylinder test, f_{co}, is the main parameter defining the concrete axial strength. However, the normal stress of the concrete section is also affected by the lateral stress due to section confinement.

Five empirical models, which considered the effects of the lateral stresses, were introduced by Park [26], Sheikh [35], Mander [21], Muguruma [23] and Fujii [7]. These models were compared by Hoshikuma et al [17] as to their effectiveness in predicting the behavior of pier walls. It was concluded that the accuracy of each

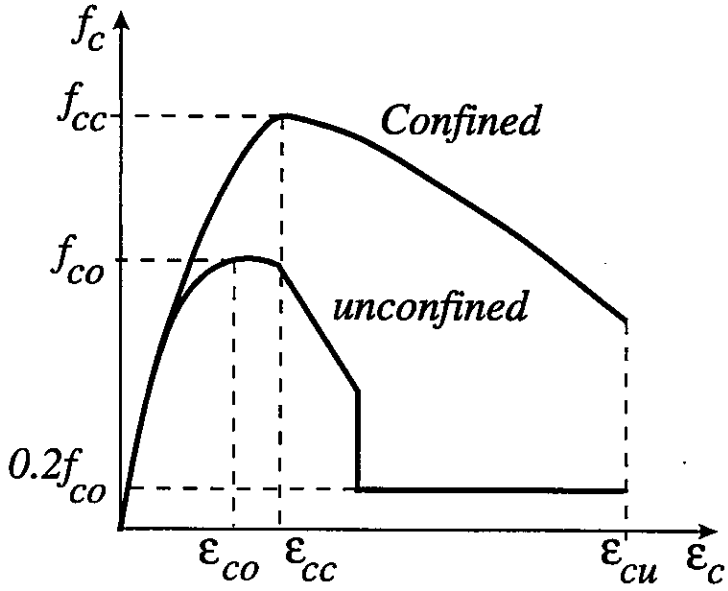

Figure 4.1: Concrete model (Hoshikuma model)

model is very dependent on the concrete section shape and the reinforcement ratio. Accordingly, Hoshikuma presented a concrete model applicable to rectangular pier walls which was adopted in this research. Figure 4.1 shows the relation between the concrete normal stress, f_c, and its corresponding strain, ϵ_c, for the confined and the unconfined models.

Equation 4.3 provides this relation where f_{cc} and ϵ_{cc} represent the concrete maximum stress and the corresponding value of strain

$$f_c = \begin{cases} E_c\ \epsilon_c\ \left(1 - \frac{1}{n}\left(\epsilon_c/\epsilon_{cc}\right)^{n-1}\right) & \text{if } \epsilon_c < \epsilon_{cc} \\ \\ f_{cc} - E_{des}\ (\epsilon_c - \epsilon_{cc}) & \text{if } \epsilon_c > \epsilon_{cc} \end{cases} \tag{4.3}$$

where E_c is the modulus of elasticity of the concrete material. The various parameters used in this equation may be calculated from Eqs. 4.4 through 4.7. The confinement effect is considered by the volumetric ratio of the lateral reinforcement ρ_s and its yield stress f_{yh}. Two parameters, α and β in Eqs. 4.6 and 4.7, are set equal to zero for the

unconfined model and equal to 0.30 and 0.55, respectively, for the confined model.

$$n = \frac{E_c\ \epsilon_{cc}}{E_c\ \epsilon_{cc} - f_{cc}} \tag{4.4}$$

$$E_{des} = 16\frac{f_{co}^2}{\rho_s\ f_{yh}} \tag{4.5}$$

$$\frac{f_{cc}}{f_{co}} = 1 + 3.70\ \alpha\ \frac{\rho_s\ f_{yh}}{f_{co}} \tag{4.6}$$

$$\epsilon_{cc} = .002 + .033\ \beta\ \frac{\rho_s\ f_{yh}}{f_{co}} \tag{4.7}$$

The strain at failure of the concrete section is calculated from Eq. 4.8 and is limited to 0.004 for the unconfined section

$$\epsilon_{cu} = \epsilon_{cc} + \frac{f_{cc}}{2\ E_{des}} \tag{4.8}$$

The stress-strain relation of the reinforcement, as introduced by Samara [34], was used in the present analysis. Equations 4.9 to 4.11 provide the relation between the stress, f_s, and its corresponding strain, ϵ_s. Figure 4.2 explains the various parameters of this equation. The possibility of buckling of the compression steel or slippage of the tension steel is not considered in this model.

$$f_s = \epsilon_s E_s \qquad if \quad \epsilon_s \leq \epsilon_y \tag{4.9}$$

$$f_s = f_y \qquad if \quad \epsilon_y \leq \epsilon_s \leq \epsilon_{sh} \tag{4.10}$$

$$f_s = f_y\left(\frac{m(\epsilon_s - \epsilon_{sh}) + 2}{60(\epsilon_s - \epsilon_{sh}) + 2} + \frac{(\epsilon_s - \epsilon_{sh})(60 - m)}{2(30r + 1)^2}\right) \qquad if \quad \epsilon_{sh} \leq \epsilon_s \leq \epsilon_{su} \tag{4.11}$$

where

$$m = \frac{(f_{su}/f_y)\,(30r + 1)^2 - 60r - 1}{15r^2}; \qquad r = \epsilon_{su} - \epsilon_{sh} \tag{4.12}$$

4.3 Calculation of Wall Displacement

A computer program, PWDUCT (Pier Wall DUCTility), was developed to evaluate the ductility parameters, and is briefly described here. In general, the total

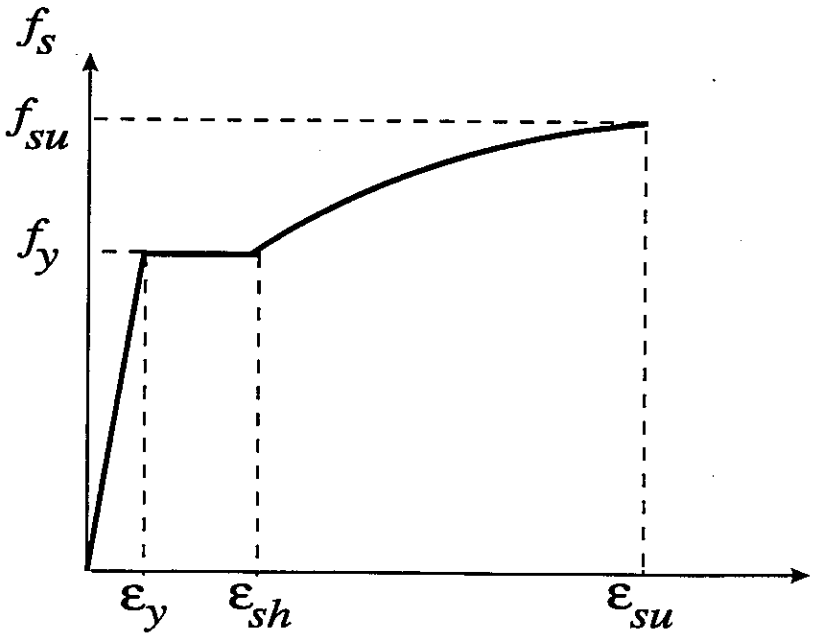

Figure 4.2: Reinforcement model

displacement at the top of the wall may be expressed as the sum of two displacement components

$$\Delta = \Delta_f + \Delta_s \tag{4.13}$$

where Δ_f is the displacement due to wall flexure and Δ_s is the deformation due to shear; the latter was ignored in this analysis as it is very small. The stiffness method is typical for displacement calculations; however, the top displacement of a cantilever wall was calculated herein according to Eq. 4.14 which is most appropriate for this structure type

$$\Delta_f = \int_0^L \phi(x) x dx \tag{4.14}$$

where $\phi(x)$ is the curvature distribution along the wall height and x is the coordinate measured from the top of the wall. Again, the theoretical yield displacement will be modified by the ratio of (Q_i/Q_y) as indicated in Eq. 4.6.

The calculation of the top horizontal displacement of each wall using Eq. 4.14 requires the knowledge of the curvature distribution over the wall height at different loading stages. To determine the relation between the bending moments and cur-

vatures under a constant axial load, it was found convenient to divide the section into a number of discrete laminas and to replace the lateral steel reinforcement by an equivalent thin strip with the appropriate thickness, as shown in Fig 4.3. The stresses in the concrete and steel in each lamina were found from the strain value at the center of the lamina and the above stress-strain relations. Two basic assumptions were utilized in the analysis to determine the laminas' strains:

- plane section remains plane after bending, and
- the bond slip between the reinforcement and the concrete was not considered.

The theoretical moment-curvature relation for a given axial load may be determined by incrementing the concrete strain in the extreme compression fiber, ϵ_{cm}. For each value of ϵ_{cm}, the depth of the neutral axis, kd, was found from Eq. 4.15 in which the sum of the internal forces equals the external axial load, P. The moment, M, corresponding to this value of ϵ_{cm} and the axial load is determined by summing the moments of the internal forces

$$P = \sum f_{cl}\ A_{cl} + \sum f_{sc}\ A_{sc} - \sum f_{st}\ A_{st} \tag{4.15}$$

where f and A represent the stress and the area of the concrete and steel laminas. Accordingly, the section curvature can be calculated as

$$\varphi = \frac{\epsilon_{cm}}{kd} \tag{4.16}$$

The yield displacement, Δ_y, and the yield curvature, ϕ_y, are defined at the case of first yielding of the flexural reinforcement, $f_s = f_y$. From the moment-curvature diagram, the curvature distribution can be constructed over the wall height as shown in Fig. 4.4 where the maximum curvature, ϕ_y, is at the bottom of the wall. Beyond the yielding stage, the curvature at the bottom section of the wall increases until it reaches its maximum calculated value. Subsequently, a plastic hinge is formed at

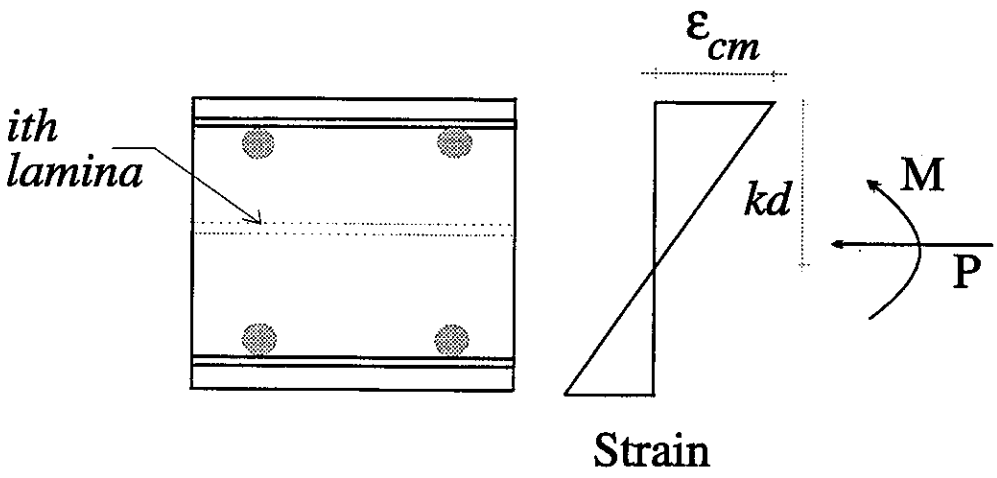

Figure 4.3: Section discrete laminas

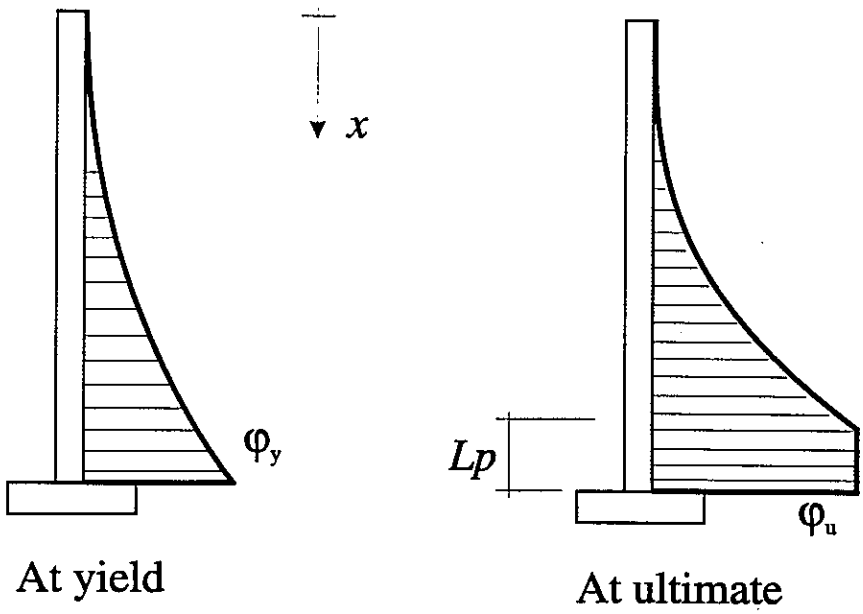

Figure 4.4: Curvature distribution

the wall base causing a significant rotation of the wall base sections. Therefore, the curvature distribution at the ultimate state is influenced by the plastic hinge length. An empirical formula developed by Priestley [30] for the plastic hinge length was used in the present analysis

$$L_p = 0.08L + 0.15 f_y d_b \tag{4.17}$$

where L is the wall height, d_b is the diameter of the longitudinal bars and f_y is the steel yield stress in ksi.

4.4 Caltrans Method for Calculating Ductility

A computer program, COL604R, was developed by Mark Seyed in 1993, for use by Caltrans designers. Even though the program is based on the same general principles described above, a few differences in the calculation of the ductility parameters were found, and are discussed here. First, the yield displacement is calculated from Eq. 4.18 which is more conservative yet not as accurate as Eq. 4.14

$$\Delta_y = \phi_y L^2/3 \tag{4.18}$$

where ϕ_y is the curvature at first yield and L is the total height of the wall. In addition, the ideal load used to calculate the idealized yield displacement is calculated from an equivalent elasto-plastic approximation of the section moment-curvature relation which possesses the same amount of the energy absorption; in other words, the area under the elasto-plastic moment-curvature idealization is set equal to the area under the true moment-curvature curve.

To calculate the ultimate displacement, an approximate method, introduced by Mander [20], is used. The total displacement of the wall is the sum of three displacement components

$$\Delta_u = \Delta_y^{'} + \Delta_p + \Delta_s \tag{4.19}$$

Wall sample	Yield displacement (inch)	Ideal load (kips)	Idealized yield displacement (inch)	Ultimate displacement (inch)	Ductility factor
HN	1.80	47.74	1.84	4.63	2.52
HP	1.86	47.82	1.93	7.92	4.10
HU	1.83	47.87	1.88	5.31	2.82
LN	1.57	31.23	1.65	4.93	3.00
LP	1.66	30.93	1.76	9.28	5.27
LU	1.62	30.96	1.71	5.86	3.43

Table 4.1: Ductility parameters calculated using the PWDUCT program

where $\Delta y'$ is the idealized yield displacement, Δ_p is the plastic deformation due to the nonlinearity of the moment-curvature response which occurs when the steel has yielded and/or the concrete enters the inelastic zone, and Δ_s is the deformation due to shear which was ignored in the analysis as it is very small. The plastic deformation can be calculated from [29]

$$\Delta_p = \theta_p(L - 0.5L_p) \tag{4.20}$$

where the plastic hinge rotation θ_p is evaluated from

$$\theta_p = \phi_p \, L_p = (\phi_u - \phi_y') \, L_p \tag{4.21}$$

in which ϕ_u is the maximum curvature at the base and L_p is the length of the plastic hinge which is empirically assumed as in Eq. 4.17. The ductility parameters calculated using the two computer programs are summarized in Tables 4.1 and 4.2.

Wall sample	Yield displacement (inch)	Ideal load (kips)	Idealized yield displacement (inch)	Ultimate displacement (inch)	Ductility factor
HN	2.20	49.53	2.34	5.70	2.44
HP	2.18	52.17	2.46	9.11	3.70
HU	2.07	50.34	2.25	7.64	3.40
LN	1.78	32.23	1.94	5.91	3.05
LP	2.02	34.27	2.36	9.49	4.02
LU	1.91	33.05	2.14	7.93	3.71

Table 4.2: Ductility parameters calculated using the COL604R program

4.5 Correlation of Experimental and Theoretical Results

The maximum horizontal load, the idealized yield displacement, the ultimate displacement and the displacement ductility factor, determined from the experimental and the theoretical programs, were compared and are presented in Figs. 4.5 to 4.8. In these figures, each sample was denoted by two letters: the first is either "H" or "L" indicating high or low vertical reinforcement ratio, whereas the second letter "N", "P" or "U" indicates the cross-ties distribution. The wall strength is illustrated in Fig. 4.5 by comparing the maximum horizontal load that the sample can carry. In addition, the main ductility parameters (the yield and ultimate displacements) are compared in Figs. 4.6 and 4.7, and the displacement ductility factor is illustrated in Fig 4.8. Inspection of these figures revealed that:

- A good correlation was found between the calculated wall strength and the observed values (Fig. 4.5). The values computed from the program COL604R

are slightly higher than those calculated using the program PWDUCT.

- The values of the yield displacement calculated by the PWDUCT program for the "L" walls are close to the experimental values; however, the difference is noticeable for the "H" walls. In contrast, the values computed using the COL604R program have a better correlation in the "H" walls than the "L" walls. It is also noted that the experimentally observed yield displacements have increased by approximately 40% in the highly reinforced walls. In addition, the cross-tie distribution does not significantly influence either the observed or the calculated values. Some difference, however, was noted for the values computed by the COL604R program because the ideal load is dependent on the confinement.

- The calculated ultimate displacements using both computer codes are in good agreement, however, these values are much less than those observed experimentally (Fig. 4.7).

- The calculated displacement ductility factors using both computer programs showed reasonable correlations with the experimental values; however, the theoretical values are always conservative.

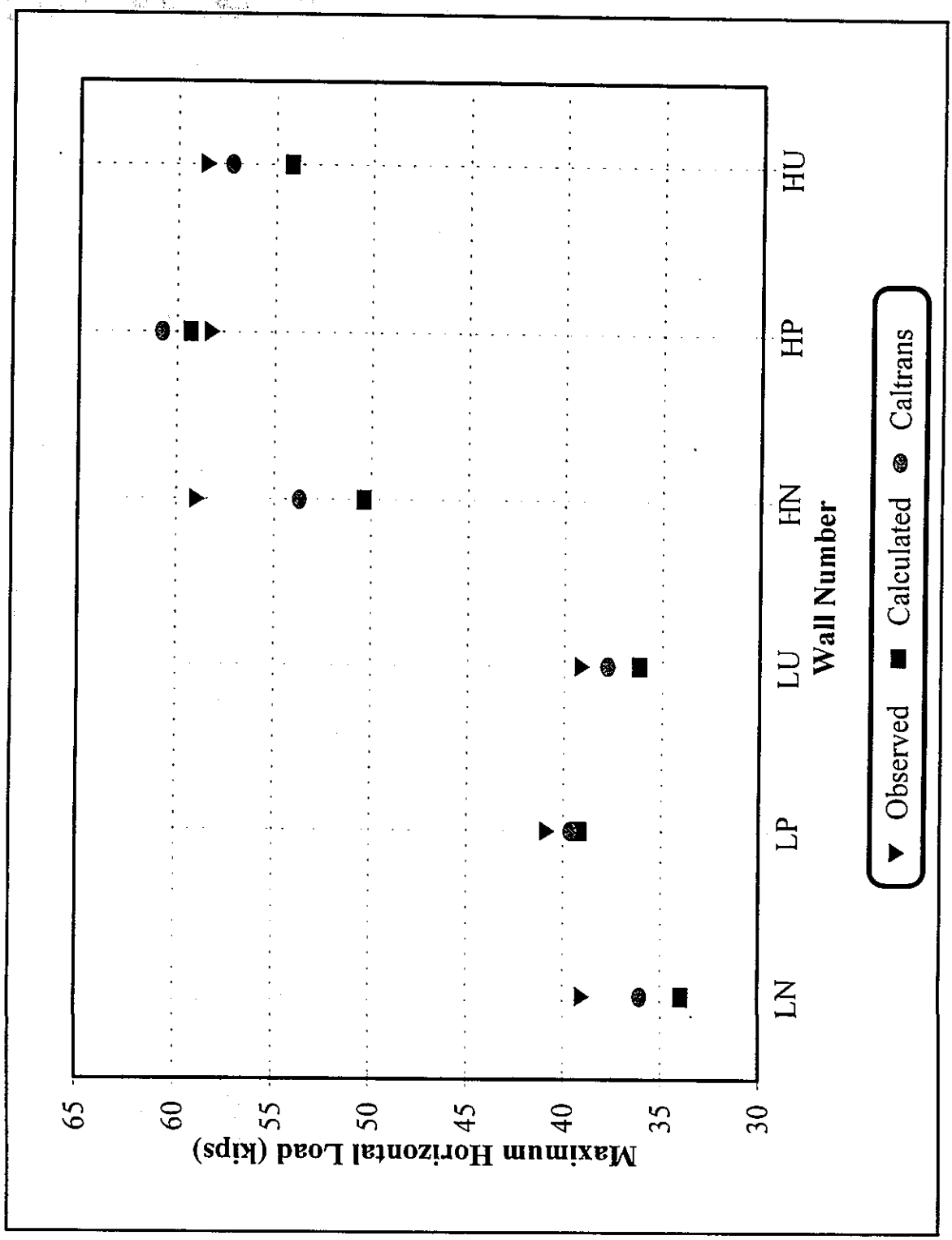

Figure 4.5: Observed and calculated maximum horizontal loads

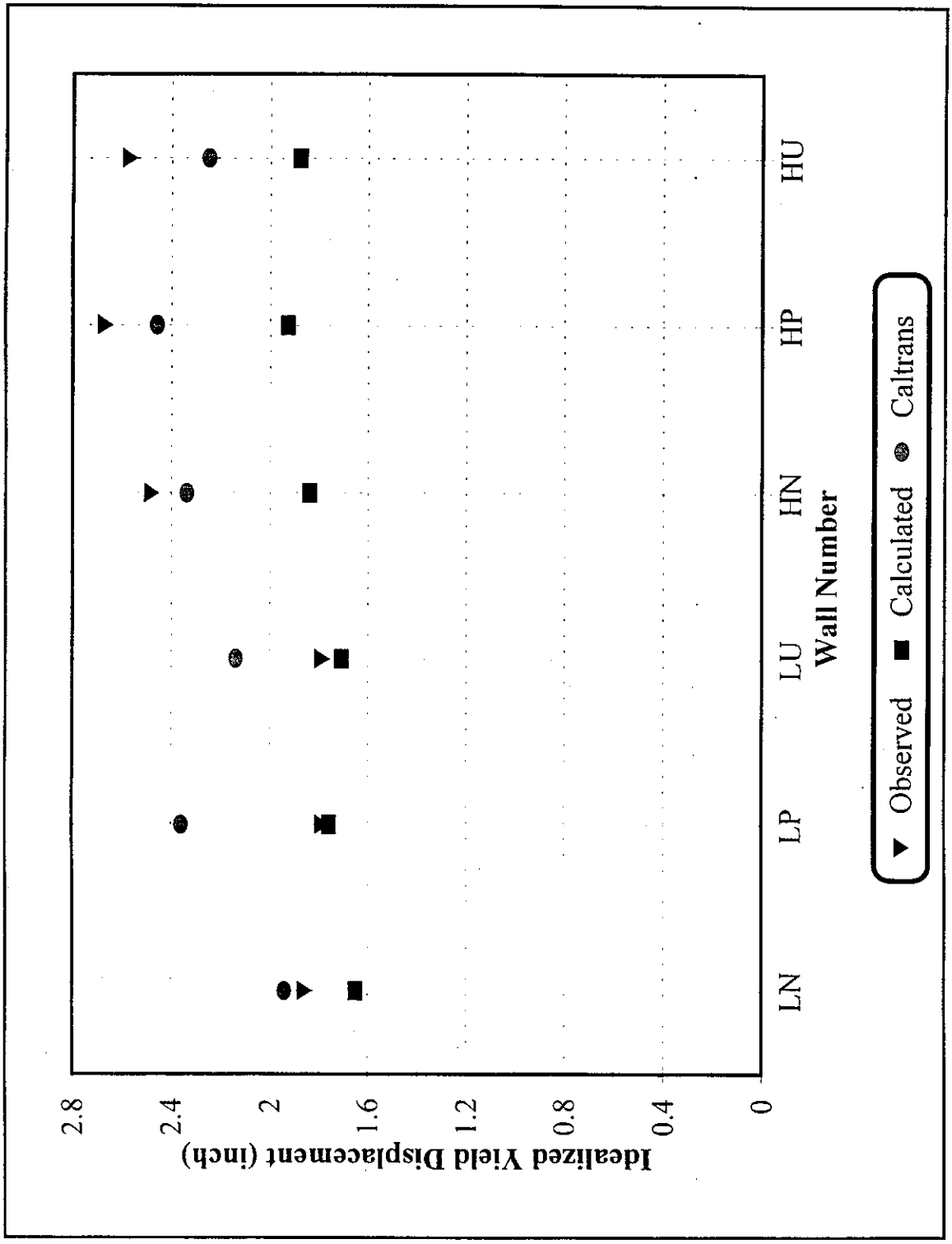

Figure 4.6: Observed and calculated idealized yield displacements

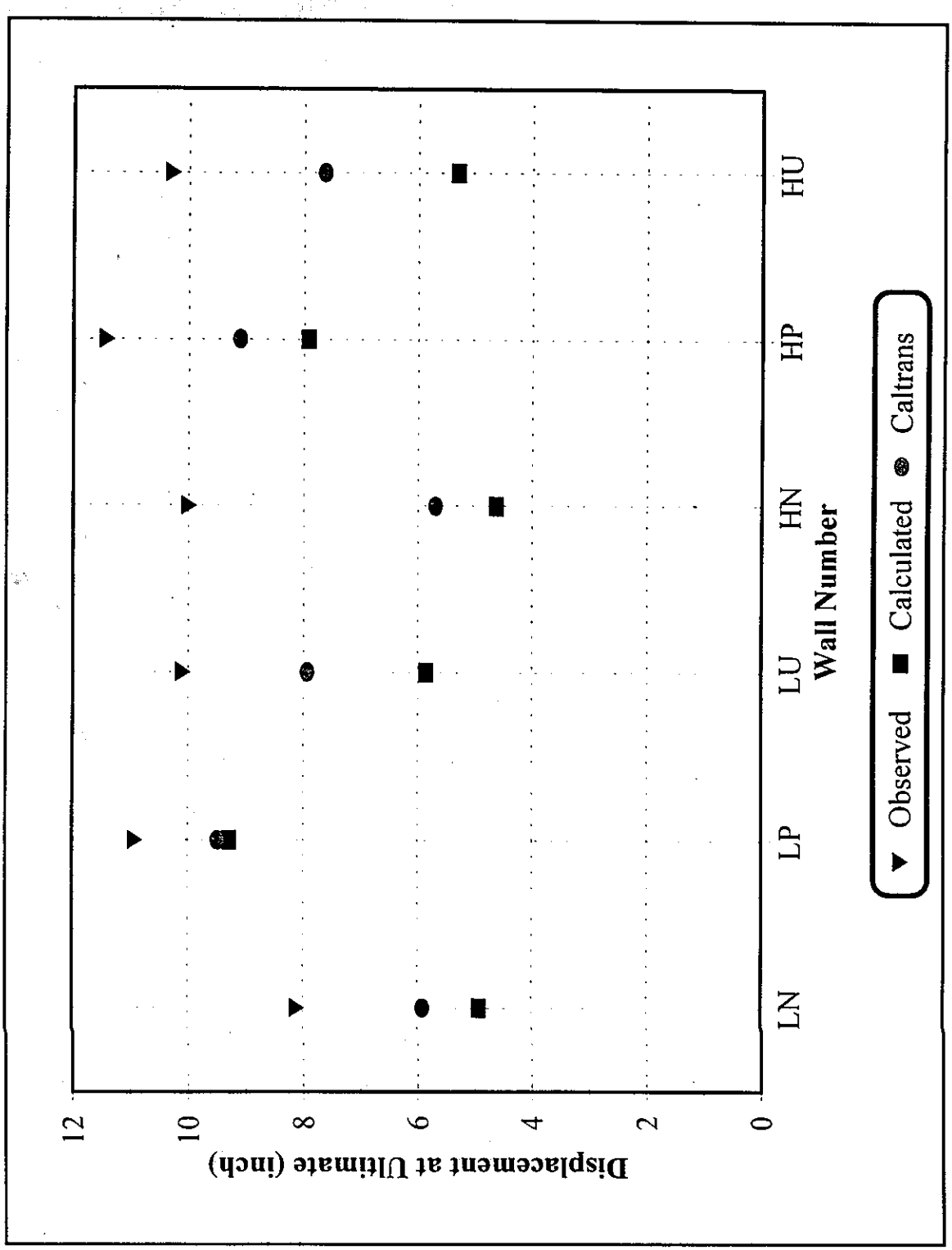

Figure 4.7: Observed and calculated ultimate displacements

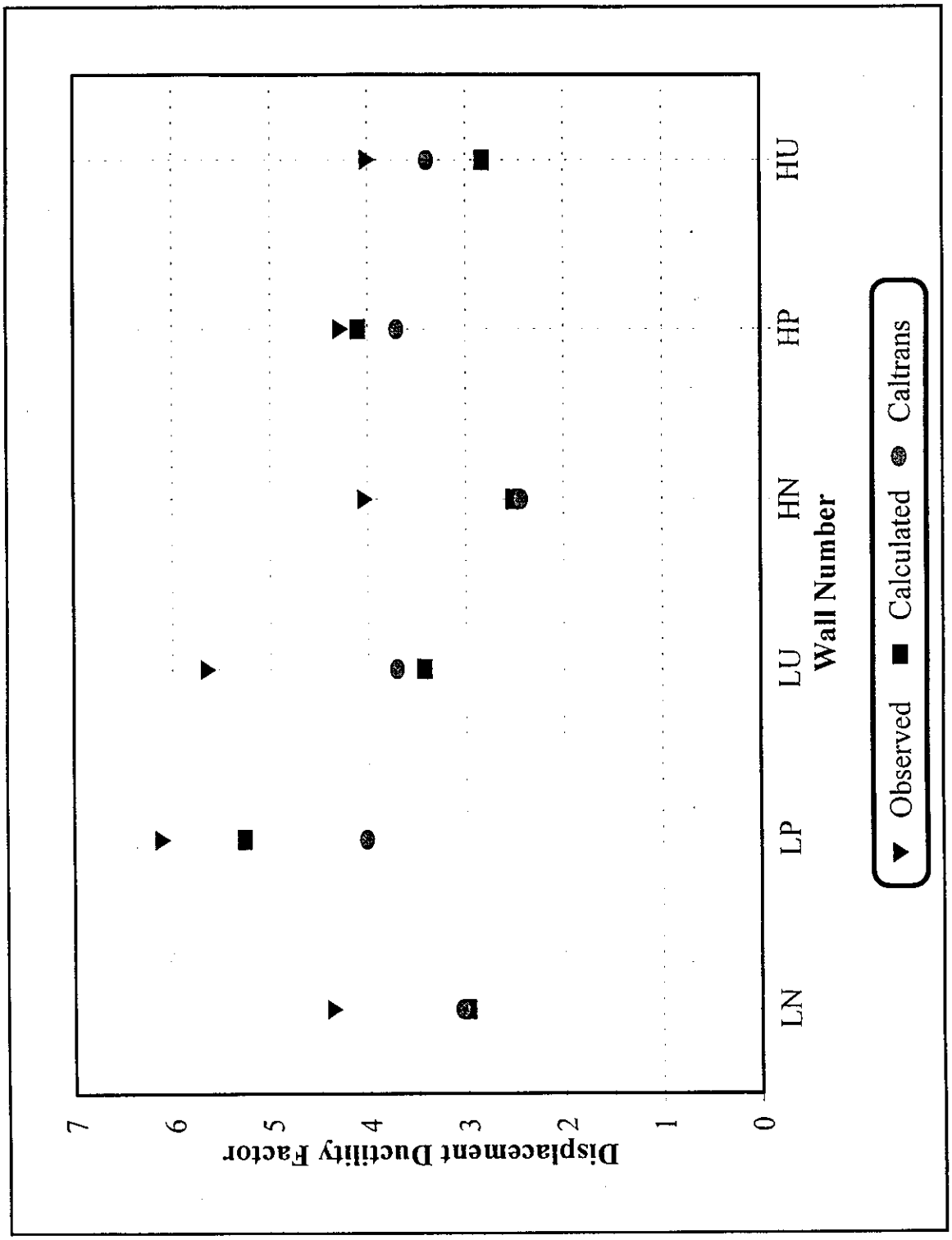

Figure 4.8: Observed and calculated displacement ductility factors

Chapter 5

Conclusions

The cyclic testing of six half-scale pier wall samples representing two ratios of the vertical reinforcement and three distributions of the cross-ties has led to the following conclusions:

1. A minimum displacement ductility factor of 4.0 was observed for all walls.

2. Based on the assumption that the yield moment is equal to 75% of the ideal moment, the average values of the idealized yield displacements were found to be 1.83 and 2.57 inch for the "L" and "H" walls, respectively.

3. All walls with the higher reinforcement ratio failed at nearly the same ductility level regardless of the distribution of the cross-ties. This is attributed to the observation that cross-ties in these samples could not provide sufficient confinement to the pier wall sections.

4. For walls with the lower reinforcement ratio, the cross-ties enhanced the ductility factor in the "LP" and "LU" walls by nearly 40% and 30%, respectively. Even though the walls with uniform and partial distributions of cross-ties achieved almost the same ductility factor, the partial distribution of the cross-ties is definitely more economic.

5. The cross-tie distribution has minimal effect on the wall stiffness and the maximum load.

6. Large lateral forces associated with bar lateral deformation were generated and transmitted to the cross-ties in the walls with the higher reinforcement ratio. These forces exceeded the ties' capacity to prevent bar buckling. It is therefore recommended not to use the larger size bars for the vertical reinforcement.

7. Failure of the cross-ties occurred by the opening of their ends. It is recommended that cross-ties with a longer hook length be used.

Bibliography

[1] American Concrete Institute, Building Code Requirements for Reinforced Concrete, ACI 318-89, Detroit, Michigan, 1989.

[2] Baker, A.L., and Amarakone, A.M., "Inelastic Hyperstatic Frames Analysis." Proceedings of the International Symposium on the Flexural Mechanics of Reinforced Concrete, ASCE-ACI, Miami, November 1964.

[3] Cheok, G.S., and Stone, W.C., "Behavior of 1/6-Scale Model Bridge Columns Subjected to Inelastic Cyclic Loading," ACI Structural Journal, No. 87-S64, November-December 1990.

[4] Corley, W.G., "Rotational Capacity of Reinforced Concrete Beams," Journal of Structural Division, ASCE, Vol. 92, October 1966, pp. 121-146.

[5] Department of Transportation, State of California, Bridge Design Specifications, June 1990.

[6] Earthquake Engineering Research Institute, Earthquake Spectra, Loma prieta Earthquake Reconnaissance Report, Vol. 6, May 1990.

[7] Fujii, M., "A Study on the Application of a Stress-Strain Relation of Confined Concrete," Annual Report on Cement Engineering, Vol. 42, 1988, pp. 311-314.

[8] Gates, J.H., "Seismic Resistant Bridge Design in California," Seismic Research for Highway Bridges, U.S.-Japan Program, 1984, pp. 1-13.

[9] Gates, J.H., "California's Seismic Design Criteria for Bridges," Journal of the Structural Division, Proceedings of the American Society of Civil Engineers, Vol. 102, December 1976.

[10] Ghee, A.B., "Ductility of Reinforced Concrete Bridge Piers Under Seismic Loading," Research Report, Department of Civil Engineering, University of Canterbury, Christchurch, New Zealand, 1981.

[11] Haggag, H.A., "Cyclic Behavior of Bridge Pier Walls for Design and Retrofit," Ph.D. Dissertation, Department of Civil and Environmental Engineering, University of California, Irvine, Winter 1995.

[12] Haggag, H.A., Haroun, M.A., Pardoen, G.C., and Shepherd, R., "Behavior of Bridge Pier Walls of Modern Design Under Cyclic Loads," Proceedings of the fifth U.S. National Conference on Earthquake Engineering, EERI, Chicago, Illinois, July 1994.

[13] Haroun, M.A. and Haggag, H.A., "Models for Evaluating the Ductility of Reinforced Concrete Bridge Pier Walls," Proceedings of the 10th US-Japan Bridge Engineering Workshop, Lake Tahoe, May 1994.

[14] Haroun, M.A., Pardoen, G.C., and Shepherd, R., "Testing of Pier Walls of Limited Ductility," Proceedings of the Second Seismic Research Workshop, California Department of Transportation, Sacramento, March 1993.

[15] Haroun, M.A., Pardoen, G.C., and Shepherd, R., "Seismic Ductility and Strength of Pier Walls," Proceedings of the third NSF Workshop on Bridge Engineering Research in Progress, San Diego, November 1992, pp. 285-288.

[16] Haroun, M.A., Pardoen, G.C., Shepherd, R., Haggag, H.A., and Kazanjy R.P., "Cyclic Behavior of Bridge Pier Walls for Retrofit," Final Report to the California Department of Transportation, December 1993.

[17] Hoshikuma, J., Kawashima, K. and Nagaya, K., "A Stress-Strain Model for Reinforced Concrete Bridge Piers Confined by Hoop Reinforcement," Proceedings of the Second US-Japan Workshop on Seismic Retrofit of Bridges, Berkeley, California, January 1994.

[18] Kawashima, K., Hasegawa, K., Koyama, T. and Yoshida T., "Hysteretic Behavior of Reinforced Concrete Bridge Piers by Dynamic Loading Tests and Shaking Table Tests," Proceedings of Ninth World Conference on Earthquake Engineering, Tokyo-Kyoto, Japan, Vol. IV, August 1988.

[19] Kent, D.C. and Park, R., "Flexural Members with Confined Concrete," Journal of the Structural Division, ASCE, Vol. 97, No. ST7, July 1971, pp. 1969-1990.

[20] Mander, J.B., "Seismic Design of Bridge Piers," Thesis, Civil Engineering Department, University of Canterbury, New Zealand, 1983.

[21] Mander, J.B., Priestley, M.N. and Park, R., "Observed Stress-Strain Behavior of Confined Concrete," Journal of the Structural Division, ASCE, Vol. 114, No. ST8, August 1988; pp. 1827-1849.

[22] Mourad, S.A., Flynn, N.H., Haroun, M.A., Pardoen, G.C., and Shepherd, R., "Seismic Retrofit of Bridge Pier Walls," Proceedings of Third U.S. Conference on Lifeline Earthquake Engineering, ASCE, Los Angeles, August 1991, pp. 176-185.

[23] Muguruma, H., "A Study on the Improvement of Bending Ultimate Strain of Concrete," 24th Structural Engineering Symposium, 1978, pp. 109-116.

[24] National Center for Earthquake Engineering Research, The Northridge, California Earthquake of January 17, 1994: General Reconnaissance Report, Technical Report NCEER-94-0005, March 1994.

[25] NZS 3101, "The Design of Concrete Structure," Part 1: Code of Practice, Part 2: Commentary, Standards Association of New Zealand, Wellington, 1982.

[26] Park, R., "Ductility of Square-Confined Concrete Columns," Journal of the Structural Division, ASCE, Vol. 108, No. ST4, April 1982, pp. 929-950.

[27] Park, R., and Paulay, T., Reinforced Concrete Structures, John Wiley and Sons, 1975.

[28] Park, R., "Evaluation of Ductility of Structures and Structural Assemblages from Laboratory Testing," Bulletin of the New Zealand National Society for Earthquake Engineering, September 1989, pp. 155-166.

[29] Paulay, T. and Priestley, M.N., Seismic Design of Reinforced Concrete and Masonry Buildings, John Wiley and Sons, 1992.

[30] Priestley, M.N., and Park, R., "Strength and Ductility of Concrete Bridge Columns under Seismic Loading," ACI Structural Journal, Vol. 84, January-February 1987, pp. 61-76.

[31] Priestley, M.N., Seible, F., Chai, Y.H., "Design Guidelines for Assessment Retrofit and Repair of Bridge for Seismic Performance," Report No. SSRP-92/01, Department of Applied Mechanics and Civil Engineering Sciences, University of California, San Diego, August 1992.

[32] Rizkalla, S.H., Saadat, F., and Higai, T., "Fundamental Characteristics and Behavior of R.C. Bridge Piers Subjected to reversed Cyclic Loading," University of Manitoba, Winnipeg, Manitoba, Canada.

[33] Saatcioglu, M. and Ozcebe, G., "Response of Reinforced Concrete Columns to Simulated Seismic Loading," ACI Structural Journal, Title no. 86-S1, January-February 1989.

[34] Samara, R.M., " Ductility Analysis of Confined Columns," Journal of Structural Engineering, ASCE, Vol. 116, No. 11, November 1990.

[35] Sheikh, S.A. and Uzumeri, S.M., "Strength and Ductility of Tied Concrete Columns," Journal of the Structural Division, ASCE, Vol. 106, No. ST5, May 1980, pp. 1079-1102.

[36] Soesianawati, M.T., "Limited Ductility Design of Reinforced Concrete Columns," Research Report 86-10, Department of Civil Engineering, University of Canterbury, Christchurch, New Zealand, March 1986.